Okinawa Institute of Science and Technology
Graduate University

Thesis submitted for the degree

Doctor of Philosophy

Investigating the Function of Strip1 in Ganglion Cell Survival and Neural Circuit Formation of the Developing Zebrafish Retina

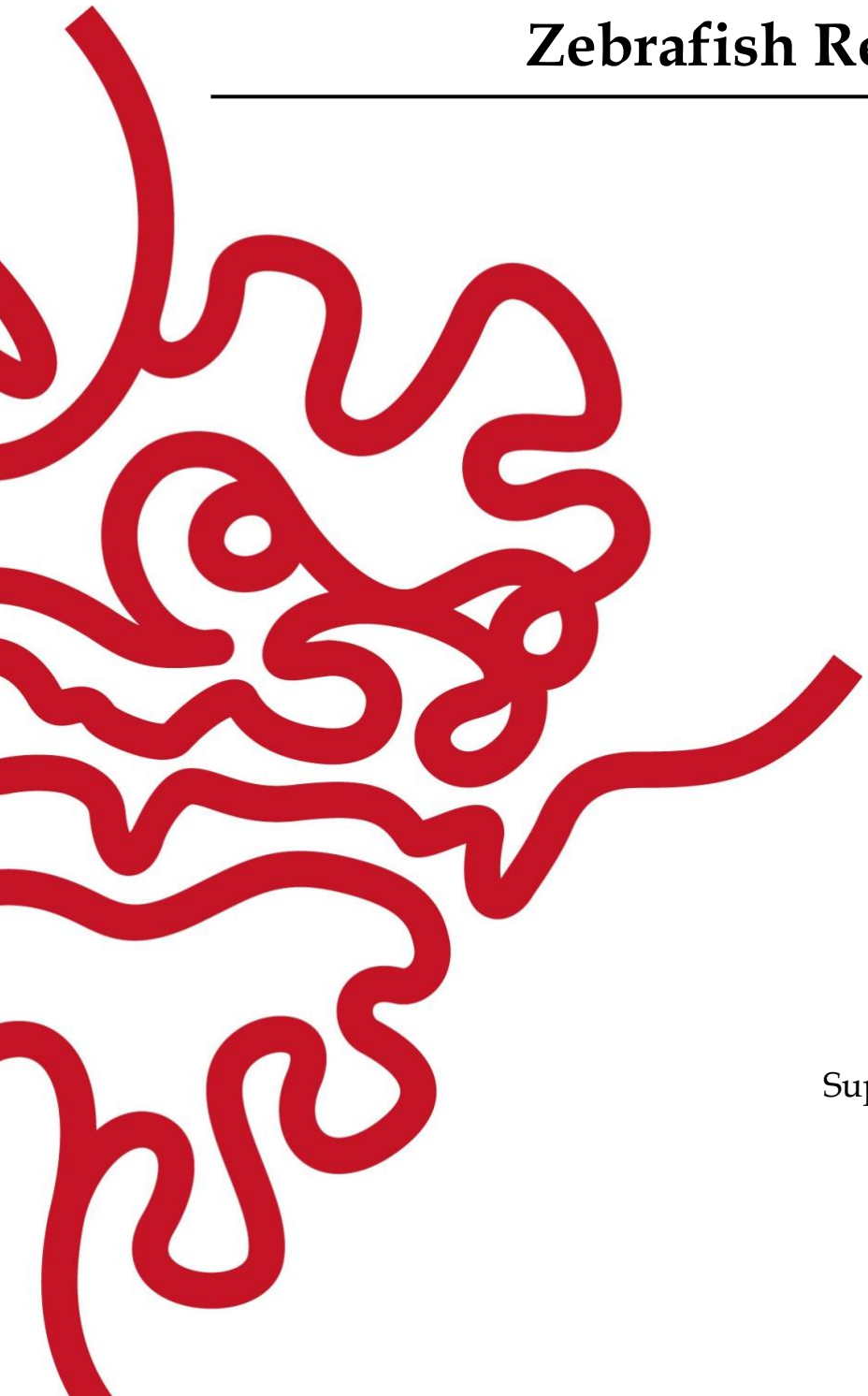

by

Mai Ahmed

Supervisor: **Prof. Ichiro Masai**

March 2022

Declaration of Original and Sole Authorship

I, Mai Ahmed, declare that this thesis entitled "Strip1 is essential for ganglion cell survival and neural circuit formation of the developing zebrafish retina" and the data presented in it are original and my own work.

I confirm that:

- No part of this work has previously been submitted for a degree at this or any other university.
- References to the work of others have been clearly acknowledged. Quotations from the work of others have been clearly indicated and attributed to them.
- In cases where others have contributed to part of this work, such contribution has been clearly acknowledged and distinguished from my own work.
- None of this work has been previously published elsewhere, with the exception of the following:

  Ahmed M, Kojima Y, Masai I. Strip1 regulates retinal ganglion cell survival by suppressing Jun-mediated apoptosis to promote retinal neural circuit formation. Elife. 2022 Mar 22;11:e74650. doi: 10.7554/eLife.74650. PMID: 35314028.

Date: March 23rd, 2022

Signature: 

Abstract

In the vertebrate retina, an interplay between retinal ganglion cells (RGCs), amacrine and bipolar cells establishes a synaptic layer called the inner plexiform layer (IPL). This circuit conveys signals from photoreceptors to visual centers in the brain. However, the molecular mechanisms involved in its development remain poorly understood. Striatin-interacting protein 1 (Strip1) is a core component of the STRIPAK complex, and it has shown emerging roles in embryonic morphogenesis. This study uncovers the importance of Strip1 in inner retina development. Using zebrafish, I show that loss of Strip1 causes defects in IPL formation. In *strip1* mutants, RGCs undergo dramatic cell death shortly after birth. Cells in the inner nuclear layer subsequently invade the degenerating RGC layer, leading to a disorganized IPL. Mechanistically, zebrafish Strip1 interacts with its STRIPAK partner, Striatin3, to promote RGC survival by suppressing Jun-mediated apoptosis. In addition to its function in RGC maintenance, Strip1 is required for RGC dendritic patterning, which likely promotes interaction between RGCs and amacrine cells for IPL formation. Taken together, I propose that a series of Strip1-mediated regulatory events coordinates inner retinal circuit formation by maintaining RGCs during development, which ensures proper positioning and neurite patterning of inner retinal neurons.

Acknowledgments

I would like to express by deepest gratitude to my supervisor Prof. Ichiro Masai for his constant support and guidance during my PhD journey. I am thankful that he gave me the freedom and resources to pursue my research questions. His insightful feedback and immense experience have brought my work to a higher level.

I would like to extend my sincere thanks to my thesis committee members; Prof. Tadashi Yamamoto and Prof. Hiroshi Watanabe for always giving me their time and constructive feedback on my research progress.

I would like to thank all the members of the Masai unit. I am grateful to Dr. Yuko Nishiwaki for her constant support and constructive feedback, and Dr. Yuki Takeuchi for providing technical advice and for teaching me how to analyze RNA sequencing data. I am thankful to the fish facility and technical staff for always taking care of my fish lines. I would also like to thank former lab members Dr. Fumiyasu Imai, Dr. Sachihiro Suzuki, and Ms. Asuka Yoshizawa for supporting initial cloning experiments and fishline generation at the Masai unit.

Special thanks to Mr. Yutaka Kojima for his constant support with genotyping, fishline maintenance, and preparation of histology samples, and Dr. Tetsuya Harakuni for helping me with molecular cloning. I also appreciate all the support I received from my lab mates, especially Swathy Babu and Manana Kutsia for always sharing ideas and constructive feedback.

I am thankful to Prof. Rachel Wong and Prof. Francesco Argenton for providing important constructs I used in my work. In addition, I am grateful to Dr. Ivan Mbogo in the Evolutionary Neurobiology Unit at OIST, and Mr. Alejandro Villar-Briones from the Instrumental Analysis section of Research Support Division at OIST for their help with mass spectrometry analysis. I am also grateful for the support I received from the Sequencing and Imaging sections at OIST. In addition, I am thankful to the Student Support section and OIST Graduate School for their tremendous support and assistance throughout my PhD.

I would like to thank my friends– Dr. Nishtha Ranawat, Dr. Amine Aladag, Nadine Wurkuttis, and Aliya Adefuin for a cherished time spent in OIST. They made graduate life a much pleasant experience.

I am forever grateful to my parents and my sisters for always supporting me and pushing me to challenge myself. Lastly, I am thankful to my beloved husband Mohieldin Youssef. Without his tremendous understanding and encouragement, it

would have been impossible for me to finish my studies, while we both took care of our wonderful children, Omar and Hana.

Abbreviations

ACs	Amacrine cells
AFs	Arborization fields
AJs	Adherens junctions
AO	Acridine Orange
aPKC	atypical protein kinase C
ath5	atonal bHLH transcription factor 7
BAX	BCL2-associated X protein
Bcl-2	B-cell lymphoma 2
BDNF	Brain-derived neurotrophic factor
BPs	Bipolar cells
BSA	Bovine serum albumin
CCM3	Cerebral cavernous malformation 3
Cka	Connector of kinase to AP-
CMZ	Ciliary marginal zone
CTTNBP2	Cortactin binding protein 2
dACs	displaced amacrine cells
DSCAM	Down syndrome cell adhesion molecule
Ena	Enabled
Erk1/2	Extracellular signal-regulated kinase 1/2
F-actin	Filamentous actin
FGFR1OP2	Fibroblast growth factor receptor 1 oncogene protein 2
GCL	Ganglion cell layer
GSKIII	Germinal center kinase III
has	*heart and soul*
HCs	Horizontal cells
hpf	Hours post fertilization
hpo	Hippo kinase cassette
hsp	Heat shock promoter
iACs	inhibitory amacrine cells
INL	Inner nuclear layer
IPL	Inner plexiform layer
JNK	Jun N-terminal kinase
LCA	Leber's congenital amaurosis
MAPK	Mitogen-activated protein kinase

MGs	Müller glia cells
mib	*mindbomb*
Mob3	Monopolar spindle-one -binder family 3
moe	*mosaic eyes*
ncad	N-cadherin
NMJ	Neuromuscular junction
nok	*nagie oko*
Oki	Okinawa wildtype
ome	*oko meduzy*
ONI	Optic nerve injury
ONL	Outer nuclear layer
ONX	Optic nerve crush
OPL	Outer plexiform layer
OT	Optic tectum
PE	Peripodial epithelium
PFA	Paraformaldehyde
PP2A	Protein phosphatase 2A
PPI	protein-protein interaction
PRs	Photoreceptors
RGCs	Retinal ganglion cells
RINs	Retinal inhibitory neurons
RIN	RNA integrity number
roy	*roy orbison*
rw147	*riken wako 147*
Sdk-1/2	Sidekick-1/2
SIKE	Suppressor of IKKe
SLMAP	Sarcolemmal membrane-associated protein
SSLP	Simple sequence length polymorphism
Strip1	Striatin-interacting protein 1
STRIPAK	Striatin-interacting phosphatase and kinase
STRN	Striatin
TBCD	Tubulin folding cofactor D
TCA	Trichloroacetic acid
TrkB	Tropomyosin-related kinase B
TUNEL	Terminal deoxynucleotidyl transferase dUTP nick end labeling
UMAP	Uniform Manifold Approximation and Projection
WISH	Whole-mount in situ hybridization

إهداء إلى أمي وأبي لحبهما وعطائهما الكبير، ودعمهما الدائم لي في مسيرتي

Dedicated to my parents, for their endless love and unwavering support.

Contents

List of Figures

List of Tables

Chapter 1.

Introduction

"The retina is the oldest and most persistent of my laboratory loves. Life never succeeded in constructing a machine so subtly devised and so perfectly adapted to an end as the visual apparatus."
–Santiago Ramón y Cajal

The neural retina is a light-sensitive tissue located at the back of vertebrate eyes. It has an impeccably organized neural circuit that has puzzled researchers for decades (Avanesov and Malicki, 2010, D'Orazi et al., 2014, Dowling, 1987, y Cajal, 1972). Owing to its intricate organization, the retina can rapidly and efficiently convert light into electric signals, which travel through the optic nerve to reach visual centers in the brain. The retina is a part of the central nervous system that presents a unique model to study mechanisms of neural circuit formation. In different brain regions, examining mechanisms of neuronal wiring is an intimidating task due to the heterogeneity and complexity of its neural circuits. On the other hand, the retina is assembled into a relatively simple architecture with known types of neurons, which can be easily manipulated. In addition, the retina is anatomically separated from the brain during early embryogenesis. Such accessibility facilitates the analysis of different developmental events. Most importantly, synaptic connections and cell bodies are segregated into distinct parallel layers called laminae. This feature renders the retina an excellent system to study mechanisms underlying synaptic layer assembly (Albrecht et al., 2020, Avanesov and Malicki, 2010).

1.1 Laminar structure of the vertebrate retina

The vertebrate retina is comprised of six major classes of neurons which are separated into three cellular layers with two synaptic or plexiform layers in between (**Figure** 1.1 **A**). At the apical side, the outer plexiform layer (OPL) harbors synapses that transmit input from photoreceptors (PRs) in the outer nuclear layer (ONL) to bipolar (BPs) and horizontal cells (HCs) in the inner nuclear layer (INL). On the other hand, the inner plexiform layer (IPL) is considered the processing hub of the inner retina. It is densely packed with synaptic connections formed between BPs

and amacrine cells (ACs) in the INL and retinal ganglion cells (RGCs) in the ganglion cell layer (GCL) at the basal side of the retina. Synaptic connections within the IPL are further distributed into different sublaminae grouped in two structurally and functionally distinct groups; the inner and outer IPL, which receive synaptic connections from ON and OFF BPs, respectively. The retina contains one type of glial cells called Müller glia (MGs) which span the apico-basal axis of the retina (Hoon et al., 2014, Huberman et al., 2010). The laminar anatomy of the neural retina is often referred to as "retinal lamination", and it is a highly conserved feature among vertebrates **(Figure** 1.1 **B).**

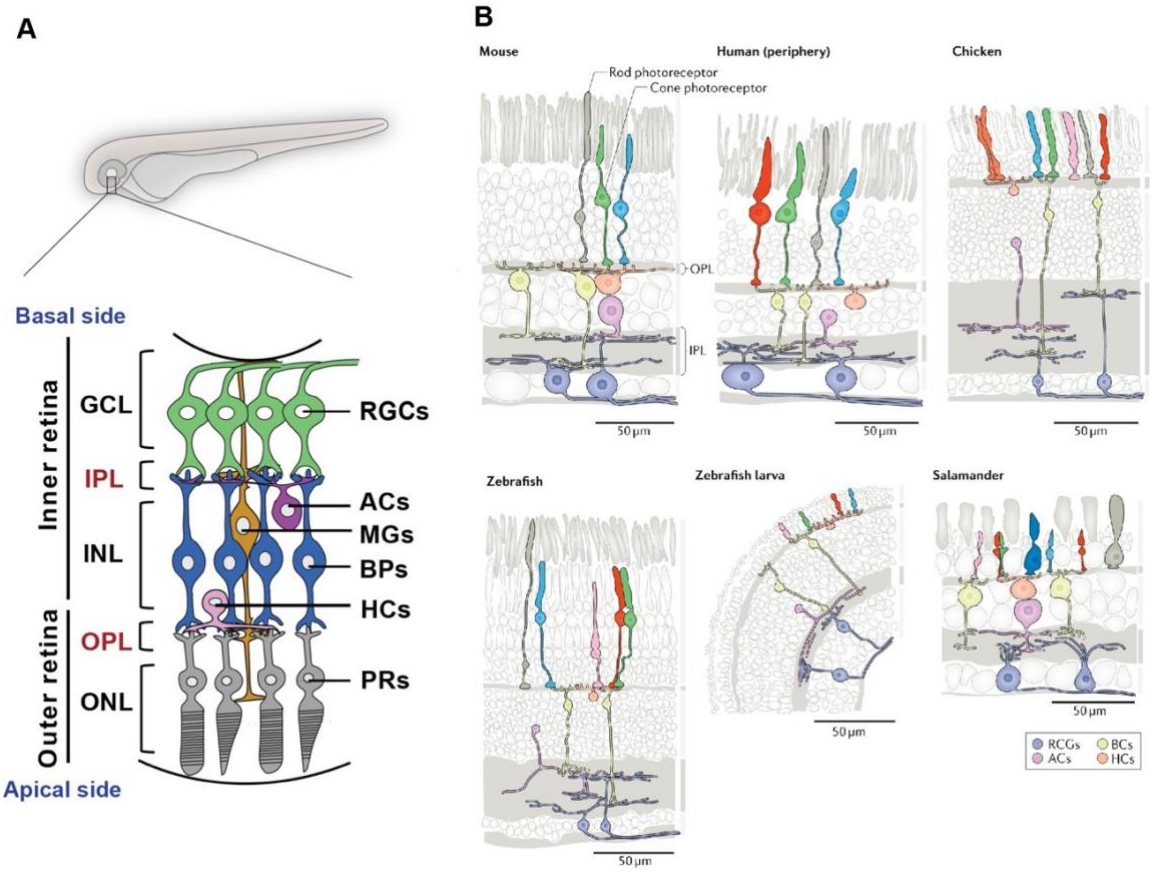

Figure 1.1. Laminar structure of the vertebrate retina.

(A) Zebrafish retinal neural circuit showing different retinal neurons and synaptic layers. (B) The laminar anatomy of the retina is conserved among vertebrates (adapted from (Baden et al., 2020)).

1.2 Lamination is a hallmark of the nervous system

The clustering of synapses with similar properties into distinct synaptic neuropils is a characteristic feature of many brain areas, like the neocortex, hippocampus, and cerebellum (Amini et al., 2018, Baier, 2013). Although the exact purpose of neuronal layering is not fully known, there have been several models that explain the function of lamination in the nervous system. The "wiring economy" or "wiring optimization" model is among the popular models, in which the wiring cost

becomes higher when the distance between connecting neurons increases. The wiring cost refers to metabolic requirements, cellular material needed or time of signal conductance (Chklovskii and Koulakov, 2004, Di Donato, 2016). This model can explain the compressed retinal anatomy to avoid scattering of light passing to the retina. In addition, parallel processing allows fast transmission of visual signals through retinal tissue (Amini et al., 2018, Hoon et al., 2014, Nassi and Callaway, 2009). Another model proposes that lamination ensures the fast assembly of functional neuronal circuits. In zebrafish astray mutants, disrupted lamination in the optic tectum leads to a delay in the assembly of direction-selective neural circuits. However, the functionality of these circuits is achieved eventually (Nikolaou and Meyer, 2015).

Perturbations in retinal lamination could compromise visual processing. Therefore, it is important to examine which developmental programs and molecular mechanisms play a role in establishing retinal lamination. Over the past decades, zebrafish has proven itself to be a valuable model to study such mechanisms owning to its many advantages; external embryogenesis, ease of genetic manipulation, transparency of embryos which provides high resolution *in vivo* imaging, and most importantly, fast development of the visual system (Fadool and Dowling, 2008). To identify important molecules in retinal lamination, we need to first understand the developmental steps involved in this process.

1.3 Developmental steps of retinal lamination

Three main events are required for precise formation of retinal layers: First, neurogenesis of different retinal cell types at specific developmental time frames. Second, neuronal migration of different cell types to designated areas in the developing retinal tissue. Third, neurite outgrowth to connect with synaptic partners (Amini et al., 2018). These events do not occur in a sequential manner, but rather in overlapping timeframes. There is a great deal of consistency in the order of these events among different vertebrate models (Fadool and Dowling, 2008, Richardson et al., 2017). However, they vary in the timeline, ranging from several hours as in zebrafish to days as in the mouse model. Next, the three developmental events underlying retinal morphogenesis will be described in detail, relying mainly on published studies from the zebrafish model.

1.3.1. Neurogenesis

In zebrafish, the eyes develop from bilateral thickenings called optic lobes that evaginate from the forebrain (Malicki et al., 2003, Schmitt and Dowling, 1994). By 22 hours post fertilization (hpf), an optic cup is formed with an inner layer that later develops into the neural retina, while the outer layer becomes the retinal pigmented epithelium. Prior to neurogenesis, the optic cup consists of a single sheet of pseudostratified neuroepithelium at around 24 hpf (Schmitt and Dowling, 1994). Shortly afterwards, the retina undergoes dynamic changes in the cell cycle and expression patterns of several genes to induce cell cycle exit, retinal cells become post mitotic and differentiate. One of the important regulators of neurogenesis is

the *atonal bHLH transcription factor 7* gene, known as *ath5* (the zebrafish homologue of mammalian *Math5*). Ath5 expression starts right before the onset of neurogenesis in a wave-like pattern spreading from the ventronasal patch onwards, such expression was found to play a central role in RGC genesis (Kay et al., 2001, Masai et al., 2000).

RGCs are the first cell types to differentiate at around 27 to 28 hpf, they are the only output neurons of the retina, which project their axons through the optic nerve to the visual centers of the optic tectum (OT), known as superior colliculus in the mammalian visual system. Shortly afterwards, from around 35 to 48 hpf, amacrine and horizontal cell precursors become post mitotic (Hu and Easter Jr, 1999). Both cell types are inhibitory interneurons, horizontal cells reside in apical side of the INL making synaptic connections with rod and cone photoreceptors while amacrine cells are mainly located facing the IPL to make synaptic connections with both ganglion and bipolar cells (Jusuf and Harris, 2009).

Rod and cone photoreceptors start to exit cell cycle at around 43-48 hpf following amacrine and horizontal cell genesis. Although both cell types differentiate in overlapping time frames, cones mature relatively faster that rods (Perkins and Fadool, 2010). Bipolar cell genesis occurs relatively late at around 60 hpf (Schmitt and Dowling, 1994), starting before the retinal neuroepithelium is fully laminated while the last-born cohorts are generated after lamination is established. Bipolar cells are the only retinal cell types that make synaptic connections in both the IPL and OPL as they serve to transmit visual information from photoreceptors to RGCs (Engerer et al., 2017). There are two types of bipolar cells which differ in their response to light stimuli; OFF bipolar cells stratify the outer IPL and they are hyperpolarized by light while ON bipolar cells are depolarized by light and elaborate their arbors in the inner IPL (Connaughton, 2011).

Müller glia cells are the only glia cells in the retina and among the last cells to be generated at around 48 hpf (MacDonald et al., 2015). It is worth mentioning that neurogenesis in the retina continues post embryonically through a small population of retinal stem cells residing at the interface between ciliary epithelium and retina, termed ciliary marginal zone (CMZ) (Raymond et al., 2006). By contrast, apoptosis occurs naturally during retinal development in a series of waves starting with RGCs and ending with photoreceptors. It is thought to function in tuning the retinal network during and after neurogenesis (Biehlmaier et al., 2001).

1.3.2. Neuronal migration

Neurogenesis normally occurs at the apical surface of the retinal neuroepithelium. Subsequent migration of different cell types to their final position is a critical step for constructing a laminar structure. In the retina, radial migration is the most common mode of migration along the apico-basal axis. For example, recent studies on RGCs show that they translocate their soma to basal areas through its basal-apical processes, after then, their apical process is lost. They postulate that this process depends largely on stabilized microtubule dynamics (Icha et al., 2016).

Studies on amacrine and horizontal cell precursors display interesting migration patterns, they both utilize bipolar processes to translocate from apical side to central retina. Afterwards, they both lose the apical process and translocate via tangential migration where amacrine cells migrate deeply in the INL while horizontal precursors return to their final positions in the apical side (Chow et al., 2015). Photoreceptors are born apically from precursor cells and reside in the most apical side of the retina. Therefore, it is expected that they don't need much translocation. However, there are some evidence that precursors of L-cones can be detected in basal areas of the retina before migrating apically for cell division (Suzuki et al., 2013). As for bipolar cells, our information is limited on how these cell types migrate to their destined positions in the INL.

1.3.3. Neurite outgrowth and formation of plexiform layers

The last step to achieve successful lamination of the retina is the elaboration of neurite arbors to make synaptic connections in destined plexiform layers. Several studies suggest that both cell migration and neurite extension can occur at overlapping time frames, as in the case of amacrine cells. Elegant time-lapse experiments demonstrate that during the events of amacrine cell migration, random neurites are extended that later become more directed to form a presumed plexus (Godinho et al., 2005). Most amacrine cells reside in the INL, and they are commonly referred to as inhibitory amacrines or iACs. However, a small population resides in the GCL and known as displaced amacrines (dACs). Initial observations proposed that at earlier stages, inhibitory amacrines are located apically, while displaced amacrines are located basally, and later with development, amacrine cells project dendritic plexus that emerges between the two different cell types separating them into different layers (Godinho et al., 2005). However, later time-lapse studies proposed a different sequence of events, where displaced amacrines initially reside in the INL and they translocate their soma through the nascent IPL, eventually leading to a shift in their dendritic polarity (Chow et al., 2015).

Time-lapse imaging of RGC dendritic patterning in zebrafish revealed that this process is highly dynamic. At earlier stages, RGCs exhibit exuberant and exploratory dendritic tips which become more stabilized later on, as lamination is established (Mumm et al., 2006). Surprisingly, although RGCs are born before their partners, amacrine cells, their dendrites target and stratify previously laminated amacrine cell plexus, which likely suggests that amacrine cells provide laminar cues for RGC dendritic stratification within the IPL.

Time-lapse imaging experiments in zebrafish show that during retinal ganglion cell migration to the basal side, after the apical migratory processes are lost, axons emerge from rudiments of the basal processes (Poggi et al., 2005, Yoshimatsu et al., 2013). It is also thought that this axonogenesis precedes the formation of dendritic arbors. Although RGC axons don't contribute to retinal lamination. They play a crucial role in the retinal circuit assembly by transmitting visual signals through the optic nerve to reach visual centers in the brain. Initial axons of RGCs exit the eyecup at around 32 hpf and reach the optic chiasm between 34 and 36 hpf (Burrill and Easter Jr, 1994, Stuermer, 1988). At 44-48 hpf , RGC axons

start to arborize the optic tectum, and by 72 hpf, retinotectal projections are completed by stratifying in 10 different arborization fields termed AF1-AF10 (**Figure** 1.2). Around the same time, the first visual-evoked and electroretinographic responses are recorded (Fadool and Dowling, 2008)

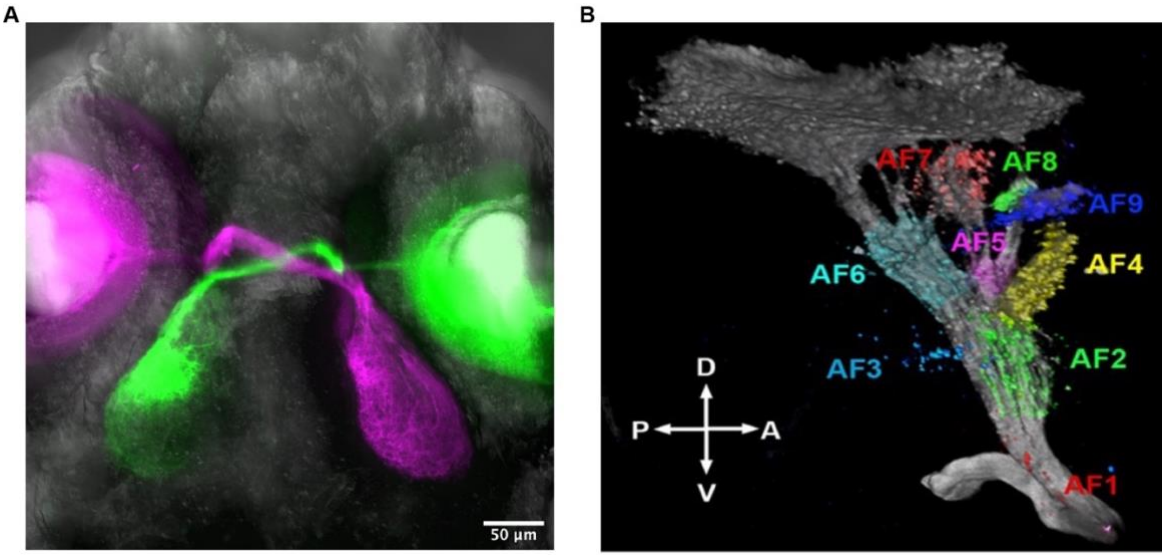

Figure 1.2. Projections of RGC axons in zebrafish visual system.

(A) Dorsal view of retinotectal projections in zebrafish at 4 dpf. (B) Medial view of zebrafish retinotectal projections showing the different arborization fields (AF1-AF10) (Robles et al., 2014).

In vertebrate retina, OPL formation follows the establishment of the IPL which occurs within hours in zebrafish. This process is mainly contributed by horizontal cells elaborating their dendrites to make connections with photoreceptors (Morris and Fadool, 2005). Bipolar cells are the last to stratify in the forming IPL and OPL. Data from mouse and zebrafish models suggest that bipolar cells develop axons and dendrites that were inherited from apical and basal neuroepithelial-like processes rather than de novo extension from the cell body (Chow et al., 2015, Morgan et al., 2006, Randlett et al., 2013). Interesting, although terminal differentiation of bipolar cells, determined by bipolar-specific markers, happens at later stages, time-lapse imaging in zebrafish and mouse models suggests that bipolars/their precursors retract their basal processes to form an axon and stratify the nascent IPL at similar time frames to those of amacrine cells and RGCs (Randlett et al., 2013). Photoreceptor synaptic terminals become distinguishable by light and electron microscopy beginning at about 62 hpf, around the same time when the retina has become fully laminated (Morris and Fadool, 2005). **Figure** 1.3 illustrates the different developmental events that establish a laminated zebrafish retina.

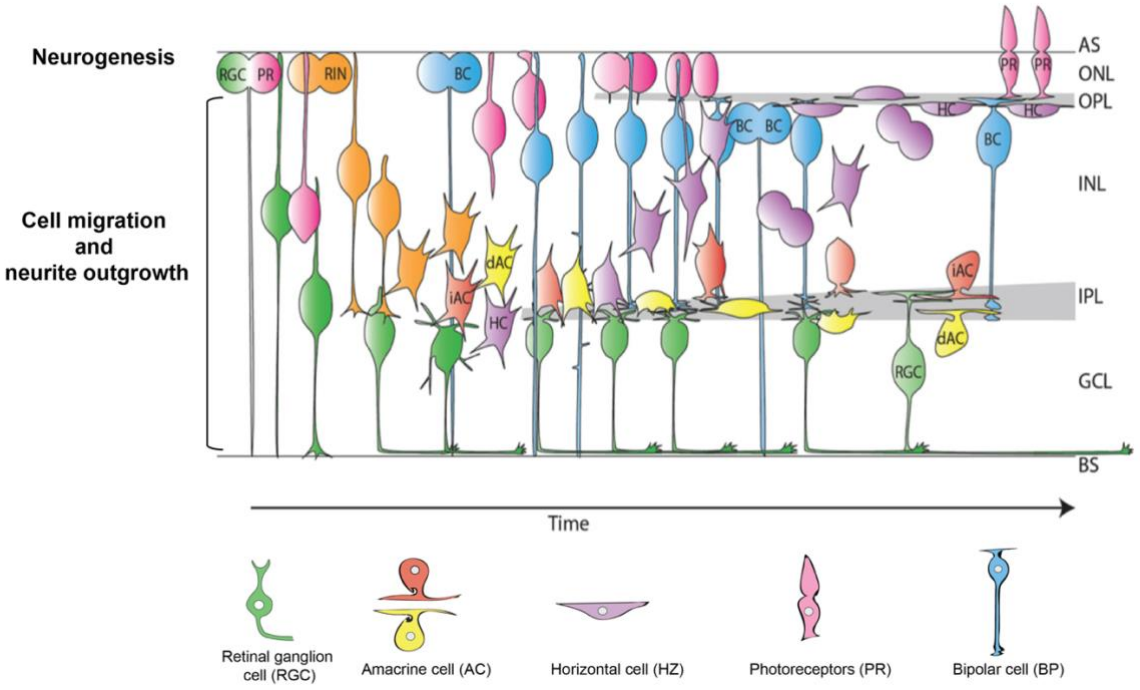

Figure 1.3. Summary of developmental events underlying retinal lamination in zebrafish.

Neurogenesis occurs at the apical side of the retina, followed by cell migration to destined layers and neurite extension to reach synaptic partners. RIN: retinal inhibitory neurons, AS: apical side, BS: basal side, ONL: outer nuclear layer, OPL: outer plexiform layer, INL: inner nuclear layer, IPL: inner plexiform layer, GCL: ganglion cell layer. Figure is adapted from (Chow et al., 2015).

1.4 Molecular mechanisms underlying retinal lamination

It is easy to understand that perturbations in any of the steps involved in retinal development would disrupt lamination. Therefore, there have been tremendous efforts using the zebrafish and mouse models to decipher the molecular cues that regulate this intricate process. Major cell polarity regulators like Stardust/Crumbs and Par3/Par6/atypical protein kinase C (aPKC) are among the well-established key players in retinal lamination. Stardust/Crumbs complex maintains the apico-basal cell polarity of the retinal neuroepithelium. Since the final mitosis linked to neurogenesis occurs at the apical surface of the neuroepithelium, defects in cell polarity cause mispositioning of mitotic cells, leading to severe disorganized retinal layers as observed in zebrafish mutants like *nagie oko (nok), oko meduzy (ome),* and *mosaic eyes (moe)* mutants (Jensen and Westerfield, 2004, Omori and Malicki, 2006, Wei and Malicki, 2002). In fact, mutations in CRB1 (the human Crumbs1 homologue) are associated with inherited retinal diseases in humans like Leber's congenital amaurosis (LCA) and retinitis pigmentosa. In addition, retinal lamination defects are observed in LCA patients with CRB1 mutations (Jacobson et al., 2003, Richard et al., 2006).

The Par3/Par6/atypical protein kinase C (aPKC) is an essential polarity regulator across different species and in many biological contexts. It localizes to the membrane apical domains and preserves their apical identity. In zebrafish, aPKCλ

maintains adherens junctions (AJs) at the apical side of retina. Therefore, in aPKCλ mutants called *heart and soul (has),* adherens junctions collapse leading to the detachment of mitotic cells from the ventricular zone of the neural retina, which causes severe retinal layering defects (Horne-Badovinac et al., 2001, Ohno, 2001). Similarly, loss of aPKCλ in differentiating photoreceptors of the mammalian retina leads to lamination defects throughout the retina, which could be attributed to disruption of adherens junctions between photoreceptors and retinal progenitors (Koike et al., 2005).

Maintenance of adherens junctions at the apical side of retinal neuroepithelium also requires the cell adhesion molecule, N-cadherin. Therefore, in zebrafish *n-cadherin* mutants (*ncad/parachute*), although retinal cell fate specification occurs normally, mitotic cells detach from the apical surface, similar to aPKCλ mutants, causing lamination phenotypes with scattered rosettes of plexiform layers (Malicki et al., 2003, Masai et al., 2003).

Substantial evidence suggests the importance of extracellular matrix components in retinal lamination and visual system development, possibly by offering a laminar positional code. One excellent example is the reelin signaling pathway. It was previously found, in two mouse knockout mutants of the pathway, reeler and scrambler, that retinal interneurons aberrantly stratify the IPL causing perturbations in retinal synaptic connectivity (Rice et al., 2001). Recently, a reelin gradient in the zebrafish tectal neuropil was found to act as a chemoattractant for the laminar targeting of RGC axons (Di Donato et al., 2018).

Semaphorins are transmembrane repulsive proteins that are known to regulate lamination in the inner retina. In the mouse retina, Semaphorins (Sema5A and Sema5B) are expressed in the outer neuroblastic layer, and they direct neurites of inner retinal neurons away from the OPL to stratify into their destined areas in the IPL. This mechanism is probably mediated through their receptors, PlexinA1 and PlexinA3. Therefore, in Sema5A/B double knockout mice, inner retinal neurons exhibit dendritic mistargeting to the outer retina, leading to inner retinal lamination defects (Matsuoka et al., 2011a). On the other hand, Sema6A is another type of Semaphorins that regulates sublamination within the IPL. Sema6A is expressed in the ON sublaminae while its receptor PlexinA4 is expressed in the OFF sublaminae. This expression restricts subsets of inner retinal neurons to the OFF sublaminae. Consequently, mice with null mutation in PlexA4 or Sema6A show aberrant dendritic stratification of subclasses of amacrine cells and RGCs within ON and OFF sublaminae of the IPL (Matsuoka et al., 2011b).

Studies on the chick retina have shed the light on the importance of the cell adhesion molecules Sidekicks (Sdk-1, Sdk-2) and Down syndrome cell adhesion molecules (Dscam and DscamL) in sublaminar targeting within the IPL through homophilic adhesion (Yamagata and Sanes, 2008, Yamagata et al., 2002). These molecules are expressed in subsets of RGCs and their presynaptic partners, and they concentrate within different IPL sublaminae. Yamagata and Sanes found that cells which project to the same sublaminae tend to express the same cell adhesion molecule. Consequently, in absence of these cell adhesion molecules, laminar patterning in the IPL is disrupted.

1.5 Zebrafish *strip1* mutant shows unique retinal lamination defects

A large-scale mutagenesis study was previously conducted by introducing random mutations in RIKEN wild-type male gametes using N-ethyl-N-nitrosourea. Mutants with defects in retinal development were isolated based on anti-acetylated α tubulin labeling (Masai et al., 2003). *RIKEN WAKO 147 (rw147*) was initially isolated based on defects in retinal layering (Ahmed et al., 2021). Morphologically, *rw147* mutant embryos have small eyes, lower jaw atrophy and cardiac edema at 4 days post-fertilization (dpf) (**Figure** 1.4 **A**). Histological examination of *rw147* retinal sections revealed an interesting retinal lamination defect; retinal layers appear to form in correct order; however, lamination is not uniform presenting in a wave-like pattern (**Figure** 1.4 **B**). This lamination defect appears more prominent in the IPL, compared to the OPL. The *rw147* mutation is lethal by 6 dpf due to cardiac edema. Mutation mapping assays using simple sequence length polymorphism (SSLP) markers, mapped the mutation to a region in chromosome no. 22, where only one protein coding gene exists, *striatin-interacting protein 1* or *strip1*. Subsequent sequencing confirmed the presence of a mis-sense mutation in *strip1* gene of *rw147* mutant located in exon no. 7 resulting in an amino acid change Leu195 to Arg (GenBank Accession Number NP_998686.2) (**Figure** 1.4 **C**).

Strip1, previously known as FAM40A, is a highly conserved protein with 208 different orthologues from yeast to humans. Zebrafish Strip1 holds 83% similarity to human STRIP1 at the protein level and 72% transcript homology. As for protein structure, zebrafish Strip1 protein has two conserved domains, N1221 and DUF3402 (**Figure** 1.5). However, The biological function of both domains is yet to be defined (Shi et al., 2016). Collectively, Strip1 could play important conserved roles among vertebrates. Zebrafish Strip1 has one paralogue, Strip2, with 69% homology to Strip1. Over a decade ago, Strip1 was initially isolated as part of an evolutionarily conserved supramolecular protein complex called the striatin-interacting phosphatase and kinase (STRIPAK) complex (Goudreault et al., 2009).

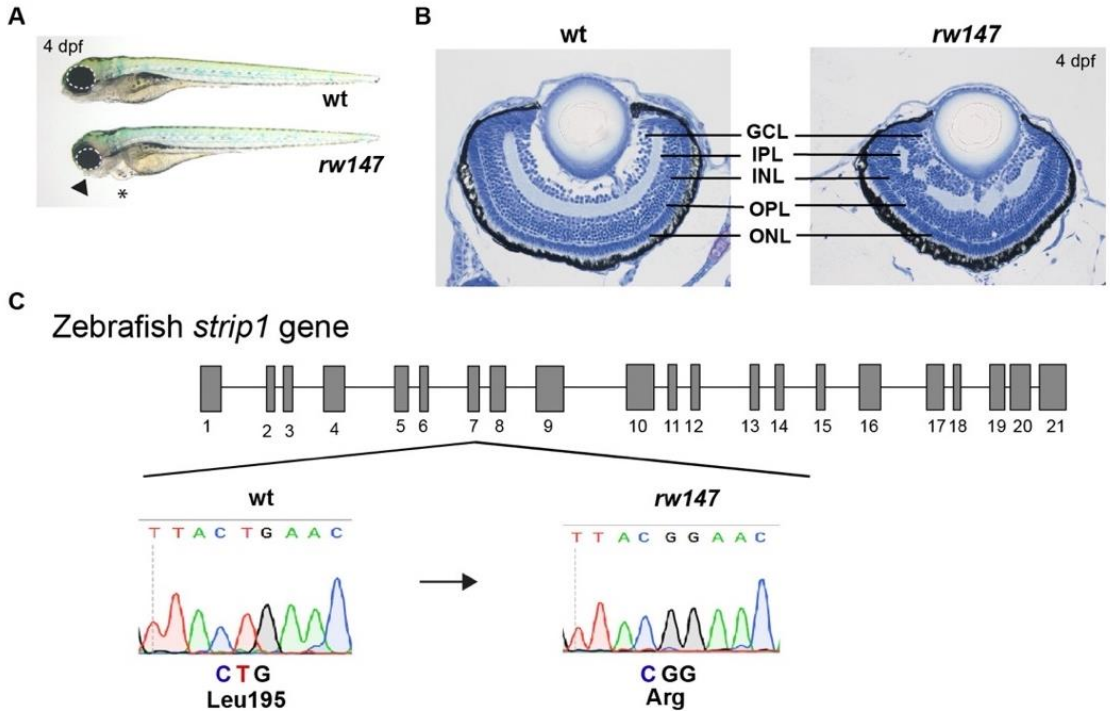

Figure 1.4. *rw147* retinal lamination mutant encodes *strip1*

(A) Morphology of wild-type and *rw147* embryos at 4 dpf. Dotted lines demarcate the eye. An arrowhead indicates abnormal lower jaw. An asterisk indicates heart edema. (B) Wild-type and *rw147* mutant retinas at 4 dpf. (C) A missense mutation occurs in *strip1* gene of *rw147* mutants.

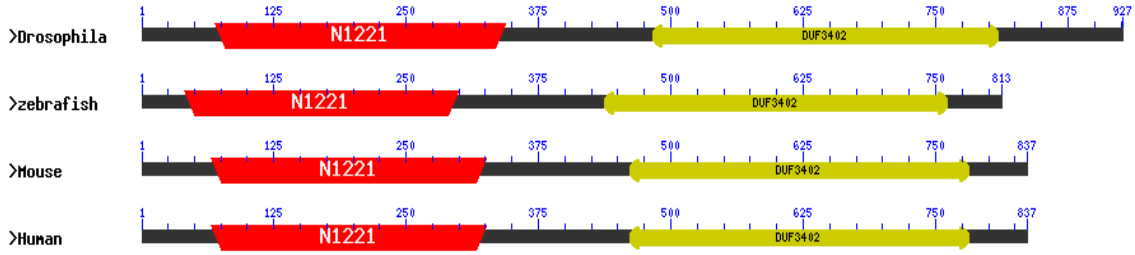

Figure 1.5. Conserved domains of Strip1 protein across species

Schematic diagram of 4 different Strip1 protein orthologues showing the conserved domains N1221 in red and DUF3402 in yellow. Figure generated using NCBI Conserved Domain Search Tool (Marchler-Bauer et al., 2014).

1.6. Strip1: A core component of STRIPAK complex

In 2009, STRIPAK complex components were identified through rigid affinity purification coupled with mass spectrometry approaches in the mammalian cell lines (Goudreault et al., 2009, Hwang and Pallas, 2014). They defined the large multiprotein assembly to consist of a set of core components; 1) serine/threonine-protein phosphatase PP2A catalytic subunit known as PP2Ac and 2) the scaffolding subunit PP2Aa together with 3) Striatin family proteins (Striatin known as STRN, Striatin3 known as STRN3/ SG2NA and Striatin4 known as STRN4 or Zinedin) which function as the regulatory B subunits. Striatins associate with three more core

components; 4) Monopolar spindle-one -binder family 3 or Mob3, 5) STRIP1/2, hence the name striatin-interacting proteins and 6) the cerebral cavernous malformation 3 (CCM3) protein. Ccm3 in turn is the binding partner that links the germinal center kinase III (GSKIII) family of Ste20 kinases and STRIPAK components. In addition to the core components, STRIPAK can make mutually exclusive interactions with either the cortactin binding proteins (CTTNBP2/CTTNBP2NL) or through the assembly of another subcomplex of sarcolemmal membrane-associated protein (SLMAP) and the close members; suppressor of IKKε (SIKE)/fibroblast growth factor receptor 1 oncogene protein 2 (FGFR1OP2). **Figure** 1.6 summarizes different STRIPAK complex components.

Members of the STRIPAK complex were found to organize in diverse signaling complexes regulating multiple cellular processes like cell cycle, apoptosis, cell migration, cell polarity, and vesicular transport in different tissues and organisms (Chen et al., 2018a, Fidalgo et al., 2010, Hwang and Pallas, 2014, La Marca et al., 2019, Neisch et al., 2017, Rodriguez-Cupello et al., 2020). Consequently, disruption of the different components of the complex by themselves or in the context of the STRIPAK complex has been implicated in many pathological conditions, including cancer progression and tumorigenesis, heart disease, diabetes, and autism (Cheung et al., 2001, Ding et al., 2005, Madsen et al., 2015, Nader et al., 2012)

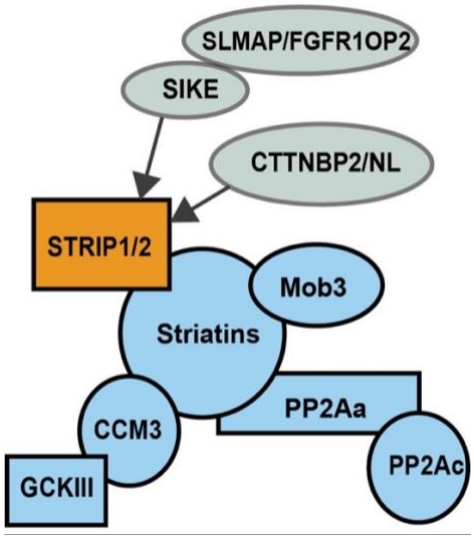

Figure 1.6. Components of mammalian STRIPAK complex.

Schematic diagram showing the core components of the mammalian STRIPAK complex and some of its accessory molecules. Core STRIPAK components include PP2Ac and PP2Aa, together with striatins (STRN, STRN3 and STRN4), Mob3, STRIP1 or STRIP2, and a germinal center kinase GCKIII bound via Ccm3. Some molecules bind in a mutually exclusive pattern to the core components. Arrows show that SLMAP and SIKE are not detected in STRIPAK complexes containing CTTNBP2/ CTTNBP2NLand vice versa. (Figure adapted from (Hwang and Pallas, 2014)).

Many studies have shown the importance of different components of STRIPAK complex in neuronal development. Striatin is abundantly expressed in the brain striatum and motor neurons. Within neurons, it has somato-dendritic localization in dendritic spines. In the absence of Striatin, dendritic growth is

perturbed, suggesting a role of Striatin in dendritic development (Bartoli et al., 1999, Li et al., 2018). Interestingly, other striatins like Zinedin and SG2NA, also localize in somato-dendritic areas with high expression in dendritic spines (Benoist et al., 2006). DMob4 (the Drosophila homologue of Mob3) was also found to localize in dendritic spines and plays an important role in synaptic assembly, axonal transport and stabilization of microtubules (Schulte et al., 2010). Similarly, CTTNBP2 localizes in dendritic spines and is proposed to regulate spine density (Chen et al., 2012).

1.7. Strip1: Emerging roles in embryonic morphogenesis

Over the past decade, several studies have provided valuable insights on the importance of Strip1 in several aspects of embryonic morphogenesis, including neuronal development. Strip1 is proposed to act as an adaptor molecule that gets recruited in multiple protein complexes, independently or in the context of the STRIPAK complex, to elicit diverse physiological functions. In this section, I will discuss the recent body of literature, from *Drosophila* and mouse models, on Strip1 function in development and the proposed molecular signaling involved.

1.7.1. Mesoderm migration

In mouse, STRIP1 is essential for mesoderm migration during gastrulation (Bazzi et al., 2017). Therefore, a missense mutation in *Strip1* causes developmental arrest at midgestation due to failure in mesoderm migration and elongation across the anterior-posterior axis. Upon culturing mesoderm explants *in vitro*, cells were compact with abnormal focal adhesions and defects in cell migration, which might be attributed to distinct enrichment of cortical filamentous actin (F-actin) (Bazzi et al., 2017). These findings are supported by *in vitro* studies, which showed that upon knockdown of Strip1 in PC3 cell line, cells became flatter with decreased cell spreading and increased F-actin in cell periphery (Bai et al., 2011).

1.7.2. Neuronal morphogenesis

In *Drosophila*, Strip (a homolog of mammalian Strip1/2) is required for axon elongation by regulating early endosome trafficking (Sakuma et al., 2014). Membrane trafficking functions in the transport of organelles and materials along the axon and it is required for elongation and guidance of neurites (Flynn et al., 2013). Retrograde axonal transport is particularly useful in the recycling of cargos from axon terminals back to the cell body, and early endosome clustering plays a critical step in this process. Two important molecules in this process are; Rab5 for targeting of early endosome to microtubules and dynein motor protein complex for translocation of cargos across microtubules (Jovic et al., 2010). Strip was reported to play a part in this process by acting as a molecular platform for early endosome organization. In a yeast two-hybrid screen, Glued (homologue of human and zebrafish Dynactin1) was found to be a Strip-binding partner. Dynactin1 is a major component of the dynactin/dynein complex where it binds to both dynein and microtubules. Sprint was also identified as a Strip-interacting molecule and it is

known to activate Rab5. Thus, authors propose that Strip functions as an adaptor molecule, which links Rab5/early endosomes with Dynactin complex for efficient clustering of early endosomes on microtubules. Subsequently, in *strip* mutants, this link is abolished leading to axon elongation defects of Drosophila olfactory projection neurons (PNs). Rab5 mutant displayed similar axon elongation defects and the phenotype was partially rescued by the expression of Rab5 constitutive active form. The function of Strip in axon elongation of PNs is proposed to be independent of the STRIPAK complex because PNs with disrupted Connector of kinase to AP-1 (Cka, Drosophila homologue for Striatins) do not exhibit axon elongation defects (Sakuma et al., 2014).

In addition to its role in early endosome trafficking, Strip is proposed to regulate neurite development and synaptogenesis by modulating cytoskeletal dynamics. Remodeling of cytoskeletal elements like actin, microtubules and intermediate filaments is essential for neuronal polarization, migration, and neurite extension (Flynn et al., 2013). *Drosophila* Strip is proposed to promote axon elongation by localizing with microtubules and stabilizing them. This role is mediated through the physical and genetic interaction of Strip with Dscam and Tubulin folding cofactor D (TBCD), an important molecule in the assembly of α and β tubulin heterodimers (Sakuma et al., 2015). A genetic interaction previously established between TBCD and Dscam was found important in *Drosophila* neurite development (Okumura et al., 2015). Collectively, these reports suggest that this tripartite Strip-TBCD-Dscam complex stabilizes microtubules, which is important for projection neuron elongation.

Strip is proposed to regulate synaptogenesis through its function in actin organization. F-actin is required for neurite extension at the growth cones by controlling microtubule advance (Flynn et al., 2013). Strip was found, together with other molecules of STRIPAK complex, to play an important role in synaptic bouton organization at the neuromuscular junction (NMJ) (Sakuma et al., 2016). In absence of strip, excessive formation of NJM boutons is observed. The molecular signaling linked to this role is the Hippo pathway. Authors demonstrate that endogenous Strip genetically and physically interacts with hippo kinase cassette (Hpo) leading to its inactivation and in turn, increase the expression of the active form of Enabled (Ena), a hippo downstream target. In absence of Strip, Hpo is activated (phosphorylated), this subsequently inactivates Ena. Eventually, inactivation of Ena activates Arp2/3, a molecule known to control actin organization and responsible for actin branching (Spence et al., 2016). Therefore, the absence of Strip leads to excessive actin branching and synaptic bouton formation. **Figure** 1.7 summarizes the molecules reported to interact with Strip1 to promote neuronal morphogenesis.

1.7.3. Cell proliferation and differentiation

Two stem cell niches exist in the *Drosophila* testis to regulate spermatogenesis; somatic stem cells that encapsulate germline stem cells. Recently, studies on *Drosophila* Strip have shed the light on its function in spermatogenesis in L3 male gonads (La Marca et al., 2019). In absence of Strip, differentiation of cells from both somatic and germline lineages is disrupted, and germline cells undergo excessive

and ectopic proliferation. Mechanistically, under physiological conditions, Strip interacts with Cka to suppress TNF-JNK during spermatogenesis, which is essential for proper somatic cell differentiation and morphology.

1.7.4. Cell fate specification

During the development of *Drosophila* compound eye, cells on one side of the progenitor epithelium adopt a retinal fate, while cells in the opposite side adopt the peripodial epithelium (PE) fate. Strip, together with other components of STRIPAK complex (Cka and SLMAP), were found to regulate the retina-PE cell fate specification. (Neal et al., 2020). Disruption of Strip/Cka leads to ectopic retina formation within presumed PE. Authors propose that STRIPAK-PP2A suppress Hippo signaling to suppress ectopic retinal phenotypes.

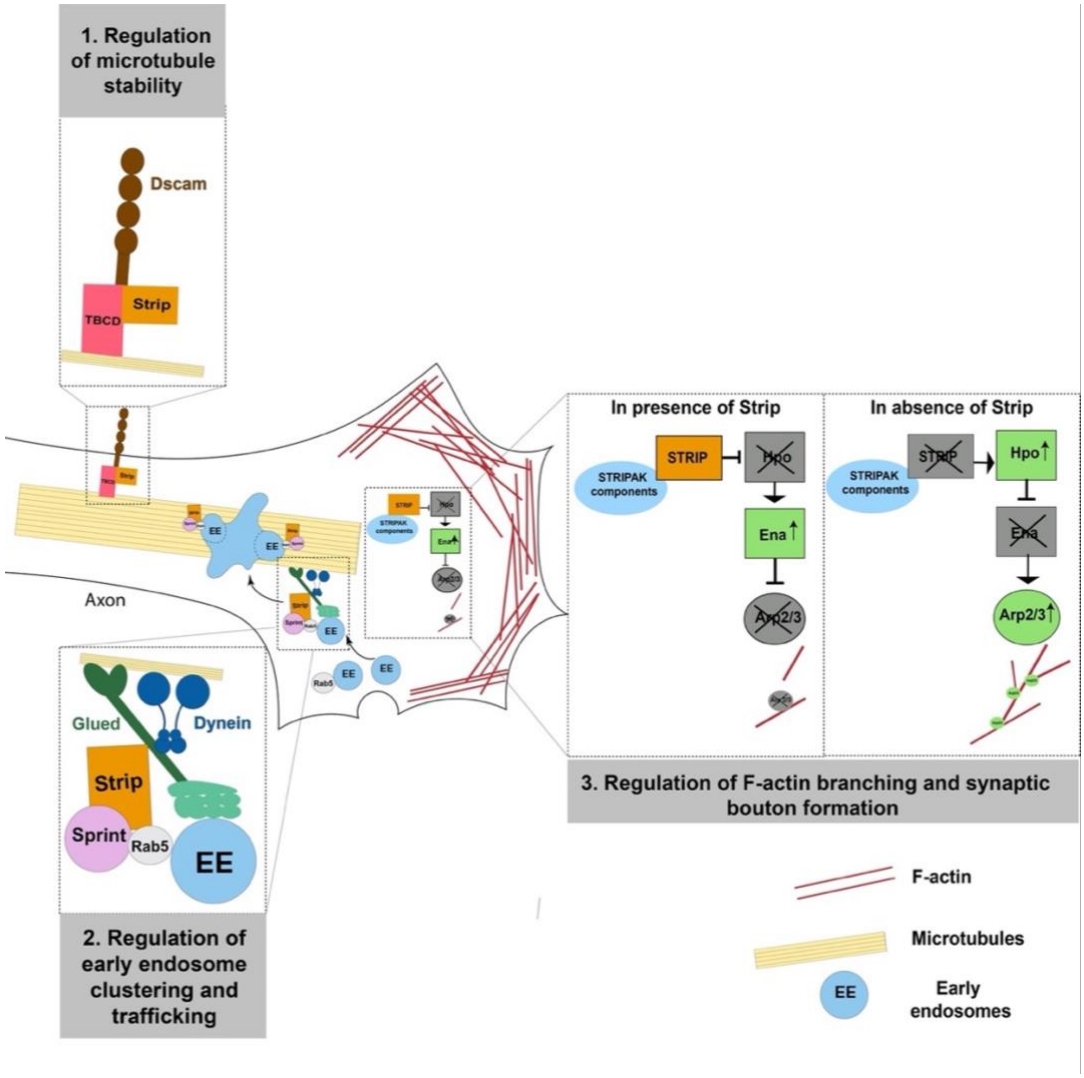

Figure 1.7. Summary of Strip-interacting partners to promote neuronal development.

Adapted from (Goudreault et al., 2009, Hwang and Pallas, 2014, Sakuma et al., 2014, Sakuma et al., 2015, Sakuma et al., 2016).

1.8. Aim and structure of the thesis

Lamination of the vertebrate retina is critical to efficiently process visual signals. To establish retinal lamination, neurogenesis, cell migration, and neurite extension must be tightly regulated, both spatially and temporally. Any defect in these events can disrupt retinal wiring and consequently compromise visual function. However, the molecular mechanisms that govern retinal neural circuit formation are not fully understood. Previous preliminary histological analysis of zebrafish *strip1* mutant retina suggested its possible function in retinal lamination. However, the function of Strip1 in vertebrate nervous system development remains elusive, owing to the embryonic lethality of mouse Strip1 knockout models.

The overall aim of this work was to **investigate the physiological role of zebrafish Strip1 in retinal neural circuit formation, at both the cellular and molecular levels**. This thesis is structured into two main parts, which discuss two different objectives I set to fulfill this aim:

a. **Phenotypic characterization of Strip1 function in retinal development**

   In **Chapter 2,** I will discuss the phenotypic study I conducted on the novel zebrafish *strip1* mutant, *rw147,* to examine Strip1 function. Using transient and stable transgenic tools coupled with live imaging, histochemical assays, and cell transplantation experiments, I investigated which cell types and developmental events are perturbed in absence of Strip1.

b. **Investigate the molecular signaling involved in Strip1 function in retinal development**

   At the biochemical level, I performed proteomic approaches to identify Strip1-interacting partners and transcriptome analysis to identify the signaling pathways affected by loss of Strip1, this part shall be described in detail in **Chapter 3.**

In **Chapter 4,** I will provide a brief conclusion of the main findings of this work and the model I propose on how Strip1 functions in the developing vertebrate retina. Finally, I will provide a brief outlook on future work that is expected to stem from this study.

Chapter 2.

Strip1 is essential for inner retina development

The retinal IPL is considered the synaptic highway of the inner retina, it is organized into different sublaminae that house multiple visual circuits established between processes of RGCs, amacrine, and bipolar cells. Therefore, the IPL is considered the perfect system to study how synaptic neuropils are formed. Moreover, understanding the mechanisms that underlie IPL development is necessary to determine how functional connections are established in the inner retina. Previous preliminary work in the Masai unit has identified Strip1 as a candidate molecule essential for retinal layered architecture. Zebrafish *strip1* mutants, *rw147,* show interesting lamination defects, which seemed more severe in the inner retina. In this chapter, I will provide a brief background on our current understanding of how the IPL is established. Afterwards, I will describe the different approaches I took and the findings I obtained that describe Strip1 as a new key player in IPL development.

2.1. Background

Over the past decades, our knowledge on the mechanisms that orchestrate inner retinal circuit development has been tremendously enriched. *In vivo* imaging studies using the zebrafish model have eloquently described the developmental events that underlie IPL formation (Chow et al., 2015, Godinho et al., 2005, Mumm et al., 2006). As we previously described, several molecular mechanisms involving extracellular matrix proteins, cell adhesion, and apico-basal cell polarity related factors are essential for overall retinal layer formation or synaptic targeting within the IPL (Jensen and Westerfield, 2004, Masai et al., 2003, Omori and Malicki, 2006, Yamagata and Sanes, 2008). However, there are still many gaps in our understanding; which cell types contribute to IPL establishment? and what dictates the precise laminar positioning of different retinal neurons?

It is widely agreed upon that amacrine cells play the dominant role in initiating an IPL. Elegant time-lapse experiments demonstrate that amacrine cells project their neurites to form laminated plexuses immediately after they become directed towards the basal retina, suggesting that they pre-pattern the IPL (Chow

et al., 2015, Godinho et al., 2005, Huberman et al., 2010). In concert with these findings, *In vivo* imaging of RGC dendritic stratification revealed that, initially, RGCs project their initial dendrites in a "waiting zone" just below the future displaced amacrine cells. Afterwards, RGCs start to stratify their dendrites into previously established amacrine strata (Baier, 2013, Mumm et al., 2006). Consistent with these reports, when RGCs aren't born due to a mutation in *ath5* gene of *lakritz* mutant, amacrine cells still manage to establish an almost normal and laminated IPL (Kay et al., 2001). However, the role of RGCs in shaping the developing IPL cannot be simply overlooked. *In vivo* imaging of *lakritz* mutant retinas at earlier time points while the IPL is being established reveal that its development is delayed and initially disrupted, which suggests a transient requirement for RGC dendrites during IPL development to stabilize amacrine cell dendrites (Kay et al., 2004).

Müller glia and bipolar cells and born at relatively later timepoints, 48 and 60 hpf, respectively (MacDonald et al., 2015). Therefore, they are considered passive players in IPL development, compared to RGCs and amacrine cells. However, several studies propose an active role for Müller glia in retinal lamination. Retinal lamination, especially in the inner retina, is perturbed in zebrafish *mindbomb (mib*) mutants, in which Müller glia differentiation is inhibited (Bernardos et al., 2005). Recently, *in vitro* cultures of retinal organoids were found to assume a distinct laminar organization that becomes disrupted in absence of Müller glia (Eldred et al., 2017).

Interestingly, IPL development is proposed to be a robust process. Randlett *et al.* utilized genetic and pharmacological approaches to inhibit the differentiation of different cell types that contribute to IPL development, either individually or in combination. Surprisingly, in absence of any given cell type, the remaining cells manage to form an IPL-like neuropil (Randlett et al., 2013). In fact, despite the combined elimination of RGCs, amacrine cells, and Müller glia, bipolar axons still manage to form a sublaminated IPL-like neuropil at the basal side of the retina. These findings suggest that each of the inner retinal neurons can autonomously establish an IPL, in absence of remaining partners. However, the question remains still, under physiological conditions, how do inner retinal neurons communicate to establish the IPL?

2.2. Materials and methods

The resources used in the phenotypic study and their corresponding catalog numbers are listed in **Table 1**.

Table 1. List of resources used in the phenotypic study.

Name	Source or reference	Identifiers	Additional information
Mouse anti-acetylated α-tubulin	Sigma-Alrich	T6793	1:1000
Rabbit anti-Pax6	BioLegned	901301	1:500
Rabbit anti-Prox1	Genetex	GTX128354	1:500

Name	Source or reference	Identifiers	Additional information
Mouse anti-PCNA	Sigma-Aldrich	P8825	1:200
Mouse Zpr1	ZIRC	ZDB-ATB-081002-43	1:100
Mouse Zpr3	ZIRC	ZDB-ATB-081002-45	1:100
Mouse anti-glutamine synthetase	Sigma-Alrich	MAB302	1:150
Rabbit anti-Strip1	This paper	N/A	IF: 1:1000 WB: 1:500
Goat anti-rabbit Alexa 488 secondary antibody	Life Technologies	A11034	1:500
Goat anti-mouse Alexa 488 secondary antibody	Life Technologies	A11029	1:500
Goat anti-mouse Alexa 546 secondary antibody	Life Technologies	A11030	1:500
Goat anti-mouse Alexa 647 secondary antibody	Life Technologies	A21236	1:500
Anti-rabbit IgG, HRP-linked Antibody	Cell Signaling	7074	1:5000
Rabbit anti β-actin	Abcam	AB8227	1:5000
Cas9 protein	FASMAC	GE-006-S	
JB-4® Embedding Kit	Polysciences	00226-1	
In Situ Cell Death Detection Kit, TMR Red	Roche	12156792910	
In Situ Cell Death Detection Kit, Fluorescein	Roche	11684795910	
DIG RNA Labeling Kit	Roche	11277073910	
Acridine Orange (AO)	Nacalai tesque	1B-307	
CellTrace™ BODIPY™ TR Methyl Ester	Thermo Fisher Scientific	C34556	
Ethyl-3-aminobenzoate de methanesulfonate (Tricaine, MS-222)	Nacalai tesque	14805-82	
PTU (N-Phenylthiourea)	Nacalai tesque	27429-22	
Fast DiO solid	Thermo Fisher Scientific	D3898	
Fast DiI solid	Thermo Fisher Scientific	D7756	
TO-PRO™-3 Iodide (642/661)	Thermo Fisher Scientific	T3605	
Hoechst 33342	Wako	346-07951	
Toluidine Blue	Nacalai tesque	1B-481	
Dextran, Tetramethylrhodamine	Thermo Fisher Scientific	D1817 LTJ	

Name	Source or reference	Identifiers	Additional information
Dextran, Alexa Flour-488	Thermo Fisher Scientific	D22910	
Dextran, Alexa Flour-647	Thermo Fisher Scientific	D22914	
Dextran, Cascade Blue	Thermo Fisher Scientific	D1976	
chopchop	chopchop	https://chopchop.cbu.uib.no	
ImageJ (Fiji)	(Schneider et al., 2012)	https://imagej.nih.gov/ij/; RRID: SCR_003070	
Imaris	Bitplane	http://www.bitplane.com/imaris; RRID: SCR_007370	
Graphpad Prism v9.1.0.	Graphpad Prism	https://www.graphpad.com/scientific-software/prism/	

2.2.1. Zebrafish husbandry

Zebrafish (*Danio rerio*) were maintained on a 14:10 hour light: dark cycle at 28°C. Collected embryos were cultured in E3 embryo medium (5mM NaCl, 0.17mM KCl, 0.33mM CaCl2, 0.33mM MgSO4) containing 0.003% 1-phenyl-2-thiouera (PTU) to prevent pigmentation and 0.01% methylene blue to prevent fungal growth. All experiments were performed on zebrafish embryos between 36 hpf and 4 dpf .

All zebrafish experiments were performed in accordance with the Animal Care and Use Program of Okinawa Institute of Science and Technology Graduate School (OIST), Japan, which is based on the Guide for the Care and Use of Laboratory Animals by the National Research Council of the National Academies. The OIST animal care facility has been accredited by the Association for Assessment and Accreditation of Laboratory Animal Care (AAALAC International). All experimental protocols were approved by the OIST Institutional Animal Care and Use Committee.

2.2.2. Transgenic lines

Details of the different transgenic lines used in this study are described in **Table 2**. To generate stable transgenic lines *for Tg[Ptf1a:mCherry-CAAX]*^{oki067}, *Tg[hsp:WT.Strip1-GFP]*^{oki068}, and *Tg[hsp:Mut.Strip1:GFP]*^{oki069}, the constructs pTol2[ptf1a:mCherry-CAAX], pTol2[hsp:WT.Strip1-GFP], and pTol2[hsp:Mut.Strip1-GFP] were injected into one-cell-stage fertilized eggs together with Tol2 transposase mRNA at the concentration 15-20 ng/µL, respectively. These injected F0 embryos were bred up to the adult stage and used to identify founder fish that produce F1 generation embryos showing stable GFP expression. Transgenic lines were established in F2 generation. The steps of plasmid construction are mentioned below in details. The mentioned transgenic lines were combined with the mutant line *strip1*^{rw147}.

Table 2. List of transgenic lines used in the phenotypic study.

Name	Description	Rationale	Reference
Tg[ath5:GFP]^{rw021}	GFP is expressed under control of the *ath5* promoter.	To visualize RGCs	(Masai et al., 2003)
Tg[Ptf1a:mCherry-CAAX]^{oki067}	Membrane-targeted mCherry is expressed under the control of *ptf1a* promoter	To visualize amacrine cells	This study
Tg(Gal4-VP16,UAS:EGFP)^{xfz43} or xfz43 and Tg(Gal4-VP16,UAS:EGFP)^{xf43} or xfz3	Enhancer trap lines that express EGFP in distinct subsets of BPs	To visualize subsets of bipolar cells	(Zhao et al., 2009)
Tg[hsp:WT.Strip1-GFP]^{oki068}	GFP-tagged wild-type Strip1 at the C-terminus is expressed under control of the heat shock promoter.	To over express wild-type Strip1	This study
Tg[hsp:Mut.Strip1:GFP] ^{oki069}	GFP-tagged *rw147* mutant form of Strip1 at the C-terminus is expressed under control of the heat shock promoter.	To over express mutant Strip1	This study
Tg[UAS:MYFP]	EYFP fused to the membrane targeting palmitoylation signal of gap43 under the control of 14XUAS E1b promoter	To label single cells in combination with cell-specific promotor-driven Gal4	(Schroeter et al., 2006).

2.2.3. Mutant line generation and genotyping

The *strip1^{rw147}* mutant line was generated from a mutagenesis screen (Masai et al., 2003) that used RIKEN Wako (RW) as a wild-type strain. Mutation mapping and subsequent experiments were carried out in the genetic background of WIK and Okinawa wildtype (oki), respectively. The *rw147* mutation was mapped on a genomic region in chromosome 22 flanked by two self-designed polymorphic markers; AL928817-12 and zk253D23-4. In addition, location of the *rw147* mutation was further restricted using another self-designed polymorphic marker Zk286J17-3 as no recombination was detected, sequences of primers used are listed in **Table 3**.

From 3 dpf, *strip1^{rw147}* homozygous mutants (*strip1$^{-/-}$*) are distinguished from wild-type siblings (*strip1$^{+/+}$* or *strip1$^{+/-}$*) by external morphology since they exhibit cardiac edema, an abnormal lower jaw, and smaller eyes. From 54 to 72 hpf, *strip1^{rw147}* homozygous mutants are screened by Acridine Orange (AO) live staining to detect apoptotic cells (Casano et al., 2016) or Bodipy TR live staining to visualize lamination defects (Choi et al., 2010). Prior to 54 hpf, genotyping of *strip1^{rw147}* mutant embryos was performed by sequencing. The 257-bp PCR amplicons were amplified using Phusion Hot Start II (Thermo Fisher Scientific) and sequenced for genotyping.

Table 3. Sequences of primers used.

Purpose	Sequences
strip1^{rw147} mutation mapping	AL928817-12: 5′-TTCAACATCTGCTTTTCCTCCT-3′ and 5′TCATGTCCCAGAAATCACACAT3′. Zk253D23-4 5′-CATTCTTCATTAAAGAGATCAGTGTGA-3′ and 5′-AGTGATCACACACCCCCACT-3′. Zk286J17-3 5′- TTCACATTTACATTTTTCTGAACATTT-3′ and 5′-CACACAGCCTTCTCTTGCAC -3′.
strip1^{rw147} mutant genotyping	5′-CGTGTGTTTTCAGGGTGTT-3′ and 5′-TCACCATCCCAAACAGCATA-3′
strip1^{crisprΔ10} or *strip1*^{oki8} mutant genotyping	5′-CGTTCCAAATCATTGAAACAGA-3′ and 5′-TGTTTGTGATGTGTTGACCTTG-3′
Strip1 cloning primers	5′-AGACTTGTGTCAGCGTGACGCGAG-3′ and 5′-ACTCTAGCAAGTGTAGTGTTGTTGATG-3′
In situ probe synthesis primers	5′-AATGCTGCCGAATAAAATGCGAG-3′ and 5′-CCCAGAGTGAACAGGATGCTCT-3′.

The *strip1*^{crisprΔ10} (officially referred to as *strip1*^{oki8}) mutant line was generated using Crispr/Cas9 gene editing technology. The gRNA sequence, 5′-CCCGCGTCCGCCTCTGACCTCAT-3′, was designed using chopchop (https://chopchop.cbu.uib.no) and it targets exon 9 of *strip1* gene. One-cell-stage embryos were injected with 200ng/µL gRNA and 500ng/µL Cas9 protein (FASMAC). F1 mutant founders were identified by sequencing. A 10-bp deletion was introduced at nucleotide 932 of the *strip1* coding sequence, resulting in a frameshift at amino acid 313 and a premature stop at amino acid 330. PCR amplicons were run on 15% polyacrylamide gel for identification of wild-type siblings and mutants. Sequences of all primers used are listed in **Table 3**.

All generated transgenic and mutant lines were combined with the zebrafish pigmentation mutant, roy orbison (roy) (D'Agati et al., 2017) to remove iridophores and enhance live imaging.

2.2.4. Molecular cloning

To generate pTol2[hsp:WT.Strip1-GFP] and pTol2[hsp:Mut.Strip1:GFP], a PCR strategy was used to amplify ~2.5 kb *strip1* cDNA from total cDNA of 4 dpf wild-type and *strip1*^{rw147} zebrafish embryos using primers listed in **Table 3**. Then, using a Gibson Assembly Cloning Kit, a *strip1* cDNA fragment was cloned into a Tol2 transposon vector pT2AL200R150G (Urasaki et al., 2006) at the *XhoI* and *ClaI* sites with a heat-shock inducible promoter (hsp) at the N-terminus (Halloran et al., 2000) and a GFP tag at the C-terminus (separated by a linker sequence, CTCGAGGGAGGTGGAGGT). For pTol2[ptf1a:mCherry-CAAX] construction, pG1[ptf1a:GFP] was used as donor plasmid, which was kindly provided by the Francesco Argenton lab. A 5.5-kb fragment of the *ptf1a* promoter sequence was retrieved at *HindIII* and *SmaI* sites and inserted into a pBluescript SK (+)

(Stratagene) shuttle vector upstream of the membrane-targeting mCherry-CAAX sequence. Then, the ptf1a:mCherry-CAAX sequence was inserted into the *XhoI and BglII* sites of pT2AL200R150G. The pB[ath5:Gal4-VP16] plasmid was constructed by inserting a 6.6-kb fragment of the *ath5* 5'-enhancer/promoter region (including 5' UTR) into the *BamHI* site of the pB[Gal4-VP16] plasmid provided by Dr. R. Köster (Koster and Fraser, 2001).

2.2.5. *In vivo* cell labeling

Single-cell mosaic labeling to visualize the morphology of RGCs was done by injecting 20 ng/mL of pB[ath5:Gal4] into 1-cell-stage embryos from intercrosses of *strip1*^{rw147} heterozygous fish combined with *Tg[UAS:MYFP]* (Schroeter et al., 2006). Likewise, pZNYX-GalVP16, a kind gift from the Rachel Wong Laboratory, was injected to visualize ON-bipolar cells (Schroeter et al., 2006). Single amacrine cell labeling was performed by injecting the DNA construct pG1[ptf1a:GFP] into 1-cell-stage embryos from intercrosses of *strip1*^{rw147} heterozygous fish at concentration 20 ng/µL (Jusuf et al., 2012).

2.2.6. Morpholino knockdown assays

Embryos produced by intercrosses of wild-type or *strip1*^{rw147} heterozygous fish were injected with antisense morpholino oligonucleotides at 1-cell stage. MO-strip1 and MO-ath5 (Pittman et al., 2008, Ranawat and Masai, 2021) were injected at a concentration of 250 mM. For each morpholino experiment, the same concentration of the standard control morpholino (STD-MO) was used as a negative control. Detailed morpholino sequences are listed in **Table 4.**

Table 4. Sequences of morpholinos used in phenotypic study.

Name	Sequence	Reference	Source/Identifier
STD-MO	5'-CCTCTTACCTCAGTTACAATTTATA-3'		Gene Tools
MO-strip1	5'-TAGCACATAAACCGACACCGTCCAT-3'	This study	Gene Tools
MO-ath5	5'-TTCATGGCTCTTCAAAAAAGTCTCC-3'	(Pittman et al., 2008)	Gene Tools ZDB-MRPHLNO-100405-2

2.2.7. Western Blotting

The heads of non-injected or MO-strip1-injected wild-type embryos were dissected at 2 dpf in Leibovitz's L-15 ice cold medium and homogenized in lysis buffer (125mM NaCl, 50 mM Tris (pH 7.5), 0.5 mM EDTA (pH 8), 1% Triton X-100 and 1× cocktail protease inhibitors). Lysates were clarified by centrifugation at 10,000 g for 10 min at 4 °C. Equal amounts of denatured clarified lysates were run on 10% Mini-PROTEAN TGX gels for SDS-PAGE and transferred to PVDF membranes using Trans-Blot Turbo PVDF Transfer system. After blocking with 5% skim milk in 0.1% tween-20 in TBS, immunoblotting was performed using anti-Strip1 (1:500) and anti-

β-actin (1:5000). HRP-linked rabbit IgG was used as a secondary antibody. Chemiluminescence signals were detected using a FUJI Las 4000 luminescence image analyzer.

2.2.8. DiI/DiO Injections

To trace the RGC axon projections into the optic tectum, 3-dpf embryos were fixed in 4% paraformaldehyde (PFA) and after washing with PBS several times, were injected with 2 mg/mL of the lipophilic dyes, DiI and DiO, in the area between the lens and retina. Large injection volumes were applied to label all RGCs. Embryos were incubated overnight at 4°C, and then mounted in 75% glycerol for confocal imaging.

2.2.9. Histological methods

Plastic sectioning and toluidine blue staining

Zebrafish embryos were embedded for JB4 plastic sectioning and toluidine blue counterstaining, as previously described (Sullivan-Brown et al., 2011). Briefly, 4 dpf embryos were fixed in 4% PFA overnight at 4°C. After washing in PBS, embryos were subjected to serial dilutions of PBS:ethanol. Then, incubated in ethanol:JB4 solution (1:1) for 3 hours at RT, followed by an overnight incubation in 100% JB4 at 4°C. Afterwards, embryos were mounted in JB4 solution A+B. Plastic sections were stained with 0.2% toluidine blue solution.

Immunohistochemistry

Immunolabeling of cryosections and paraffin sections were carried out according to standard protocols (Imai et al., 2010, Masai et al., 2003). Cryosections were permeabilized in PBTr buffer (Westerfield, 1995) (PO_4 buffer (0.1M, pH7.3)+0.1% Triton X-100) and blocked using 10% goat serum in PBTr for 1 hour. Sections were incubated overnight with primary antibody diluted in PBTr + 1% goat serum at 4°C. Slides were washed with PBTr and incubated in secondary antibody at 1:500 dilution together with a nuclear stain (1nM TOPRO3 or 1ng/mL Hoechst 33342) at RT for 2 hours. After washing in PBTr, slides were mounted with Fluoromount medium. As for paraffin sections, deparaffinization with done using xylene washes, followed by rehydration in serial dilutions of ethanol:PBS. An antigen retrieval step was performed on paraffin sections by heating in 10 mM citrate buffer pH 6.0 for 5 min at 121°C. Staining was performed as described above.

The antibodies used in the phenotypic study are listed in **Table 1** with their corresponding dilutions. Antibody against the peptide sequence of zebrafish Strip1 (amino acids 344-362: EKDPYKADDSHEDEEENDD) was generated using a synthetic peptide and used for immunostaining at 1:1,000. For adsorption control, purified antibody was preincubated with 3.6 mg/mL of corresponding blocking peptide for 1 h at room temperature. TUNEL (terminal deoxynucleotidyl transferase dUTP nick end labeling) was performed using an In Situ Cell Death

Detection Kit (Roche). Sections were incubated in enzyme solution:labeling solution at the ratio 1:9.

For whole-mount immunostaining against acetylated α-tubulin, 3-dpf embryos were fixed at room temperature for 3 h in 2% trichloroacetic acid (TCA). Then, embryos were washed in PBTr, followed by permeabilization in 0.2% trypsin for 4 min at 4°C. After washing, a post-fixation step in 4% PFA for 5 min at 4°C was applied. Next, blocking was done in 10% goat serum in PBTr for 1 h at room temperature followed by incubation in mouse anti-acetylated α-tubulin in 1% goat serum/PBTr overnight at 4°C. After washing, embryos were incubated in secondary antibody diluted in 1% goat serum in PBTr overnight at 4°C. After staining, embryos were mounted in 75% glycerol for confocal imaging.

Whole-mount in situ hybridization (WISH)

WISH was performed on wild-type zebrafish embryos at specific developmental stages as previously described (Xu et al., 1994). Hybridization was performed overnight at 65°C using *strip1* RNA probe at the concentration 2.5 ng/mL in hybridization buffer. *strip1* probe synthesis was performed according to standard protocols (Thisse and Thisse, 2008). Template regions were amplified from *strip1* cDNA using the primers listed in **Table 3** to amplify a 744 bp fragment flanking exons 1-9 of *strip1* gene. Antisense and sense probes were synthesized by *in vitro* transcription using a DIG RNA Labeling Kit (Roche). Following labeling, whole embryos were mounted in 75% glycerol for imaging. To visualize expression patterns in the retina, cryosections were prepared from whole mount embryos post-hybridization.

2.2.10. Live staining

To visualize lamination patterns, live staining of retinal landmarks was performed by incubating live zebrafish embryos in 100 nM solution of Bodipy TR methyl ester (Thermo Fisher Scientific) in E3 embryo rearing media for 1 h at room temperature, followed by several washes in E3 embryo rearing media. To examine DNA condensation of apoptotic cells in the GCL, zebrafish embryos were incubated for 30 min in 5 µg/mL of AO stain dissolved in egg water. Following staining, embryos were extensively washed with egg water and observed using epifluorescence or imaged using confocal microscopy.

2.2.11. Overexpression experiments

For rescue experiments, the wild-type and *rw147* mutant forms of Strip1 were overexpressed in *strip1*^{rw174} mutants by heat shock treatment using the transgenic lines *Tg[hsp:WT.Strip1-GFP]* and *Tg[hsp:Mut.Strip1:GFP],* respectively. To perform heat shock, embryos from heterozygous intercrosses were incubated for 1 h at 39°C starting from 27-30 hpf and applied every 12 hours until 4 dpf. After screening for transgenic embryos, embryos were fixed in 4% PFA for histological assays.

2.2.12. Cell transplantation assays

Single-cell transplantations were performed at blastula stage, as previously described (Kemp et al., 2009). Genotypes of donor and host embryos were determined at 3-4 dpf based on morphological phenotype or they were genotyped at earlier time points by sequencing or AO live-staining of apoptotic cells. To trace transplanted donor cells in host retinas, 2-5% lysine-fixable dextran rhodamine, Alexa-488 dextran, Alexa-647 dextran or cascade blue dextran were injected in 1-2-cell-stage donor embryos, depending on study design. To assess the cell autonomy of Strip1 in RGC death, donor embryos from intercrosses of *strip1*^{rw147} heterozygous fish were transplanted into wild-type host embryos. Host embryos with successful retinal transplants were fixed in 4% PFA at 60 hpf and processed for TUNEL. To assess the cell autonomy of Strip1 in RGC dendritic patterning, donor embryos from intercrosses of *strip1*^{rw147} heterozygous fish combined with *Tg[ath5:GFP]* were transplanted into wild-type host embryos. Live imaging of wild-type host retina was done at 57-58 hpf. To assess the cell autonomy of Strip1 in amacrine or bipolar development, donor embryos from intercrosses of *strip1*^{rw147} heterozygous fish combined with *Tg[ptf1a:mCherry-CAAX]* or *Tg[Gal4-VP16,UAS:EGFP]xfz3/xfz43* were transplanted into embryos from intercrosses of *strip1*^{rw147} heterozygous fish, live imaging of host retinas with successful transplants was done at 3-4 dpf to assess the morphology of donor amacrine cells labeled with mCherry or donor bipolar cells labeled with EGFP. To visualize the retinal lamination phenotype, some hosts were stained with Bodipy TR live stain prior to imaging.

2.2.13. Microscopy

Imaging of toluidine blue-stained sections and retinal sections following *in situ* hybridization was performed using a Zeiss upright Axioplan2 equipped with an AxioCam HRC camera, while imaging of whole-mount *in situ* hybridization embryos was done using a Keyence BZ-X700. An inverted Zeiss LSM 780 was used to scan immunostained retinal sections with a 40x / 1.40 Plan-Apochromat Oil objective and whole-mount immunostained embryos using a 40x / 1.0 Plan-Apochromat water objective. Glycerol-mounted embryos were placed on glass-bottom depression slides for scanning. For live imaging, zebrafish embryos were anesthetized using 0.02% tricaine (3-amino benzoic acid ethyl ester) dissolved in E3 embryonic medium and mounted laterally in 1% low-melting agarose, except for imaging of optic nerve development, which was performed by scanning embryos from ventral view. Live image acquisition of embryo retinas was carried out using an upright Zeiss LSM 710 with a 40x / 1.0 W Plan-Apochromat objective or an upright Fluoview FV3000 (Olympus) confocal microscope with a 40x / 0.8 water immersion objective.

To perform time-lapse imaging of retinal development, several embryos from intercrosses of *strip1*^{rw147} heterozygous fish carrying the transgenes *Tg[ath5:GFP;ptf1a:mCherry-CAAX]* were mounted simultaneously in a culture dish covered with E3 embryonic medium containing 0.003% PTU and 0.02% tricaine and overlayed with a thin layer of mineral oil to prevent evaporation of E3 medium to

minimize embryotoxicity. Retinal z-stacks were acquired consecutively in 1-µm steps every ~2 hrs, starting at 48 hpf with undetermined genotypes. Scanning was done using the Multi Area Time Lapse (MATL) Software module of the FV3000 (Olympus) confocal microscope and a motorized XYZ-rotation stage, Image acquisition was performed at the highest scanning speed and resolution 512X512 to minimize embryo toxicity.

All Images were processed using ImageJ (NIH, v2.1.0/1.53C), Imaris (Bitplane, v9.1.2) and Adobe Illustrator software. 3D rendering and analysis of time-lapse movies were performed on Imaris software. Whenever necessary, brightness and contrast display levels for the whole image were adjusted to aid visualization or decrease background noise.

2.2.14. Quantification and statistical analysis

To quantify RGC area, masks were generated for areas with strong ath5+ signals in the retina and quantified using the Color Threshold tool in ImageJ (Schneider et al., 2012). Afterwards, the retinal outline was defined using the lasso tool and retinal area was calculated. Data were represented as the percentage of ath5+ area to total retinal area.

To quantify apoptotic cells, the number of TUNEL+ cells in GCL or retina was calculated manually within a single retinal section. To quantify the number of ptf1a+ cells that contribute to IPL formation (amacrine cells), cells were manually counted in a unified area (8,500 μm^2) across all samples. Ptf1a+ cells that contributed to the OPL (presumably horizontal cells) were excluded from quantification. To quantify the migration patterns of ptf1a+ cells that contribute to the IPL, cells located at the apical side relative to the IPL were assigned INL+, while cells located at the basal side of the IPL or near the lens were assigned GCL+. To determine the distribution of ptf1a+ cells within transplanted columns, ptf1a+ cells that contributed to the IPL were manually calculated in a z-stack and the distribution pattern was represented as the percentage of basally or apically located ptf1a+ cells to the total number of ptf1a+ cells. Numbers of strong Pax6+ and Prox1+ cells were calculated using the analyze particles tool in ImageJ and the distribution of cells (INL+ or GCL+) was assigned based on their location relative to the IPL, according to the nuclear stain pattern. Distribution data were represented as the percentage of INL+ or GCL+ to the total number of Prox1+ or Pax6+ cells.

Statistical analysis was conducted using Graphpad Prism 9.1.0. Data are represented as means ±SD. Comparisons between two samples were done using Student's t test with Welch's correction for normally distributed data or the Mann Whitney U test for data which doesn't follow a normal distribution. For multiple comparisons, 2-way ANOVA with the Tukey post hoc test was used. Details of statistical tests and number of samples used are in figures and figure legends. Significance level is indicated as $*p < 0.05$, $**p < 0.01$, $***p < 0.001$, $****p < 0.0001$, n.s. indicates not significant.

2.3. Results

2.3.1. Retinal defects of *rw147* mutant are due to loss of Strip1

Zebrafish *rw147* mutants show severe retinal lamination defects. Previous data from the Masai unit have identified a missense mutation in *strip1* gene of *rw147* mutant genome. To confirm that loss of Strip1 is indeed the cause of *rw147* retinal lamination defects, I performed Crispr/cas9-mediated targeted mutagenesis of *strip1* gene and generated a 10-base deletion mutant, $strip1^{crisprΔ10}$ (**Figure** 2.1 **A**). $strip1^{crisprΔ10}$ deletion occurs in exon 9 and leads to a premature stop codon. $strip1^{crisprΔ10}$ mutants and $strip1^{crisprΔ10/rw147}$ trans-heterozygotes showed similar morphology and retinal lamination defects to those of *rw147* mutants, which will be named from now on $strip1^{rw147}$ mutants (**Figure** 2.1 **B-F**).

Next, I performed knockdown experiments of zebrafish Strip1 using translation-blocking morpholinos (MO-Strip1). *strip1* morphants phenocopy the retinal defects of $strip1^{crisprΔ10}$ and $strip1^{rw147}$ mutants (**Figure** 2.1 **G and H**). I verified the specificity of MO-Strip1 by generating a custom-made zebrafish Strip1 antibody that fails to detect a 93-kDa protein band corresponding to zebrafish Strip1 in the morphants, when compared to wild-type controls (**Figure** 2.1 **I**).

Furthermore, I performed rescue experiments to confirm that wild-type Strip1 can rescue $strip1^{rw147}$ mutant retinal defects. To this end, I generated two transgenic constructs; pTol2[hsp:wt.Strip1-GFP] and pTol2[hsp:Mut.Strip1-GFP] to express GFP-tagged wild-type and *rw147* mutant forms of Strip1 under the control of the heat shock promotor. Single-cell labeling revealed that wild-type Strip1 protein localization is mostly cytoplasmic (**Figure** 2.2). However, abnormal aggregation of *rw147*-mutant form was observed (**Figure** 2.2), which suggests that *rw147* mutation causes mis-folding of Strip1 protein, probably leading to loss of function. Next, I utilized the above-mentioned constructs to generate two transgenic lines; *Tg[hsp:wt.Strip1-GFP]* and *Tg[hsp:mut.Strip1-GFP]* and combined each line with $strip1^{rw147}$ mutant line. Wild-type Strip1, but not the mutant form, rescued the retinal defects of $strip1^{rw147}$ mutant following heat shock application (**Figure** 2.3 **A and B**). Taken together, the *strip1* mutation is the cause of $strip1^{rw147}$ mutant defects.

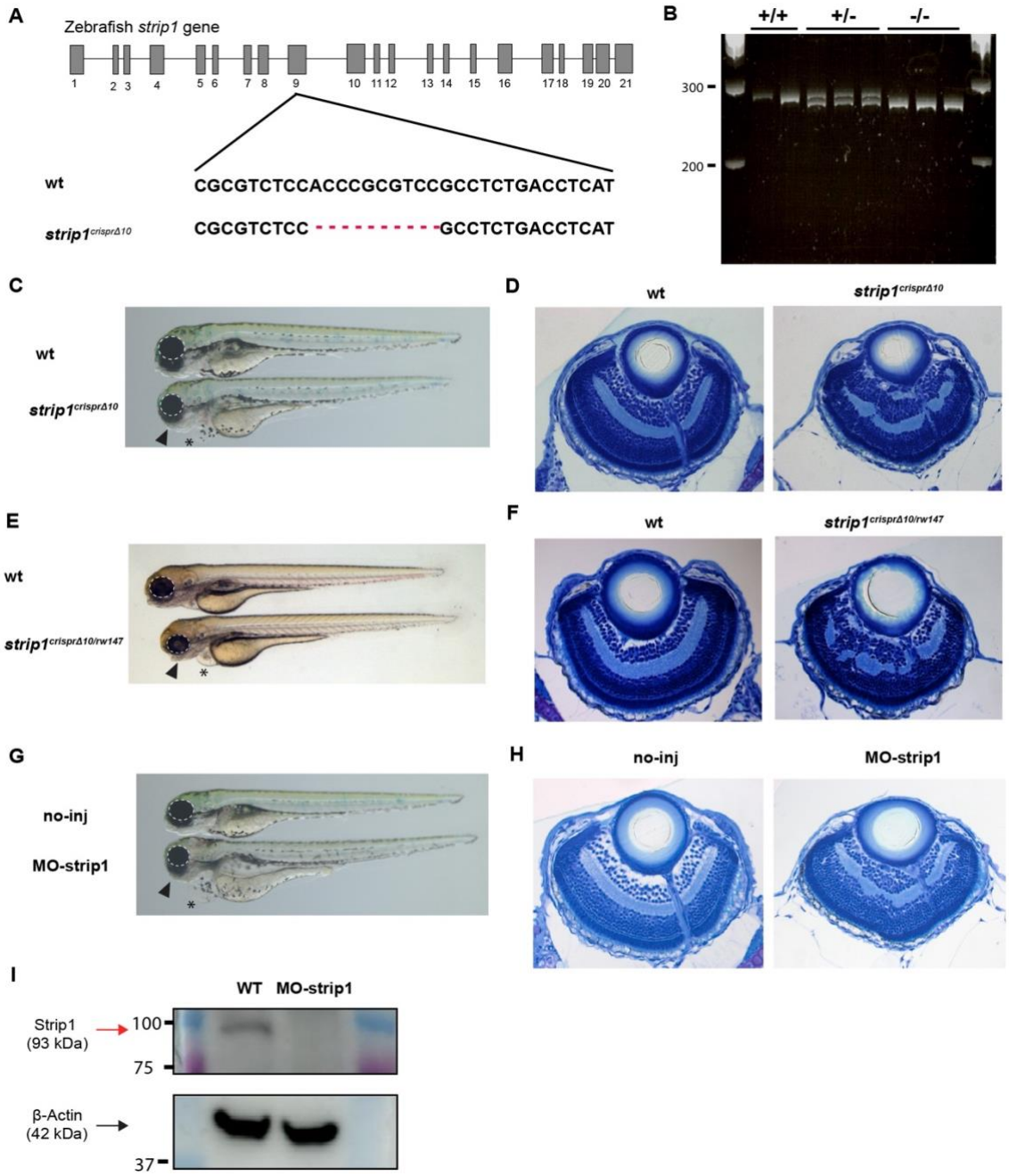

Figure 2.1. *strip1*^{crisprΔ10} mutants and *strip1* morphants phenocopy *rw147* mutant retinal defects.

(A) CRISPR-mediated, mutagenesis of zebrafish *strip1* gene. A 10-bp deletion was introduced into exon 9, leading to a premature stop codon. (B) A polyacrylamide gel image showing PCR amplicons using primers that flank the 10-base deletion of *strip1*^{crisprΔ10}. Wild-type and *strip1*^{crisprΔ10} mutant bands are expected to appear at 279 and 269 bps, respectively. (C,D) Morphology and plastic sections of wild-type and *strip1*^{crisprΔ10} embryos at 4 dpf. (E,F) Morphology and plastic sections of wild-type and trans-heterozygote *strip1*$^{crisprΔ10/rw147}$ embryos at 4 dpf. (G,H) Morphology and plastic sections of non-injected and MO-strip1 injected wild-type embryos at 4 dpf. Dotted lines demarcate the eye outline. The arrowhead indicates an abnormal lower jaw. An asterisk indicates heart edema. (I) Western blotting of 2-dpf head lysates from non-injected and MO-strip1 injected wild-type embryos.

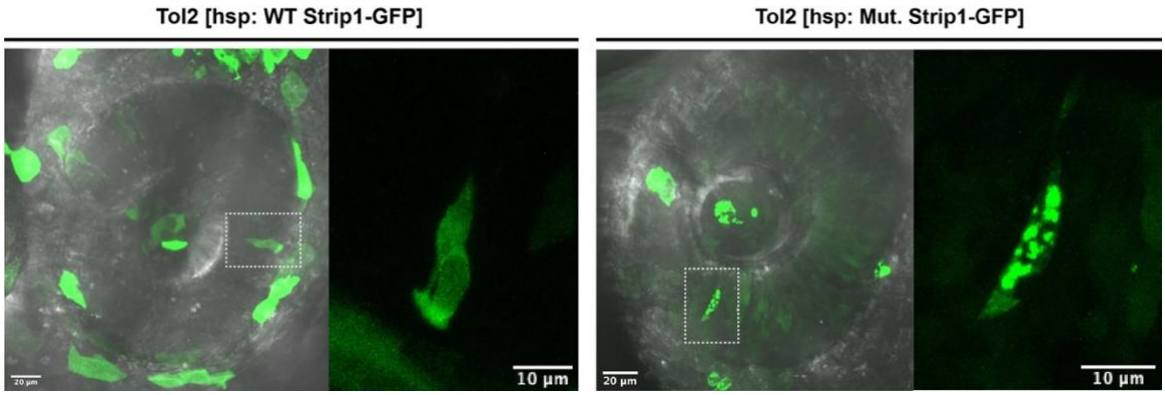

Figure 2.2. intracellular expression patterns of wild-type and *rw147* mutant forms of Strip1.

Maximum projection images of single retinal cells at 31 hpf expressing GFP-tagged wild-type (hsp:wt.Strip1-GFP) and *rw147* mutant (hsp:Mut.Strip1-GFP) forms of Strip1 at 31 hpf. Images on the right show higher magnification of outlined areas.

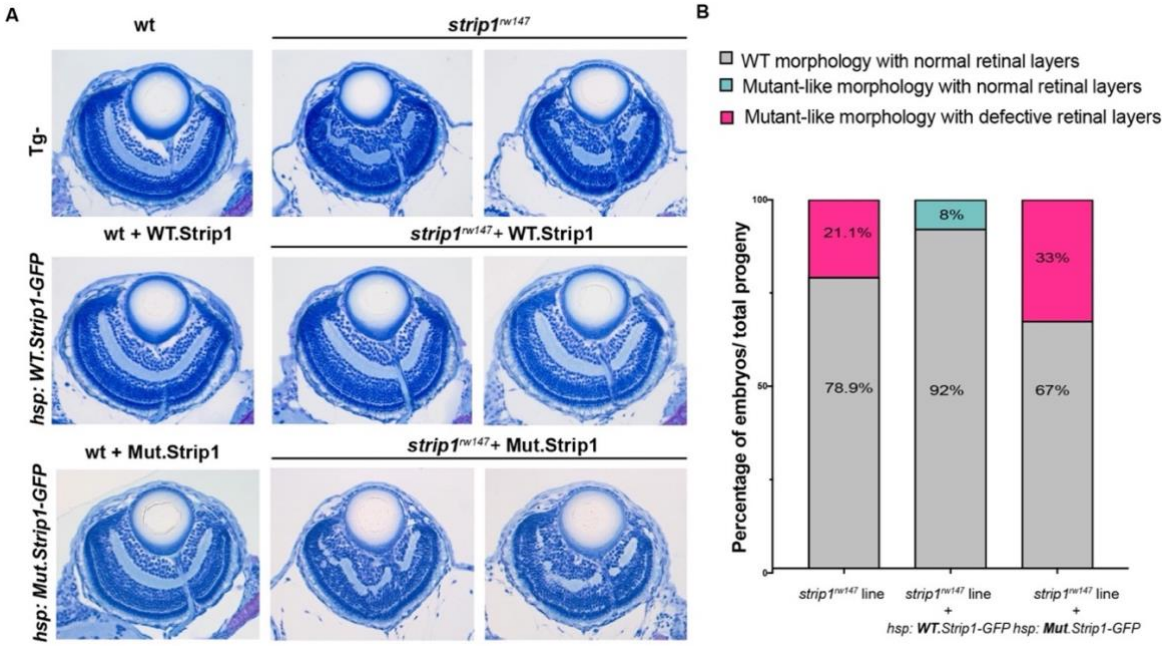

Figure 2.3. Overexpression of wild-type Strip1 rescues *rw147* mutant defects.

(A) Plastic sections of 4 dpf wild-type and *strip1*^{rw147} mutant retinas without transgene (top panels), and with the transgenes *Tg[hsp:WT.Strip1-GFP]* (middle panels) or *Tg[hsp:Mut.Strip1-GFP]* (bottom panels) post heat shock treatment. (B) A staggered bar graph, which represents the percentage of *strip1*^{rw147} mutants with a defective retina vs. mutants with a rescued retina in *strip1*^{rw147} mutants without transgenes, and with *Tg[hsp:WT.Strip1-GFP]* or *Tg [hsp:Mut.Strip1-GFP].*

2.3.2. Strip1 is expressed in inner retinal neurons

To understand how Strip1 functions in retina development, I performed whole mount *in situ* hybridization to examine *strip1* expression patterns in wild-type zebrafish embryos at different developmental stages. Zebrafish *strip1* mRNA is expressed maternally, and zygotic mRNA is ubiquitously expressed until the

gastrula stage (**Figure** 2.4 **A**). At 1-2 dpf, *strip1* expression becomes restricted to the heart and central nervous system (brain and eyes). Afterwards, expression levels decrease and become mostly retained in the optic tectum (OT). At 2 dpf, *strip1* mRNA appears to be predominantly expressed RGCs and amacrine cells (**Figure** 2.4 **B and C**). I confirmed a similar expression pattern by immunolabeling with zebrafish Strip1 antibody, which shows high expression in RGCs and amacrine cells at 2 dpf (**Figure** 2.5**).**

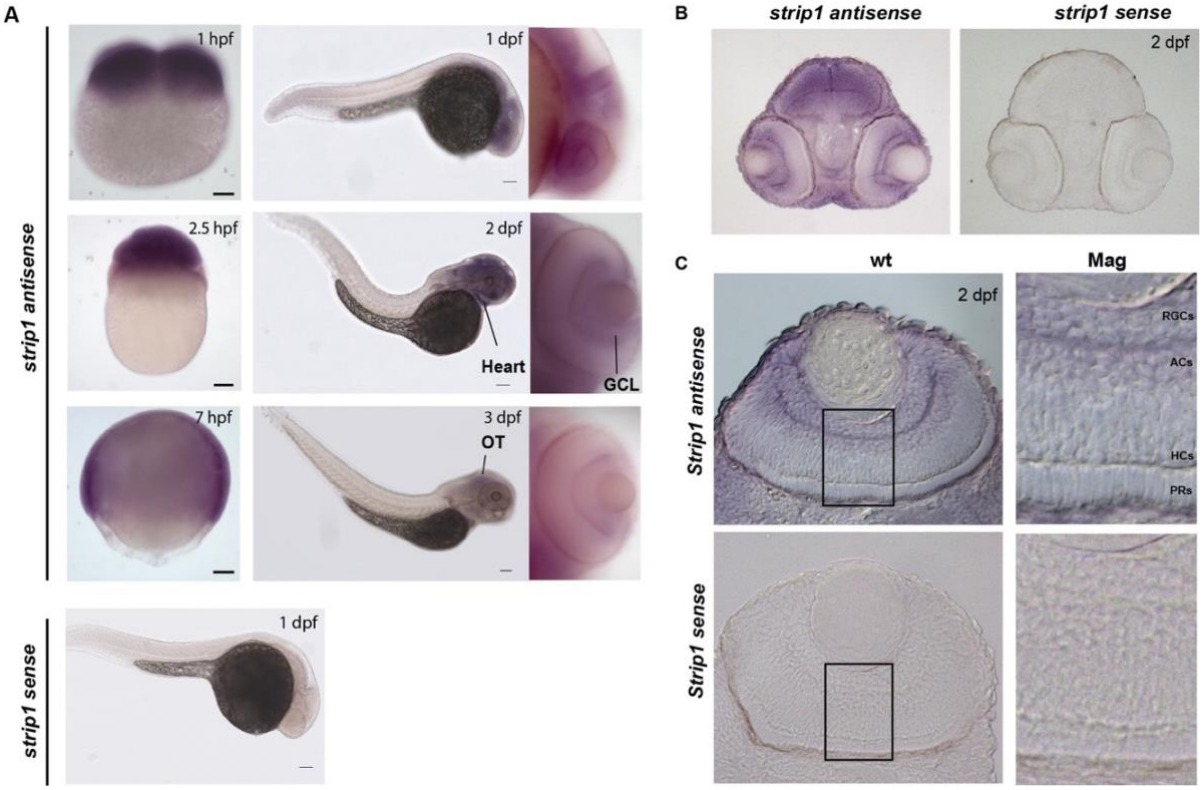

Figure 2.4. *strip1* mRNA expression pattern in the developing zebrafish embryo.

(A) *In situ* hybridization using a *strip1* antisense probe is shown at different developmental stages: 4-cell, blastula, 75% epiboly, 1 dpf, 2 dpf and 3 dpf. *In situ* hybridization using the sense probe at 1 dpf is shown as a negative control. Ventral view of 2-dpf retina shows a stronger signal in GCL (left panels). GCL, ganglion cell layer. Scale bar: 100 µm. (B) Frontal cryosections of 2-dpf heads following *in situ* hybridization show that *strip1* mRNA is predominantly expressed in the inner retina and the optic tectum. (C) Retinal cryosections show higher expression in RGCs and amacrine cells. Right panels show higher magnification of outlined areas. RGCs, retinal ganglion cells; ACs, amacrine cells; HCs, horizontal cells; PRs, photoreceptors.

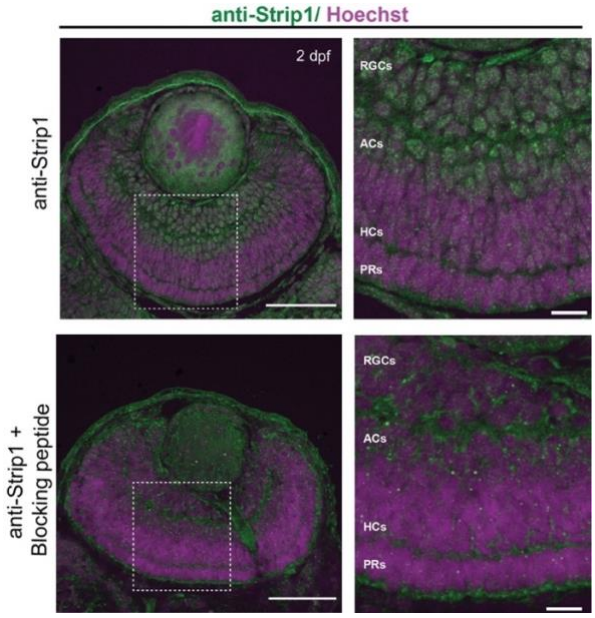

Figure 2.5. Retinal expression pattern of Strip1 protein.

Wild-type retinas labeled with anti-Strip1 antibody (upper panels) and anti-Strip1 plus Strip1 blocking peptide as a negative control (lower panels). Nuclei are stained with Hoechst. Scale bar, 50 μm. Right panels show higher magnification of outlined areas. Scale bar, 10 μm.

2.3.3. Absence of Strip1 causes defects in IPL formation

To have a better visualization of *strip1*^{rw147} lamination defects, I performed whole-mount staining of the retina with anti-acetylated α-tubulin antibody. In wild-type retinas, retinal lamination including IPL and OPL is evident at 3 dpf. In contrast, IPL shows abnormal morphology, whereas OPL is relatively normal in *strip1*^{rw147} mutants (**Figure** 2.6 **A**). We tracked IPL development using Bodipy TR live stain. In wild-type siblings, a rudimentary IPL was formed as early as 52 hpf; however, it was less defined in *strip1*^{rw147} mutants (**Figure** 2.6 **B**). At 62 hpf, *strip1*^{rw147} mutants exhibited a wave-like abnormal IPL. This temporal profile coincides with development of RGCs and amacrine cells. Next, I visualized neurite morphology of the different neurons that contribute to IPL development (RGCs, amacrine cells, and bipolar cells) by transiently expressing fluorescent proteins under control of *ath5* (Masai et al., 2003), *ptf1a* (Jusuf and Harris, 2009), and *nyx* promoters (Schroeter et al., 2006) respectively. In wild-type siblings, RGCs and amacrine cells normally extend their dendrites toward IPL; however, *strip1*^{rw147} mutants show randomly directed dendritic patterns of RGCs and amacrine cells (**Figure** 2.6 **C and D**). In wild-type siblings, bipolar cells normally extend their axons and dendrites towards IPL and OPL, respectively; however, *strip1*^{rw147} mutants show mis-routed axons and abnormally branching dendrites of bipolar cells (**Figure** 2.6 **E**). Taken together, Strip1 is required for IPL formation and correct neurite patterning of RGCs, amacrine cells, and bipolar cells.

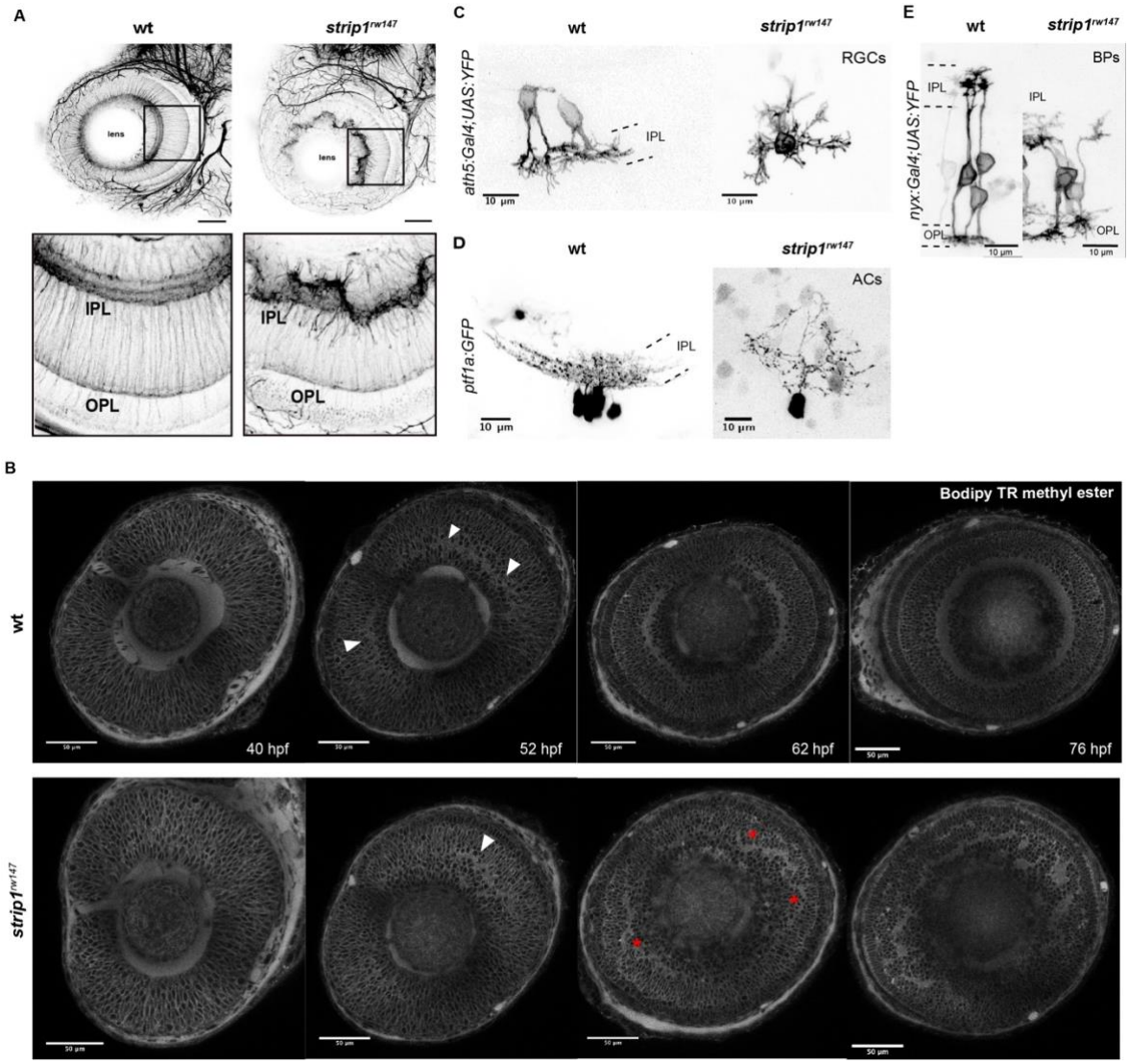

Figure 2.6. Loss of Strip1 cause defects in IPL formation.

(A) Whole-mount labeling of 3-dpf wild-type and *strip1*^{rw147} mutant retinas with anti-acetylated α-tubulin antibody. Bottom panels show higher magnification of outlined areas. Scale bar, 50 μm. (B) Live confocal snapshots of the same wild-type and *strip1*^{rw147} mutant retinas at different developmental stages stained with Bodipy TR. Arrowheads indicate rudimentary IPL. Asterisks show IPL defects in *strip1*^{rw147} mutants. Scale bar: 50 μm. *(C)* Projection images of single RGCs at 2 dpf expressing *ath5:Gal4VP16; UAS:MYFP* in wild type and *strip1*^{rw147} mutants. Scale *bar*, 10 μm. *(D)* Projection images of single amacrine cells at 3 dpf expressing *ptf1a:GFP* in wild type and *strip1*^{rw147} mutants. Scale *bar*, 10 μm. *(E)* Projection images of single bipolar cells at 3 dpf expressing *nyx:Gal4VP16; UAS:MYFP* in wild type and *strip1*^{rw147} mutants. Scale bar, 10 μm.

2.3.4. RGCs are reduced and INL cells infiltrate the GCL in *strip1* mutants

To examine how the IPL is disrupted in *strip1* mutant retinas, I combined *strip1*^{rw147} mutants with two transgenic lines, *Tg[ath5:GFP; ptf1a:mCherry-CAAX]*, to visualize RGCs and amacrine cells, respectively. In *Tg[ath5:GFP]*, GFP is expressed strongly in RGCs and weakly in amacrines and photoreceptors under control of the *ath5* retinal enhancer (Masai et al., 2003). In *Tg[ptf1a:mCherry-CAAX]*, membrane-targeted mCherry is expressed in retinal inhibitory neurons (RINs), amacrine and horizontal cells, under control of *ptf1a* promoter (Jusuf and Harris, 2009). Live imaging of 3-dpf retinas revealed that RGCs are dramatically reduced in *strip1*^{rw147} mutants (**Figure** 2.7 **A and B**). On the other hand, there was no significant change in the number of ptf1a+ amacrine cells between *strip1*^{rw147} mutants and wild-type siblings (**Figure** 2.7 **A and C**). However, ptf1a+ amacrines abnormally extended their dendrites to form an irregular pattern of IPL (**Figure** 2.7 **A**). In addition, in *strip1*^{rw147} mutant retina, a significant fraction of ptf1a+ cells were abnormally located in the GCL (**Figure** 2.7 **A**, bottom panels and **Figure** 2.7 **D**). I confirmed the positioning defects of amacrine cells by immunolabeling using anti-Pax6 antibody, which strongly labels ACs and weakly labels RGCs (Macdonald and Wilson, 1997). In wild-type siblings, most strong Pax6+ cells were in the INL, and only 9.84±4.13% were in the GCL (**Figure** 2.7 **E and G**). On the other hand, in *strip1*^{rw147} mutants, a significant percentage of strong Pax6+ cells (44.26±17.8%) was in the GCL (**Figure** 2.7 **E and G**). The total number of strong Pax6+ cells did not differ between wild-type siblings and *strip1*^{rw147} mutants (**Figure** 2.7 **F**).

It was also observed that such abnormal positioning of amacrine cells is highly correlated with the severity of IPL defects (**Figure** 2.8**).** The observed positioning defects and IPL malformation are reminiscent of the retinal phenotypes in *ath5* mutants, namely *lakritz*. RGCs fail to undergo neurogenesis in *lakritz*, leading to infiltration of amacrines into the GCL and transient IPL formation defects (Kay et al., 2001, Kay et al., 2004). I knocked down *ath5* using morpholino-antisense (Pittman et al., 2008) in wild-type embryos and compared its phenotype to that of *strip1* mutants. As previously reported, *ath5* morphants exhibited abnormal IPL at 3 dpf (**Figure** 2.9), although IPL defects were weaker than those of *strip1*^{rw147} mutants and the published phenotype of the *lakritz* mutant. In addition, a significant fraction of amacrine cells resided in the basal side of the IPL in *ath5* morphants.

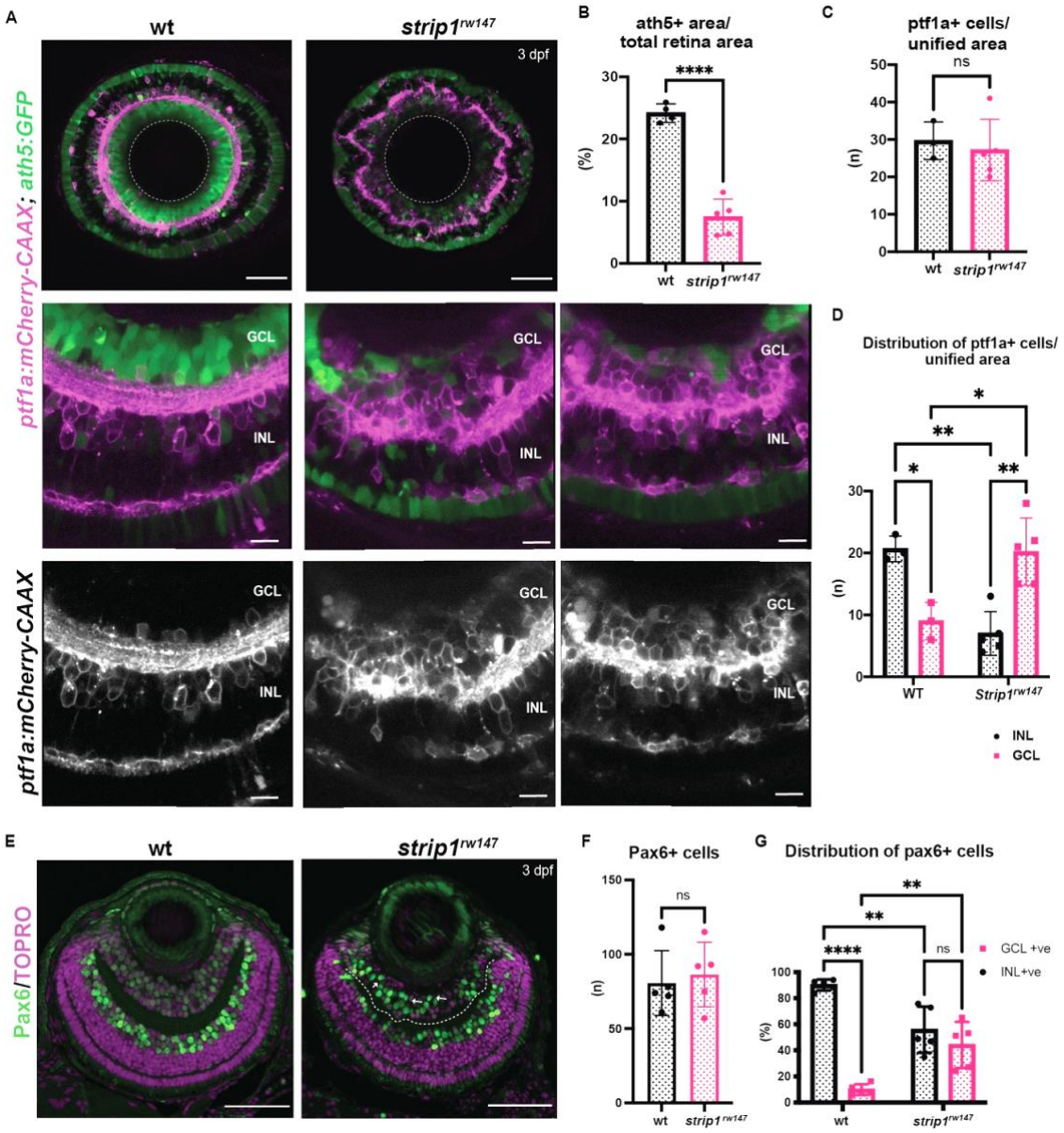

Figure 2.7. RGCs are reduced and amacrine cells infiltrate the GCL of *strip1* mutants.

(A) Live sections of wild-type and *strip1*^{rw147} mutant retinas combined with the transgenic line *Tg[ath5:GFP; ptf1a:mCherry-CAAX] to* label RGCs and amacrine cells. Middle and lower panels represent higher magnification. INL, inner nuclear layer; GCL, retinal ganglion cell layer. Scale *bar*, 50 µm (upper panels) and 10 µm (middle and lower panels). (B) Percentage of ath5+ area relative to total retinal area. Student's t test with Welch's correction, n≥4. (C) Amacrine cell numbers per unified retinal area (8,500 µm^2). Student's t test with Welch's correction, n≥3. (D) Distribution of amacrine cells (GCL or INL) per unified retinal area. Two-way ANOVA with the Tukey multiple comparison test, n≥3. (E) Wild-type and *strip1*^{rw147} mutant retinas at 3 dpf labeled with anti-Pax6. Arrows indicate strong Pax6+ cells that infiltrate the GCL. Nuclei are stained with TOPRO. Scale *bar*, 50 µm. (F) The number of strong Pax6+ cells per retina. Student's t test with Welch's correction, n=5. (G) Percentage of strong Pax6+ cells (GCL+ or INL+) to the total number of strong Pax6+ cells. Two-way ANOVA with the Tukey multiple comparison test, n=5.

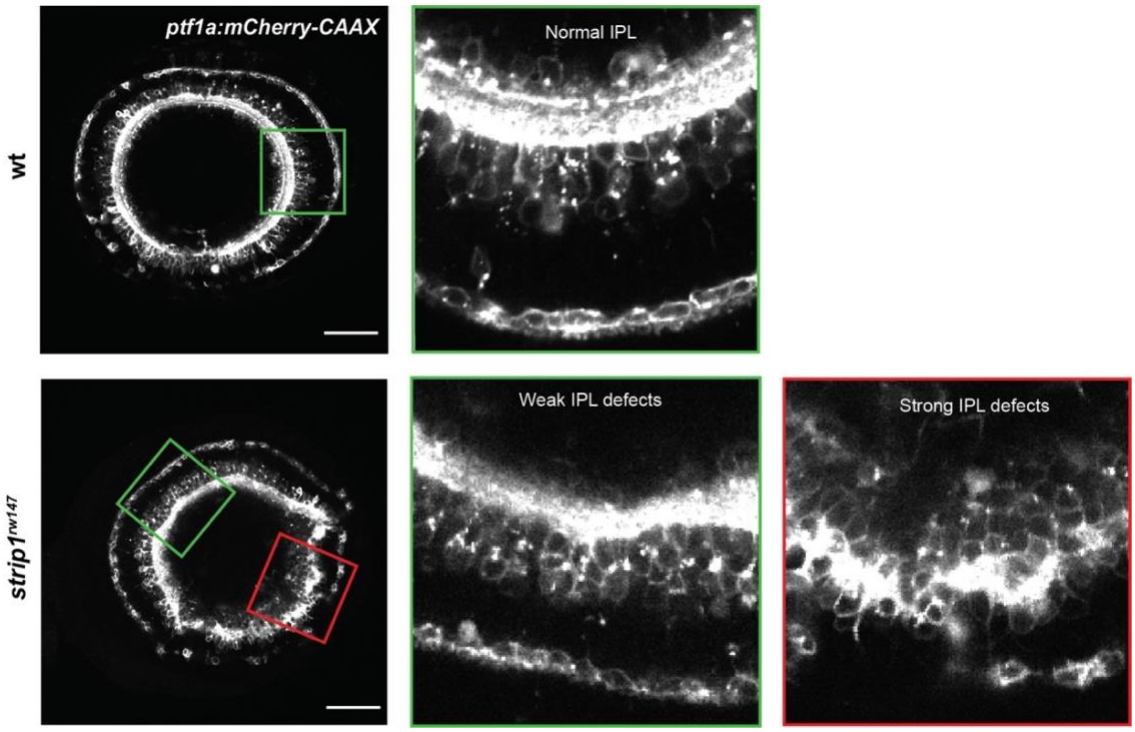

Figure 2.8. IPL defects in *strip1* mutants are associated with amacrine cell positioning defects.

Live confocal images of wild-type and *strip1*^{rw147} mutant retinas at 3 dpf combined with the transgenic line *Tg[ptf1a:mCherry-CAAX]*, which labels amacrine cells. Right panels show higher magnification of outlined areas. Scale bar, 50 µm.

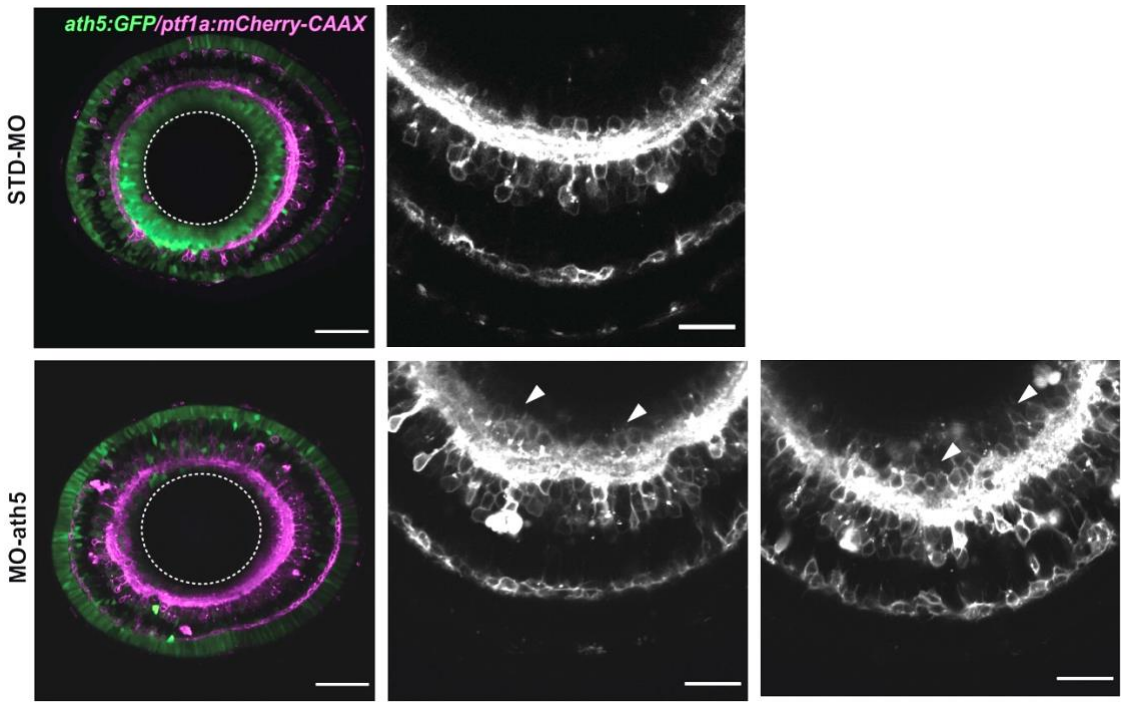

Figure 2.9. *ath5* morphants phenocopy IPL defects of *strip1* mutants.

Live confocal images of 3-dpf retinas of STD-MO and MO-ath5 injected wild-type embryos combined with the transgenic line *Tg[ath5:GFP; ptf1a:mCherry-CAAX],* which labels RGCs and amacrine cells. Panels on the right show higher magnification images to show abnormal localization of amacrine cells in GCL (arrowheads) and disrupted IPL. Scale bar, 50 µm (left panels) and 20 µm (middle and right panels).

Since bipolar cells contribute to IPL formation, immunostaining was performed using Prox1 antibody, which labels bipolar and horizontal cells (Jusuf and Harris, 2009). In wild-type, 100% of Prox1+ cells were in the INL (**Figure** 2.10 **A and C**). However, 10.6±6.26% of Prox1+ cells were abnormally located in the GCL (**Figure** 2.10 **A and C**). The total number of Prox1+ cells did not differ between wild-type siblings and *strip1*^{rw147} mutants (**Figure** 2.10 **B**). I confirmed the abnormal localization of both bipolar and horizontal cells by mosaic labeling using constructs that express YPF under the control of *nyx* and *cx55.5* promotor, respectively (Schroeter et al., 2006, Shields et al., 2007). A fraction of labeled cells resided close to the lens area (**Figure** 2.10 **D and E**). Taken together, these findings suggest that, in the absence of Strip1, INL cells abnormally infiltrate the GCL and seem to replace the reduced RGCs.

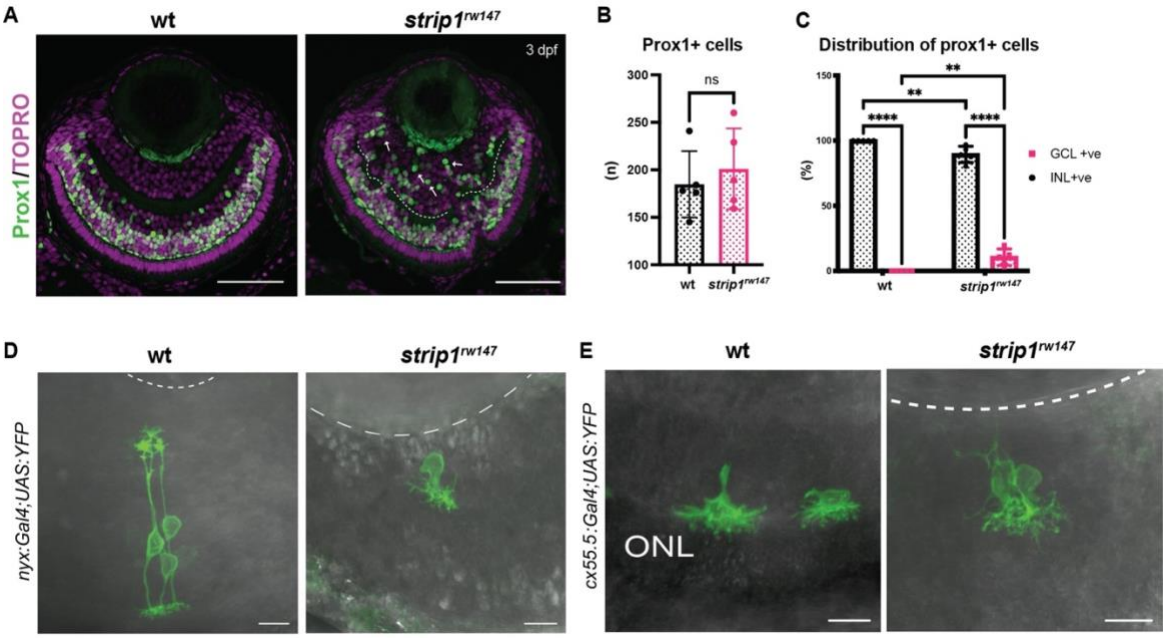

Figure 2.10. abnormal localization of bipolar and horizontal cells in the GCL.

(A) Wild-type and *strip1*^{rw147} mutant retinas at 3 dpf labeled with anti-Prox1. Arrows indicate Prox1+ cells that infiltrate the GCL. Nuclei are stained with TOPRO. Scale bar, 50 µm. (B) The number of Prox1+ cells per retina. Student's t test with Welch's correction, n=5. (C) Percentage of Prox1+ cells (GCL+ or INL+) to the total number of Prox1+. Two-way ANOVA with the Tukey multiple comparison test, n=5. (D) Projection images of single bipolar cells at 3 dpf expressing *nyx:Gal4VP16; UAS:MYFP* in wild type and *strip1*^{rw147} mutants. (E) Projection images of single horizontal cells at 3 dpf expressing *cx55.5:Gal4VP16; UAS:MYFP* in wild type and *strip1*^{rw147} mutants. Scale bar, 10 µm.

Next, to investigate if other retinal cells are affected by *strip1* mutation, immunolabeling of double-cone and rod photoreceptors was conducted using zpr1 and zpr3 antibodies, respectively (Nishiwaki et al., 2008). Apart from occasional mildly disrupted areas, the photoreceptor cell layer appeared to be largely intact, with no positioning defects (**Figure** 2.11 **A and B**). In addition, Müller glia cells and proliferating cells at the ciliary marginal zone (CMZ) were visualized using anti-glutamine synthetase (GS) (Peterson et al., 2001) and anti-PCNA antibodies (Raymond et al., 2006), respectively. Both cell types showed grossly normal positioning in *strip1*^{rw147} mutant retinas (**Figure** 2.11 **C and D**).

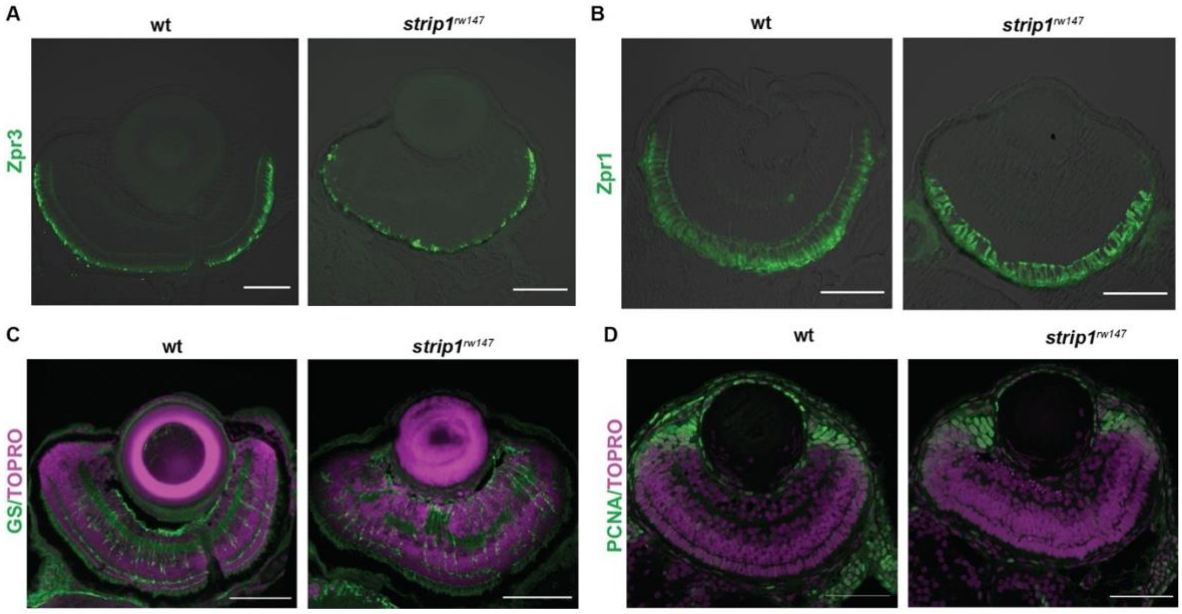

Figure 2.11. Photoreceptors, Müller glia and CMZ are grossly not affected by *strip1* mutation.

Labeling of wild-type and *strip1*^{rw147} mutant retinas with zpr3 (A), zpr1 (B), anti-glutamine synthetase (GS) (C) and anti-PCNA (D) antibodies, which visualize rod photoreceptors, double cone photoreceptors, Müller glia, and proliferative cells in the ciliary marginal zone (CMZ), respectively. Scale bar, 50 μm.

2.3.5. Strip1 is essential for RGC survival during development

In zebrafish, RGC-genesis starts in the ventronasal retina at 25 hpf, spreads into the entire retina by 36 hpf and is completed by 48 hpf (Avanesov and Malicki, 2010, Hu and Easter Jr, 1999). The reduction of RGCs in *strip1* mutants at 3 dpf could either be due to compromised RGC neurogenesis or it could be due to RGC death following birth. To clarify which, I examined RGC genesis by monitoring ath5:GFP expression, and retinal apoptosis by TUNEL from 36 to 96 hpf. In *strip1*^{rw147} mutants, RGCs are normally produced at 36 hpf; however, apoptosis occurred in the GCL as early as 48 hpf (**Figure** 2.12 **A**). The number of apoptotic cells in GCL reached its highest level at 60 hpf, and apoptotic cells were eliminated by 96 hpf (**Figure** 2.12 **A and B**). Accordingly, RGCs were significantly lower in *strip1*^{rw147} mutants than in wild-type siblings at 60 hpf and progressively reduced by 96 hpf. At 96 hpf, the ath5:GFP+ fraction in the total retina was 5.12±2.46% in *strip1*^{rw147} mutants, which is significantly lower than in wild-type siblings (21.49±4.17%) (**Figure** 2.12 **C**). In contrast, other retinal layers of *strip1*^{rw147} mutants showed slightly, but not significantly increased apoptosis at 72 hpf when compared to apoptosis within the GCL (**Figure** 2.12 **D**). In addition, there is no significant difference in apoptotic cell number in other retinal areas between 72 hpf and other time points (36, 60, 96 hpf). These findings suggest that Strip1 serves a specific function in RGC survival. Furthermore, despite the reduction in ath5:GFP+ area, the total presumptive GCL area, which was defined by area of nuclear stain between the lens and the IPL, was unchanged in *strip1*^{rw147} mutants throughout the stages from 36 to 96 hpf (**Figure** 2.12 **E**), confirming that infiltrating INL cells replace the lost RGCs.

A similar pattern of RGC death was also observed in *strip1*^{crisprΔ10} mutants (**Figure** 2.13), as visualized by acridine orange staining of apoptotic cells (Casano et

al., 2016). Interestingly, I observed a significant fraction of TUNEL+ cells in the optic tectum of *strip1*^{rw147} mutants compared to wild-type siblings (**Figure** 2.14), suggesting a common Strip1-dependent survival mechanism in the optic tectum. RGCs are the only retinal neurons whose axons exit the eyes and project to the optic tectum. In *strip1*^{rw147} mutants, RGC axons appeared to exit from the eye cup and formed an optic chiasm at 3 dpf, as shown by anterograde labeling using the axonal tracers DiI and DiO (**Figure** 2.15). However, consistent with the reduction of RGCs, the optic nerve was much thinner in *strip1*^{rw147} mutants than in wild-type siblings and showed elongation defects towards the optic tectum.

To determine whether Strip1 cell-autonomously promotes RGC survival, I conducted cell transplantation from *strip1*^{rw147} mutant donor cells into wild-type host embryos at the blastula stage. Then, I performed TUNEL of transplanted retinas at 60 hpf and found that *strip1*^{rw147} mutant donor RGCs underwent significant apoptosis in wild-type host retinas (**Figure** 2.16 **A-C**). Thus, Strip1 is cell-autonomously required for survival of RGCs.

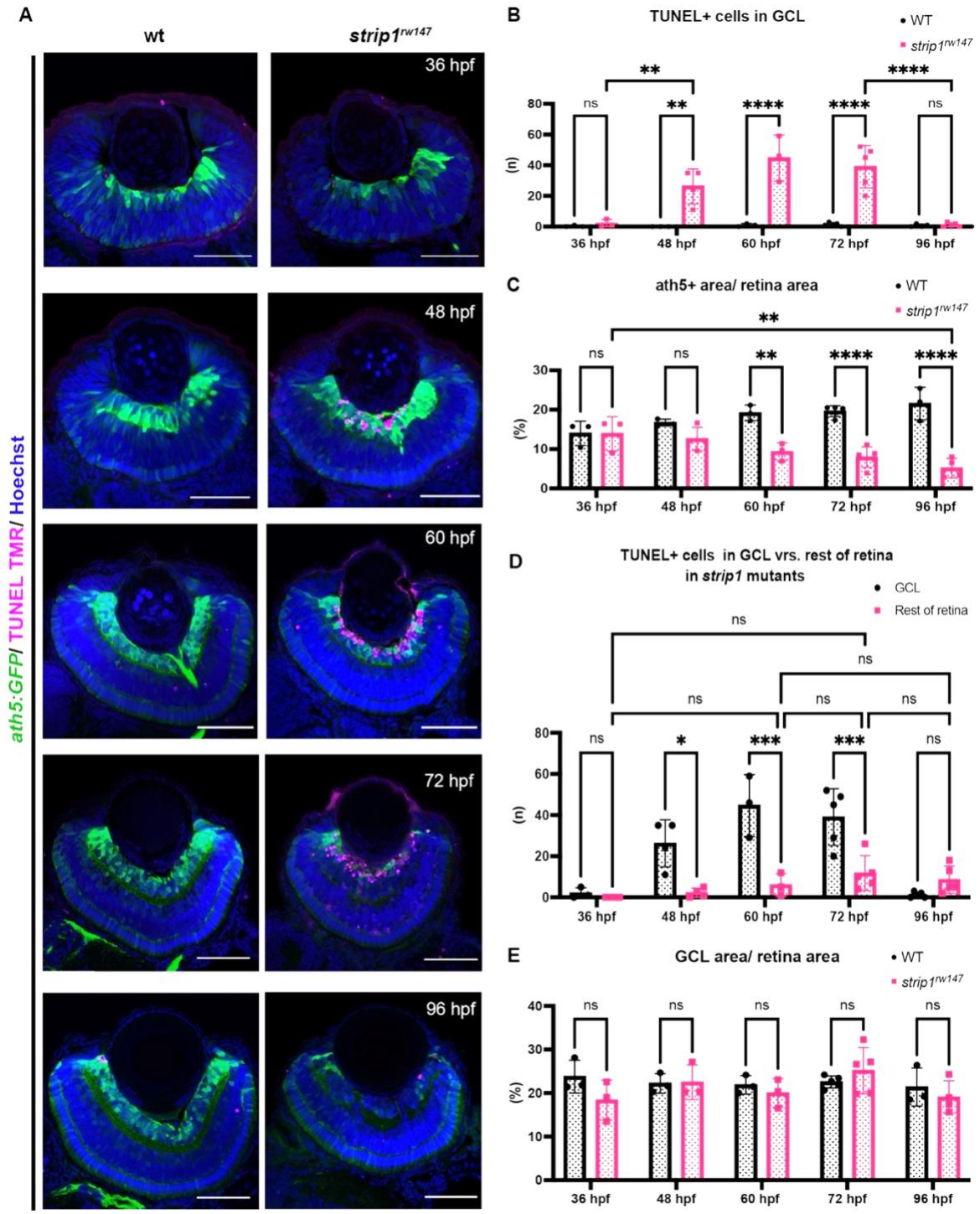

Figure 2.12. RGCs undergo cell death shortly after birth in *strip1*^{rw147} mutants.

(A) TUNEL of wild-type and *strip1*^{rw147} mutant retinas carrying the transgene *Tg[ath5:GFP] to* label RGCs at different timepoints. Nuclei are stained with Hoechst. Scale bar, 50 µm. (B) The number of TUNEL+ cells in GCL at different timepoints. (C) Percentage of ath5+ area relative to total retinal area at different timepoints. (D) The number of TUNEL+ cell in the GCL compared to the rest of the retina at different timepoints. (E) Percentage of GCL area (area between the lens and IPL) relative to the total retinal area at different timepoints. For all graphs, Two-way ANOVA with the Tukey multiple comparison test, n≥3.

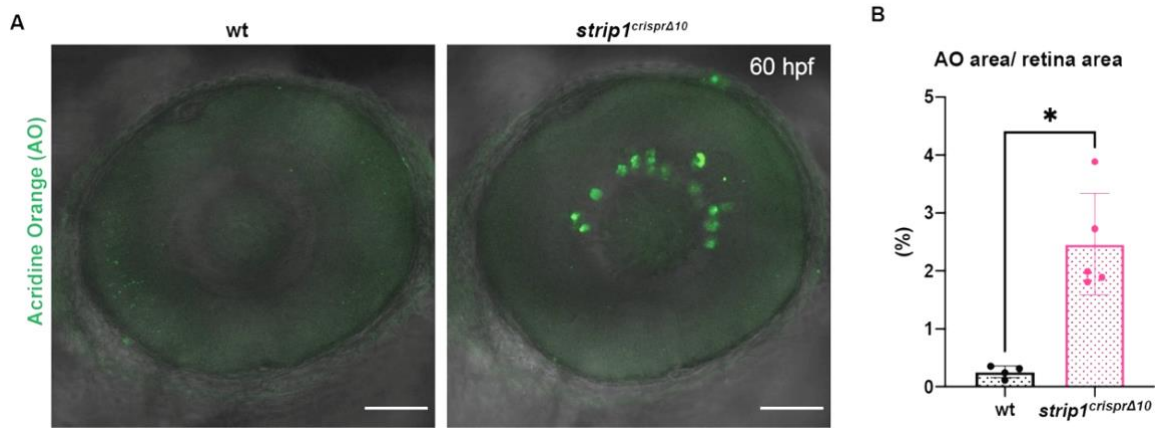

Figure 2.13. RGCs undergo cell death in *strip1*^{crisprΔ10} mutants.

(A) Live confocal images of wild-type and *strip1*^{crisprΔ10} mutant retinas stained with acridine orange (AO) to label apoptotic cells at 60 hpf. Scale bar, 50 µm. (B) Percentage of AO+ area relative to total retina area. Mann Whitney U test, n=5.

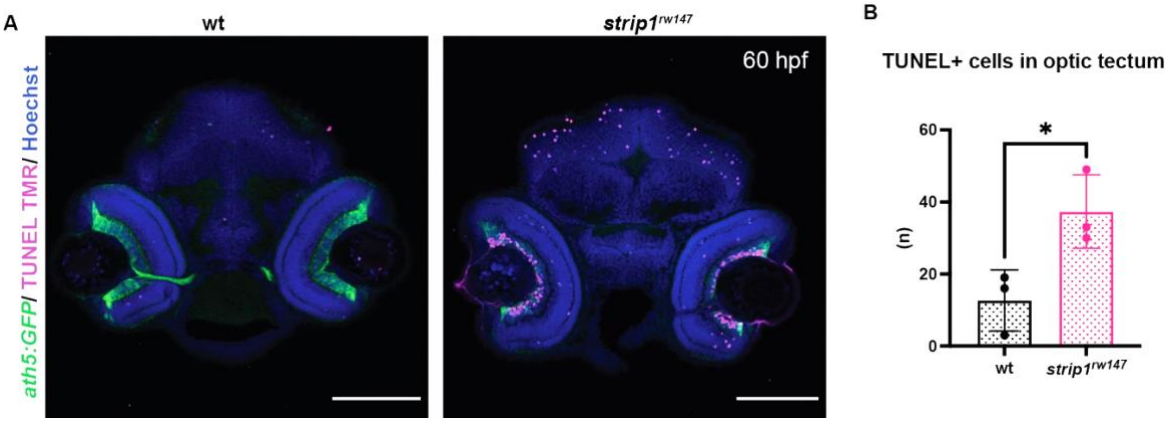

Figure 2.14. Cell death in the optic tectum of *strip1* mutants.

(A) TUNEL of 60 hpf wild-type and *strip1*^{rw147} mutant heads combined with *Tg[ath5:GFP] to* label RGCs. All nuclei are counterstained with Hoechst. Scale bar, 100 µm. (B) The number of TUNEL+ in the optic tectum. Student's t test with Welch's correction, n=3.

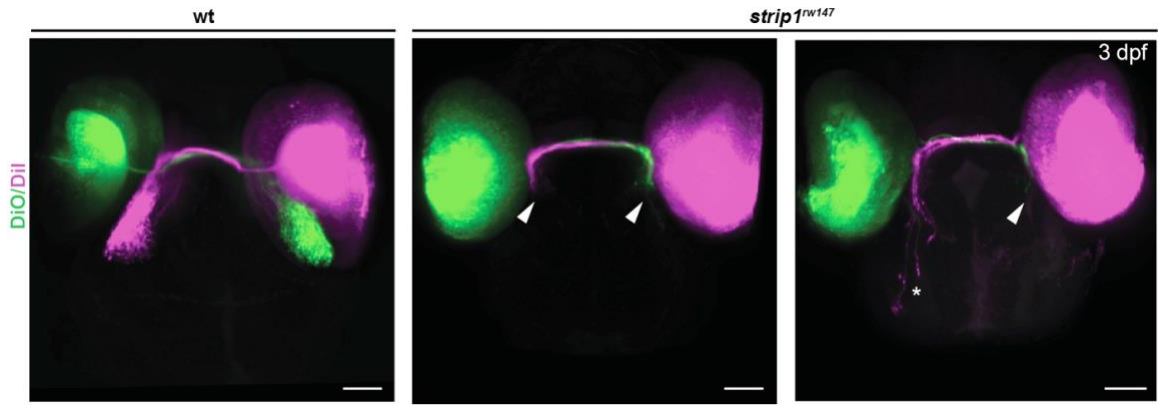

Figure 2.15. Defects in retinotectal projections of *strip1* mutants.

Dorsal view of the optic tectum of 3-dpf wild-type and *strip1*^{rw147} mutants. Most RGC axons fail to elongate properly and do not arborize within the optic tectum (arrowheads) or very few axons elongate poorly to reach more posterior arborization fields within the optic tectum (asterisk). Scale bar: 50 µm.

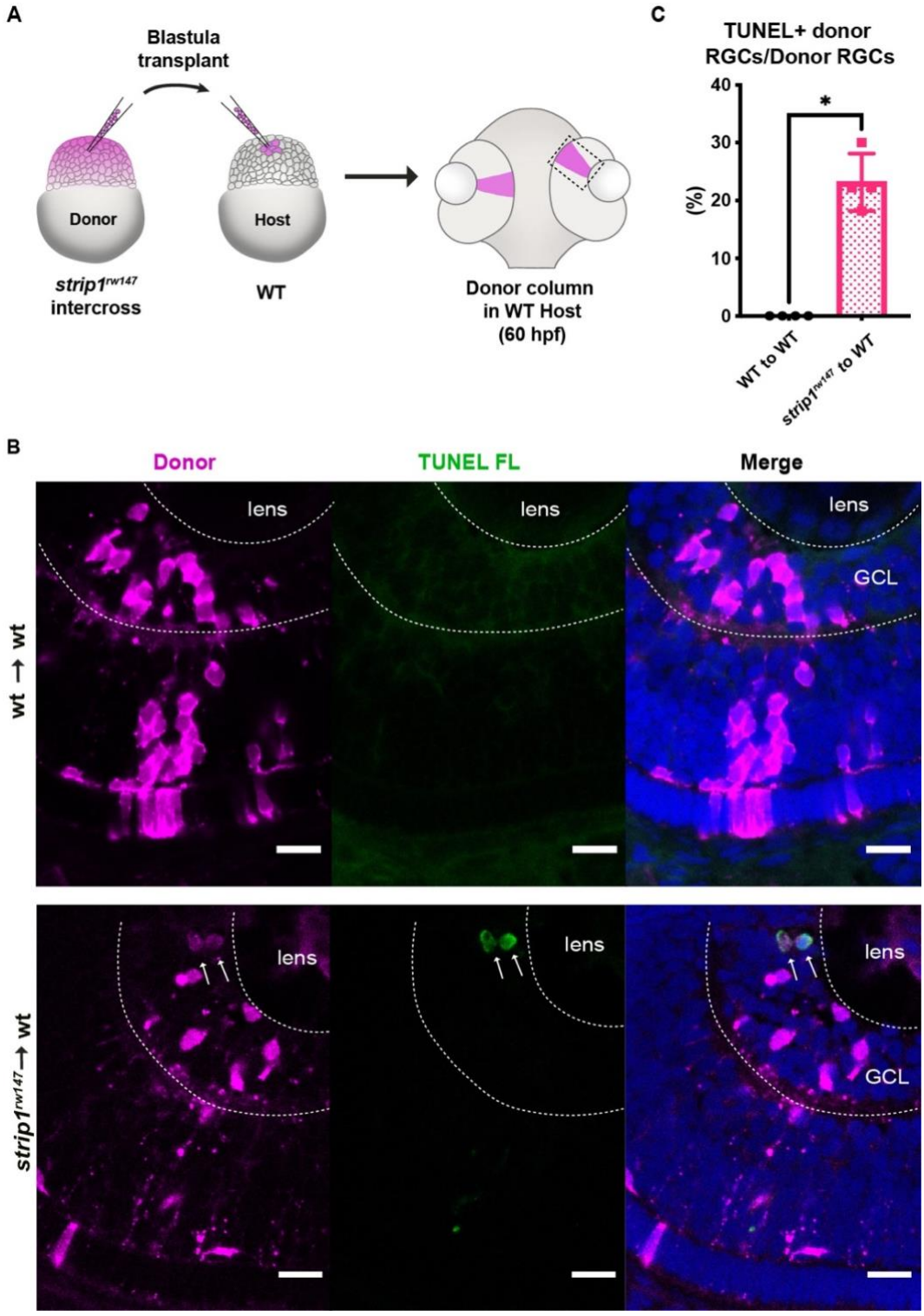

Figure 2.16. Strip1 is cell-autonomously required for RGC survival.

(A) Cell transplantation design to evaluate the cell autonomy of Strip1 in RGC survival. Donor embryos from a *strip1*^{rw147} mutant background are labeled with dextran rhodamine and transplanted into host wild-type embryos. Hosts that show transplanted retinal columns at 60 hpf were subjected to TUNEL. (B) 60-hpf host retinas stained with TUNEL FL to visualize apoptotic cells in wild type to wild type (upper panel) or *strip1*^{rw147} mutant to wild type (lower panel). Arrows indicate the presence of apoptotic donor cells. Scale bar, 10 µm. (C) Percentage of TUNEL+ donor RGCs relative to total donor RGCs. Mann-Whitney U test, n=4.

2.3.6. IPL defects occur downstream of RGC death

To clarify how loss of RGCs influences infiltration of amacrine cells into GCL and IPL disruption, I performed time-lapse imaging of retinas in *strip1*^{rw147} mutants combined with the transgenic line *Tg[ath5:GFP; ptf1a:mCherry-CAAX]*, to visualize RGCs and amacrine cells during development. At 48 hpf, there were no apparent differences in position or morphology of RGCs and amacrine cells between *strip1*^{rw147} mutants and wild-type siblings (**Figure** 2.17). At this stage, few ptf1a+ cells still retain bipolar like morphology. However, the majority lost their apical process and reside in the presumptive INL apical to RGCs, consistent with previous reports (Chow et al., 2015). Although previous histological examination of *strip1*^{rw147} mutant retinas revealed that cell death starts as early as 48 hpf, the number of apoptotic cells is likely too low to see changes in GCL at this stage.

In *strip1*^{rw147} mutants at around 52 hpf, RGCs started to disappear, creating empty spaces in the GCL (**Figure** 2.17, asterisks). However, amacrine cells were still located in the INL. At around 55 hpf, a rudimentary IPL was observed in the central retina of both wild-type siblings and *strip1*^{rw147} mutants. At around 59 hpf, amacrine cells started to invade the empty spaces in the GCL (**Figure** 2.17, arrows). Infiltration of amacrine cells into the GCL was more prominent at 62 hpf, resulting in formation of a fluctuating IPL. These findings suggest that loss of RGCs triggers infiltration of amacrine cells into the GCL in *strip1*^{rw147} mutants.

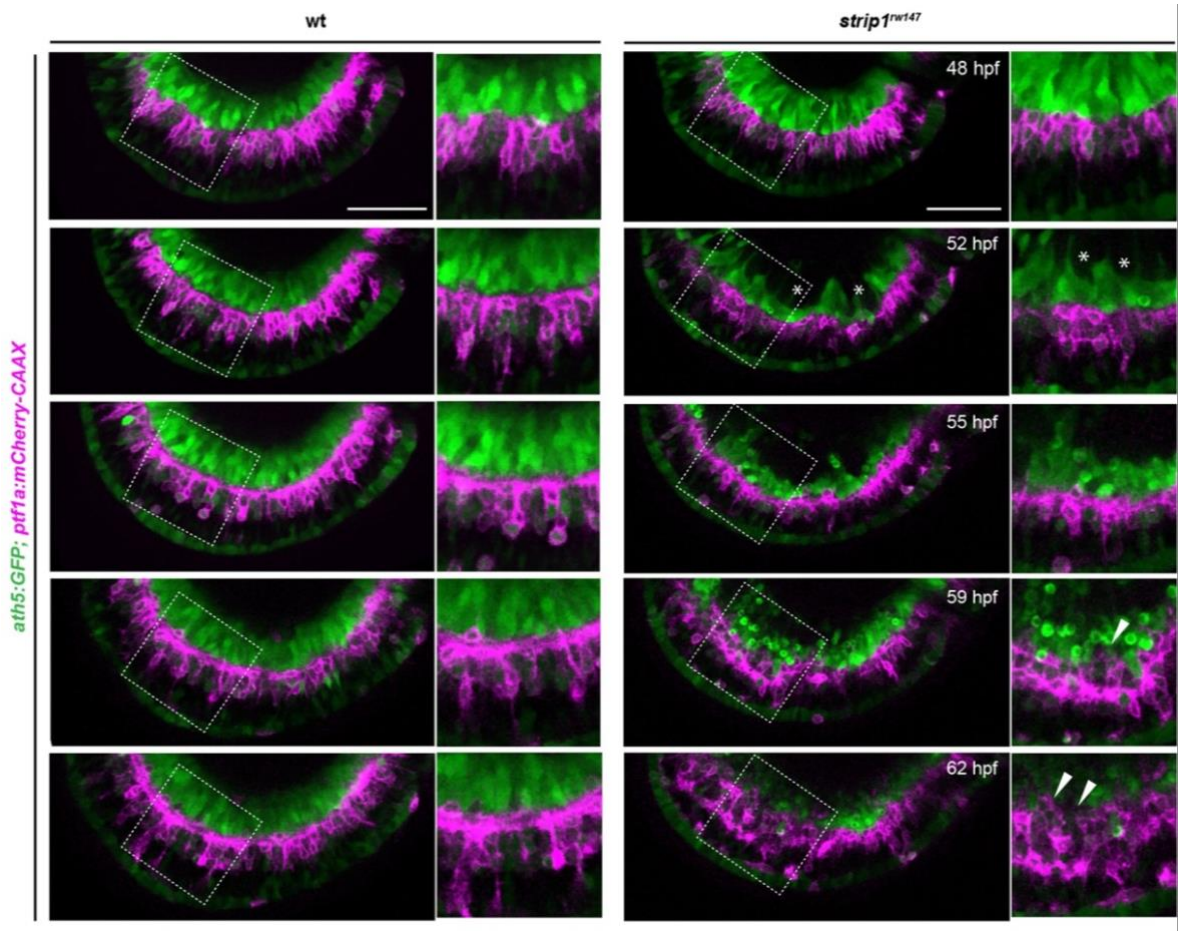

Figure 2.17. RGC death is followed by amacrine cell positioning defects and IPL malformation.

Figure 2.17. ***(continued)*** Time-lapse of wild-type and *strip1*^{rw147} retinas combined with the transgenic line *Tg[ath5:GFP; ptf1a:mCherry-CAAX]* to track RGCs and amacrine cells during IPL formation. Asterisks denote empty areas in the GCL. Arrowheads represent infiltration of ACs into empty spaces in the GCL. Scale bar, 50 μm.

2.3.7. Strip1 is non-cell autonomously required in INL cells for IPL formation

Amacrine cells are proposed to be the main cell type responsible for IPL formation (Godinho et al., 2005, Huberman et al., 2010). To examine whether Strip1 is required in amacrine cells for IPL development, I performed cell transplantation at the blastula stage using donor embryos carrying the transgene *Tg[ptf1a:mCherry-CAAX]* (**Figure** 2.18 **A**). Mutant amacrine cells transplanted into wild-type host retinas showed that most donor amacrines were normally positioned in the INL, and they extended their dendrites toward the IPL, as in the case of wild-type donor amacrine cells transplanted into a wild-type host retina (**Figure** 2.18 **B-D**). Occasionally, I observed three amacrine cells extending 2 dendritic trees instead of 1 among 73 transplanted amacrines; however, such dendritic mis-projection did not perturb IPL formation (**Figure** 2.18 **D**). On the other hand, as with mutant donor amacrine cells transplanted into mutant host retinas, when wild-type donor amacrine cells were transplanted to mutant host retinas, they showed irregular neurite projection with many somas abnormally located toward the basal side, resulting in IPL formation defects (**Figure** 2.18 **B-D**). These data suggest a non-cell autonomous function of Strip1 in amacrine cells for IPL formation.

Similarly, cell transplantation was conducted to assess the role of Strip1 in bipolar cells. Mutant donor bipolar cells labeled with the transgene *Tg[xfz43]* (Zhao et al., 2009) projected their axons toward a normal IPL in wild-type host retinas, in the same fashion as wild-type donor bipolar cells (**Figure** 2.19 **A-C**). Few transplanted columns of mutant donors showed extra lateral branching and excessive elongation of bipolar arbors (**Figure** 2.19 **C**, arrows). However, such arbor defects did not disrupt the IPL. On the other hand, when wild-type donor bipolar cells labeled with the transgene, *Tg[xfz3]*, were transplanted into a mutant host retina, they displayed neurite projection defects and their axons failed to project toward the mutant host IPL, but rather seemed to be guided toward the wild-type donor IPL (**Figure** 2.19 **D-F**). These findings suggest that Strip1 is not required in amacrine cells or bipolar cells for neurite projection to the IPL, although we cannot exclude the possibility that Strip1 is cell-autonomously required in a small subset of amacrine and bipolar cells to regulate dendritic branching and to limit neurite extension. Taken together, it is very likely that Strip1-mediated RGC maintenance is essential for proper neurite patterning of amacrine/bipolar cells and subsequent formation of the IPL.

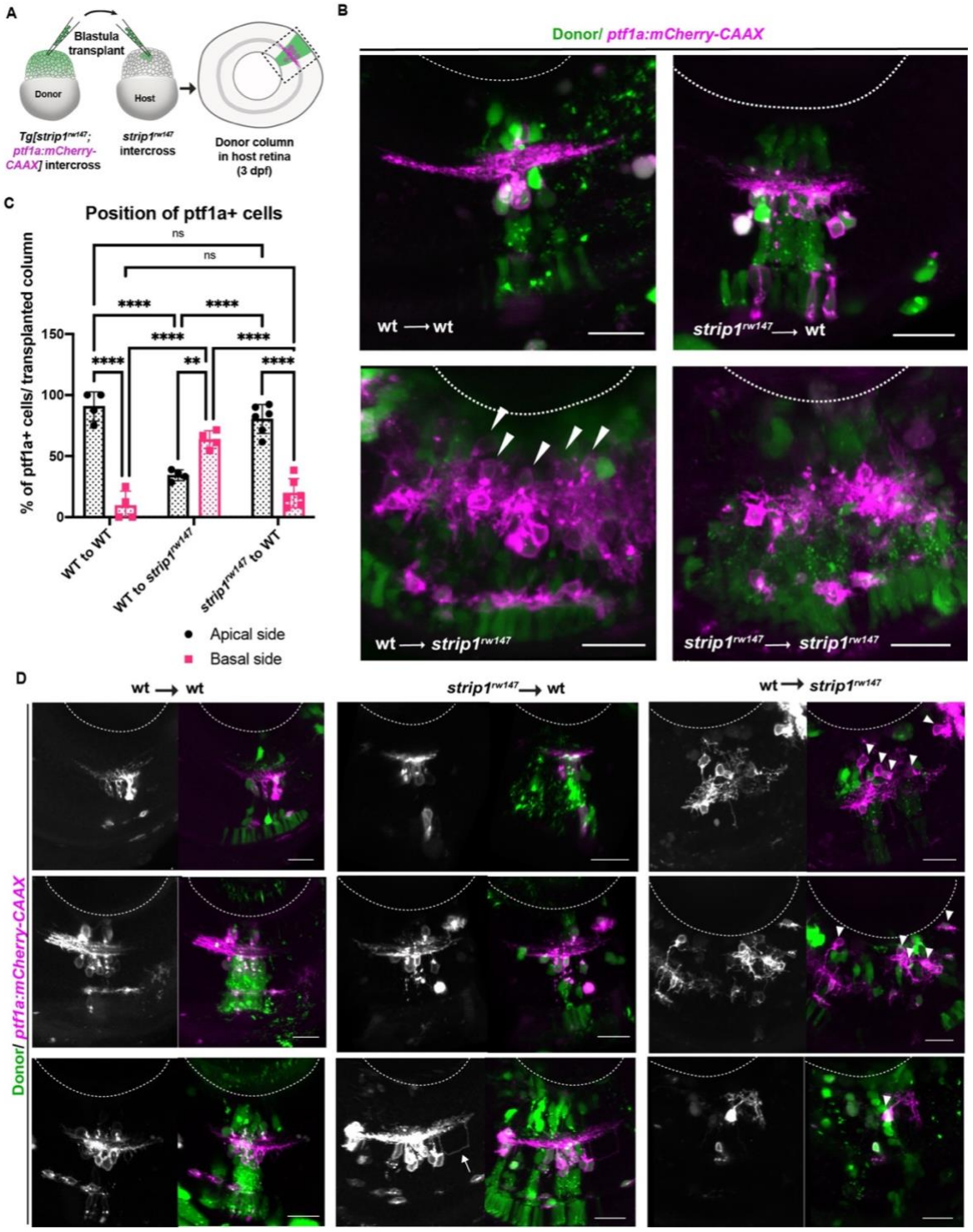

Figure 2.18. Strip1 is not cell-autonomously required in amacrine cells for IPL formation.

(A) Cell transplantation design to evaluate the cell autonomy of Strip1 in amacrine cell-mediated IPL formation. Donor embryos are from intercross of *strip1*^{rw147} heterozygous fish combined with *Tg[ptf1a:mCherry-CAAX]* to label amacrine cells. Host embryos are generated by non-transgenic intercross of *strip1*^{rw147}heterozygous fish. Donor cells are labeled with dextran Alexa-488 and transplanted into host embryos to make chimeric host retinas with donor-derived retinal columns. (B) Confocal images of four combinations of transplantation outcomes. Arrowheads represent abnormal positioning of amacrine cells in basal side of IPL. (C) Percentage of amacrine cells (either at the apical or the basal side of the IPL) relative to total number of amacrine cells within a transplanted column. Two-way ANOVA with the Tukey multiple comparison test, n≥4.

Figure 2.18. ***(continued)*** (D) 3D confocal live images showing a collage of different examples of transplant outcomes. Mutant donor amacrine cells show a normal dendritic pattern and normal projection to the IPL in wild-type host retina. On rare occasion, mutant amacrine cells display two dendritic trees (arrow in the bottom middle panel). Wild-type donor amacrine cells transplanted into mutant host retinas show abnormal projection patterns and infiltrate the GCL (arrowheads in the right panels). Scale bar, 20 µm.

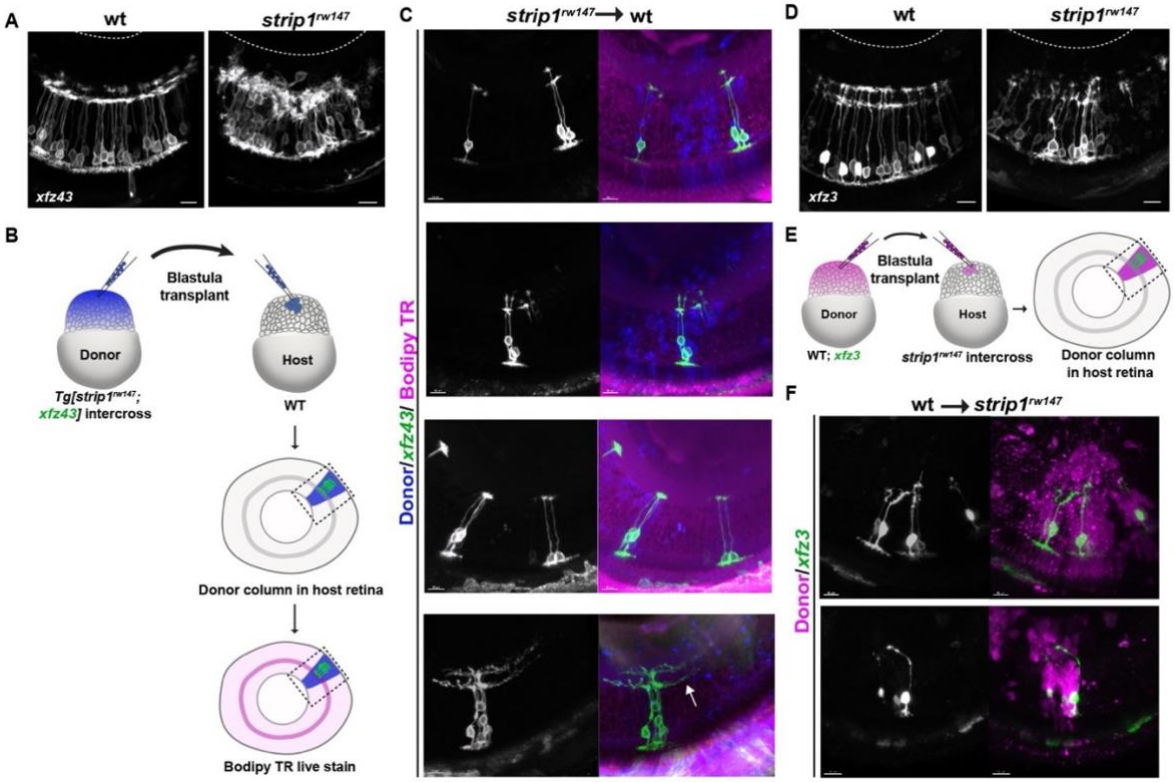

Figure 2.19. Strip1 is not cell-autonomously required in bipolar cells for IPL formation.

(A) Confocal images of 3-dpf live wild-type and *strip1*^{rw147} mutant retinas combined with the transgenic line, *xfz43*, to label subsets of bipolar cells. (B) Schematic drawings of cell transplantation design to evaluate cell autonomy of Strip1 in bipolar development. *strip1*^{rw147} mutant donor cells carrying the transgene *xfz43* (green) are labeled with dextran-cascade blue or dextran-Alexa-flour 647 (blue) and transplanted into wild-type host embryos at blastula stage, leading to chimeric wild-type retina with *strip1*^{rw147} mutant retinal columns. Retinal lamination of the host retina is visualized with Bodipy TR (magenta). (C) 3D live images of four wild-type host retinas with *strip1*^{rw147} mutant donor retinal columns outlined in (B). *strip1*^{rw147} mutant donor bipolar cells show normal neurite projection patterns to the IPL in wild-type host retina. Occasionally, bipolar axon terminals are abnormally extended laterally (arrow in the bottom panel). (D) Confocal image of 3-dpf live wild-type and *strip1*^{rw147} mutant retinas combined with the transgenic line, *xfz3*, to label subsets of bipolar cells. (E) Schematic drawings of cell transplantation design to evaluate the cell autonomy of Strip1 role in bipolar development. Wild-type donor cells carrying the transgene *xfz3* (green) are labeled with dextran-rhodamine (magenta) and transplanted into *strip1*^{rw147} mutant host embryos at blastula stage, leading to chimeric *strip1*^{rw147} mutant retinas with wild-type retinal columns. (F) 3D confocal live images of two different *strip1*^{rw147} mutant host retinas with wild-type donor retinal columns outlined in (E). Wild-type donor bipolar cells show misguided neurite projections. (A, C, D, F) Scale bar, 10 µm.

2.3.8. Strip1 is required for RGC neurite morphogenesis

The data presented so far suggest that Strip1 is not autonomously required within INL cells for IPL development. However, Strip1 functions cell-autonomously to promote RGC survival. Next, I sought to determine whether Strip1 is required cell-autonomously for RGC dendritic patterning. Answering this question was challenging because Strip1-deficient RGCs degenerate very early. Therefore, I carried out cell transplantation assay at the blastula stage using donor embryos from heterozygous *strip1*^{rw147} intercross carrying the transgene *ath5:GFP* to label RGC dendrites (**Figure** 2.20 **A**). I examined the dendritic phenotype in donor columns of host embryos between 57-58 hpf because at this stage, at least half of mutant RGC population hasn't undergone cell death yet. At the same time, at this stage, wild-type RGCs acquire apically directed dendritic patterns towards the nascent IPL.

Wild-type RGCs display normal dendritic patterns. The majority have one primary dendritic tree with diffuse arbors which seem to project towards a uniform layer when transplanted into wild-type host (**Figure** 2.20 **B).** A single axon existing basally can be observed in several cells (**Figure** 2.20 **A,** arrowheads). However, the majority of mutant RGCs show abnormal dendritic patterns when transplanted into wild-type hosts, they exhibit multiple distant dendritic trees, dendritic misguidance, and excessive branching/filopodia extensions (**Figure** 2.20 **C,** asterisks). In addition, many mutant RGCs do not project an axon or display axon defects like misguidance and bifurcation (**Figure** 2.20 **C**, red arrowheads). Collectively, these data propose a cell-autonomous role for Strip1 in RGC dendritic morphogenesis.

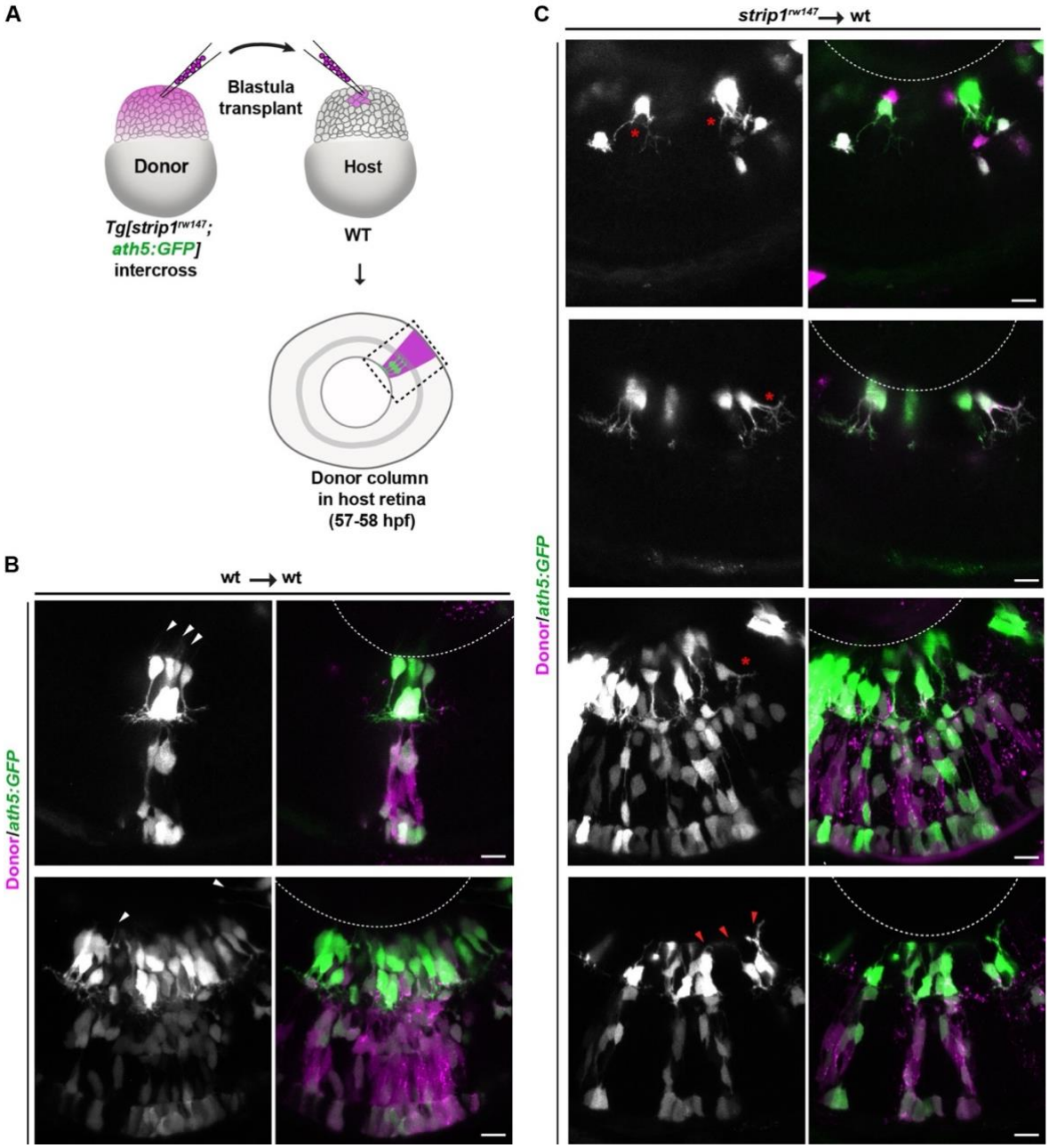

Figure 2.20. Strip1 is cell-autonomously required to promote RGC dendritic patterning.

(A) Schematic drawings of cell transplantation design to evaluate cell autonomy of Strip1 in RGC dendritic patterning. Donor cells from *strip1*^{rw147} heterozygous intercross carrying the transgene *ath5:GFP* (green) are labeled with dextran-rhodamine (magenta) and transplanted into wild-type host embryos. (B) Maximum projection images of wild type to wild type transplanted columns as outlined in (A), arrowheads depict RGC axons. (C) Maximum projection images of *strip1*^{rw147} to wild type transplanted columns. Asterisks show dendritic projection defects, red arrowheads depict RGC axon defects. Scale bar: 10 µm

I previously reported severe axon elongation defects of RGCs in *strip1*^{rw147} mutants at 3 dpf **(Figure** 2.15**),** which was expected because most of the population underwent significant apoptosis by this stage. However, cell transplantation assays suggest that mutant RGCs might have axon projection defects prior to cell death. To further investigate this phenotype, I aimed to track RGC axon projections at earlier timepoints prior to onset of apoptosis. RGCs axons exit the eyecup at 30-32 hpf and reach the optic chiasm between 34-36 (Burrill and Easter Jr, 1994). Imaging of RGC axon projection in wild type and *strip1*^{rw147} mutants was performed at three different timepoints; 36-38 hpf, 40-42 hpf, and 48-50 hpf. In both wild-type and mutant retinas, axons have already crossed the chiasm by 36 hpf. However, compared to wild-type siblings, mutant optic nerve is much thinner and the diameter at the chiasm is significantly smaller (**Figure** 2.21 **A and B**), which suggests that a fraction of RGC axons is delayed or fails to project properly.

To further confirm these findings, RGC axon projections were visualized at an earlier timepoint, 31-32 hpf, when axons have exited the eyecup but haven't crossed the chiasm yet. Based on our observations, the journey between axon exiting and crossing the chiasm is very rapid. Due to technical challenges with regards to the scanning time needed for imaging individual samples, there is considerable variation in axon projection length among different samples. However, we consistently observe shorter RGC axon projections in *strip1* mutants, compared to wild-type siblings (**Figure** 2.22 **A and B**)**.** Collectively, these findings strongly suggest that Strip1 is required for RGC axon elongation.

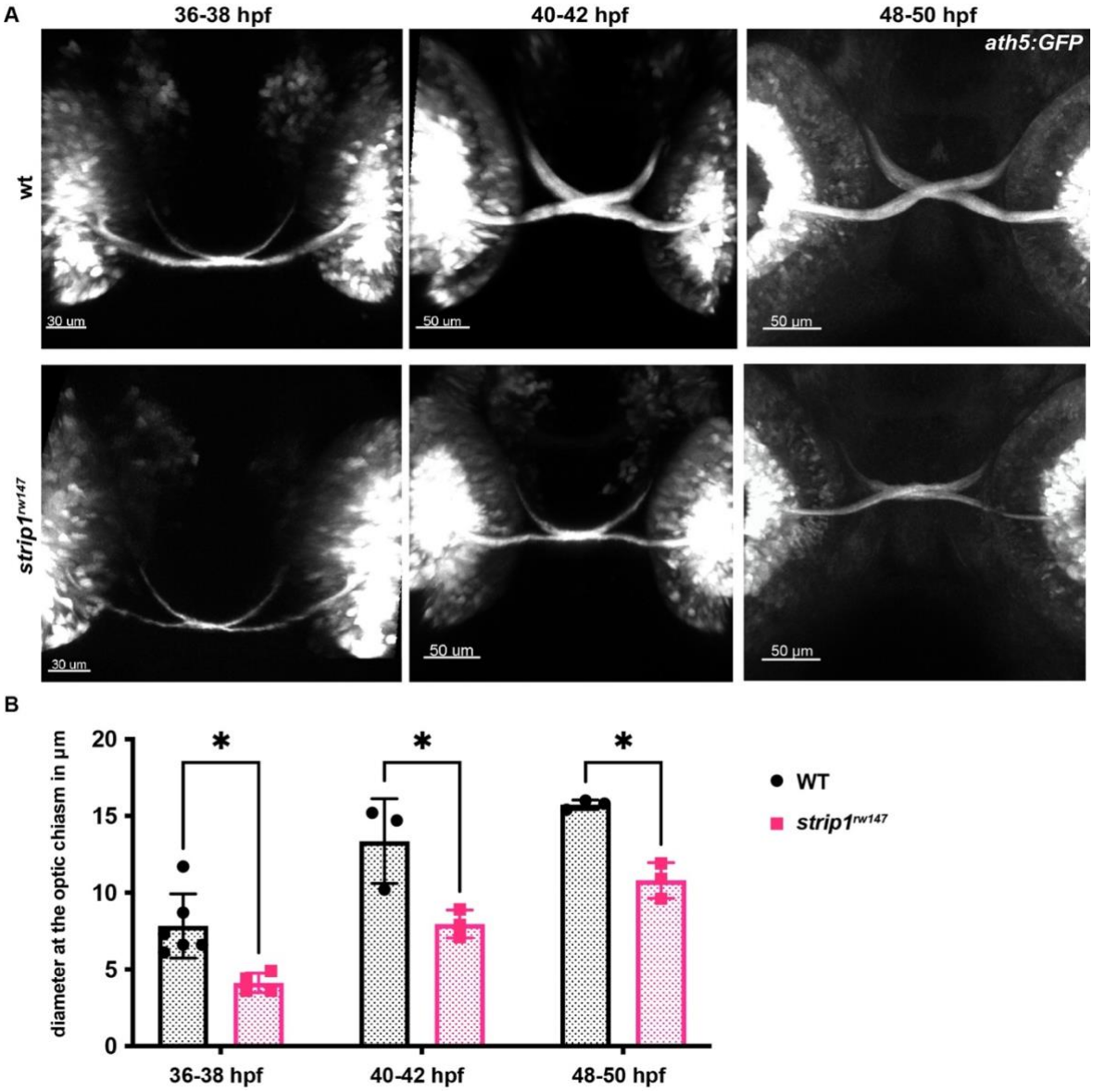

Figure 2.21. Optic nerve thinning in *strip1* mutants at early developmental stages.

(A) Maximum projection images showing ventral view of wild-type and *strip1*^{rw147} mutant retinas labeled with *ath5:GFP* to visualize RGC axon projections. Panels show samples imaged at different timepoints; 36-38 hpf, 40-42 hpf , and 48-50 hpf. (B) Quantification of optic nerve diameter at the chiasm. Two-way ANOVA with the Tukey multiple comparison test, n≥3.

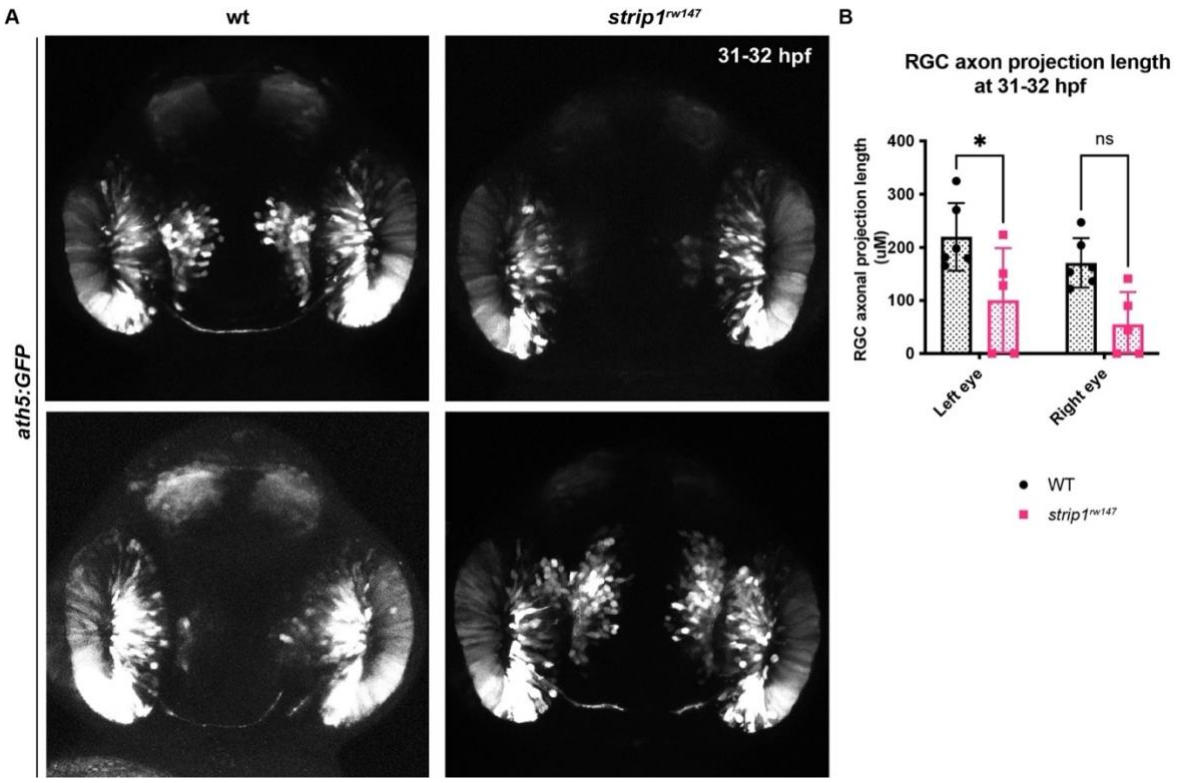

Figure 2.22. RGC axons of *strip1* mutants are delayed in their journey to the optic chiasm.

(A) Maximum projection images showing ventral view of wild-type and *strip1*^{rw147} mutant retinas labeled with *ath5:GFP* to visualize RGC axon projections at 31-32 hpf. (B) Quantification of the length of RGC axonal projections for both the left and right eyes. Two-way ANOVA with the Tukey multiple comparison test, n≥5.

2.4. Discussion

Over the past few years, Strip1/Strip has emerged as an essential protein in embryonic development by regulating diverse processes like cell migration, proliferation, cell fate specification, cytoskeletal dynamics, and endocytic trafficking (Bazzi et al., 2017, La Marca et al., 2019, Neal et al., 2020, Sakuma et al., 2014, Sakuma et al., 2015, Sakuma et al., 2016). So far, understanding the function of Strip1 in vertebrate nervous system development has been challenging due to the embryonic lethality of mouse Strip1 knockout models (Bazzi et al., 2017, Zhang et al., 2021). In this part of the study, I demonstrated a novel function of Strip1 in neural circuit wiring of the vertebrate inner retina, by maintaining RGCs during development.

In absence of Strip1, severe inner retinal lamination defects are observed, which are consistent with the predominant expression patterns of zebrafish Strip1 in inner retinal neurons (RGCs and amacrine cells). Using live imaging combined with histological assays, I showed that RGCs undergo dramatic cell death in *strip1* mutants, INL cells infiltrate the empty areas in GCL, and the IPL is disrupted. Several findings suggest that RGC death is the primary and main cause of the observed structural defects in the inner retina. First, time-lapse imaging shows that, invasion of amacrine cells into the GCL starts after RGC death and amacrine cells seem to invade empty areas within the degenerating GCL. Second, although IPL disruption is caused by neurite projection defects of INL cells, mainly amacrine cells, such defects occur due to a non-cell autonomous role of Strip1 in amacrine/bipolar dendritic patterning for IPL development. On the other hand, Strip1 is cell-autonomously required within RGCs for their survival. Collectively, these findings suggest that Strip1-mediated RGC maintenance is essential for laminar positioning of other retinal neurons and structural integrity of the IPL.

Amacrine cells are the main cells that pre-pattern a rudimentary IPL (Chow et al., 2015, Godinho et al., 2005). However, our findings, together with previous reports, suggest an active role for RGCs in this process. The phenotype of *strip1* mutants concedes with that of *lakritz* mutant in which similar amacrine positioning defects and transient IPL problems occur when RGC genesis is inhibited altogether (Kay et al., 2004). In addition, knockout mice in which atypical Cadherin Fat3 is absent in both RGCs and amacrine cells, amacrine cells invade the GCL abnormally. However, amacrine cell-specific knock out mice do not exhibit such positioning defects (Deans et al., 2011), which suggests that RGC-driven cues are necessary for proper amacrine cell positioning. Therefore, I re-introduce a model proposed by (Kay et al., 2004), in which both RGCs and amacrine cells play distinct roles in shaping the developing IPL. In this model, RGCs provide positional cues for migrating amacrine cells to initiate proper IPL program, whereas amacrine cells subsequently project their dendritic plexus and establish the foundation for a proto-IPL.

I observe similar inner retinal defects in *strip1* mutants and *ath5* morphants. However, the IPL defects of *strip1* mutants appear to be stronger. It was reported

that in *ath5 (lakritz)* mutants, the IPL defects are transient. During development, amacrine cells remodel their interactions to make an almost normal IPL (Kay et al., 2004). On the other hand, there are dynamic changes in amacrine-amacrine and amacrine-RGC interactions in *strip1* mutant retinas. Initially, most interactions are likely amacrine-RGC, but with time as RGCs degenerate, amacrine-RGC interactions are lost, and amacrine-amacrine interactions are increased. It is possible that such dynamic changes in *strip1* mutants render it more difficult for amacrine cells to remodel their dendrites, leading to severe IPL defects.

Our cell transplantation experiments demonstrate that Strip1 is cell-autonomously required for RGC dendritic patterning and axon elongation. In addition, Strip1 is likely to play a cell autonomous role on discrete populations of ACs and BPs to regulate the rate of branching or neurite extension. These findings are supported by previously established roles for *Drosophila* Strip in regulating dendritic branching and axon elongation of olfactory projection neurons (Sakuma et al., 2014). The underlying molecular mechanism is currently unknown. However, possible candidates are retrograde transport machinery and microtubule stabilization. *Drosophila* Strip is essential for recruitment of Rab5/early endosomes to retrograde transport system (Sakuma et al., 2014). Interestingly, in the *Xenopus* visual system, Rab5 was found to accumulate in axon growth cones of retinal ganglion cells and plays important role in its elongation (Falk et al., 2014). In other reports, Strip regulates neurite morphogenesis by stabilizing microtubules through the tripartite STRIP1-TBCD-DSCAM complex (Sakuma et al., 2015). Recently, mouse DSCAM was found to play critical role in retinal ganglion cell axon elongation and fasciculation (Bruce et al., 2017). Future studies on cell specific/conditional Strip1 knockout models will help us understand how Strip1 functions in retinal neurite morphogenesis and the molecular machinery involved.

We report that Strip1 is essential for both RGC survival and RGC dendritic/axonal patterning. Based on these findings, an important question must be addressed, does RGC death in *strip1* mutant occur independent of the observed neurite projection defects? Or RGC death occurs due to failure in connectivity? Secondary neuronal loss is a term that describes neuronal cell death due to loss of synaptic connections. This often happens due to disruption of retrograde transport of neurotrophic signals from post synaptic targets or failure of anterograde signaling from presynaptic inputs (Fricker et al., 2018). In fact, adult RGC degeneration is often a secondary defect in glaucoma and optic nerve injury models (Claes et al., 2019). In the developing wild-type zebrafish retina, based on our observations and published reports, RGCs start to project apically-directed dendrites between 55-60 hpf (Choi et al., 2010). In addition, our time-lapse imaging and other reports suggest that a nascent IPL is observed between 50-55 hpf (Chow et al., 2015, Kay et al., 2004), and synaptogenesis in the IPL starts at around 60 hpf (Schmitt and Dowling, 1999). However, in *strip1* mutants, significant apoptosis in the GCL occurs as early as 48 hpf, prior to normal dendritic stratification. Therefore, it is highly unlikely that RGC dendritic defects are linked to RGC death.

The question to be raised next is whether RGC axon elongation defects can cause the observed RGC cell death. Previous studies reported an acute and

significant loss of RGCs in neonatal rats following ablation of their post-synaptic target, the superior colliculus (zebrafish counter part of the optic tectum) (Claes et al., 2019, Harvey and Robertson, 1992). There are no clear reports on the requirement of retrograde signaling for survival of embryonic zebrafish RGCs and its exact timing. However, complete optic nerve transection in 5 dpf zebrafish larvae does not induce prominent RGC death (Harvey et al., 2019). Similarly, although disruption of Kinesin I motor protein in zebrafish *kif5aa* mutants leads to a delay in RGC axon innervation within the tectum, RGC population appears largely intact (Auer et al., 2015). In the developing zebrafish visual system, RGC axons begin to innervate the optic tectum between 44 and 48 hpf, and arborization is completed by 72 hpf (Burrill and Easter Jr, 1994, Stuermer, 1988). In *strip1* mutant RGCs, pro-apoptotic molecular signaling is probably initiated at/prior to 48 hpf and by 72 hpf, the majority of RGC population is lost. Taken together, the early onset and progressive degeneration of RGCs suggests that soma-mediated apoptosis, is the major cause of RGC death in *strip1* mutants. However, we cannot exclude the possibility that aberrant neurite projections and possible connectivity defects might play an additional contributing role.

Chapter 3.

Molecular signaling underlying Strip1 role in RGC survival

RGCs are the sole projection neurons of the retina. Their axons exit the eye cup to form the optic nerve, through which signals are conveyed to visual centers in the brain (D'Souza and Lang, 2020, Kolsch et al., 2021, Robles et al., 2014). RGCs are indispensable for vision. In knock out mouse and zebrafish models, when RGCs are absent or exhibit defects in axon projections, vision is compromised (Kay et al., 2001, Moshiri et al., 2008, Rick et al., 2000). Furthermore, RGC degeneration is often a secondary defect in optic neuropathies and a leading cause of blindness worldwide. Therefore, tremendous ongoing efforts are being dedicated to decipher and target signaling pathways involved in RGC death to maintain vision (Almasieh et al., 2012, Khatib and Martin, 2017, Munemasa and Kitaoka, 2012). The results of the phenotypic study have shown that Strip1 promotes RGC survival during development, which is important for maintaining the structural integrity of the IPL. However, the molecular mechanism that underlies Strip1 neuroprotective role within RGCs remains elusive.

In this chapter, I will provide a brief background on some of the known molecular mechanisms involved in RGC death. Afterwards, I will describe the proteomic, transcriptomic, and genetic approaches I used, which identified Striatin3 (Strn3) as Strip1-interacting partner with overlapping functions in RGC survival and Jun activation as a key mediator of RGC death in absence of Strip1.

3.1. Background

RGCs serve as essential communication channels between the retina and the brain. However, they are the most susceptible retinal neurons to cell death, both during development and in response to injury. During development, it is estimated that nearly 50% of mammalian RGCs undergo naturally occurring cell death during late gestation and early postnatal days (Bahr, 2000, Beros et al., 2018, Fawcett et al., 1984). Moreover, RGCs are the principal cell types that undergo cell death in response to different acute optic neuropathies, like optic nerve injury or chronic optic neuropathies as in the case of glaucoma (Almasieh et al., 2012, Munemasa and

Kitaoka, 2012, Qu et al., 2010). Over the past years, several molecular mechanisms underlying RGC death have been elucidated, with the hope to provide possible neuroprotective targets that could help mitigate RGC degeneration.

Deprivation of target-driven neurotrophic support is among the well-documented mechanisms that underlie developmental and injury-induced RGC death. Brain-derived neurotrophic factor (BDNF) and its receptor, Tropomyosin-related kinase B (TrkB) are among most reported pro-survival mechanisms involved (Almasieh et al., 2012, Johnson et al., 2009). Introduction of exogenous BDNF into the superior colliculus of newborn hamsters reduced the levels of developmental cell death in RGCs (Ma et al., 1998). Furthermore, Introduction of BDNF alone or in combination with TrkB promotes RGC survival in glaucoma and optic nerve injury models (Feng et al., 2016, Johnson et al., 2009, Martin et al., 2003, Osborne et al., 2018). The binding of BDNF to TrkB induces several pro-survival pathways, including extracellular signal-regulated kinase (ERK) 1/2, a member of mitogen-activated protein kinases (MAPK) (Cheng et al., 2002, Osborne et al., 2018). In addition, ERK1/2 activation slows RGC death in rat model of experimental glaucoma (Zhou et al., 2005). Taken together, BDNF/TrkB-mediated ERK1/2 activation is among the possible pro-survival mechanisms involved in RGC maintenance.

In contrast to the pro-survival role of ERK1/2 in RGCs, Jun N-terminal kinase (JNK) pathway, another member of the MAPK family, is an established pro-apoptotic factor in RGC death. JNK/c-Jun signaling is a key regulator of stress-induced apoptosis (Dhanasekaran and Reddy, 2008, Ham et al., 2000). Activation of the JNK pathway involves a series of phosphorylation events that ends with c-Jun phosphorylation and transactivation, which in turn activates *c-jun* gene expression (Eilers et al., 1998). C-jun is a transcription factor that induces pro-apoptotic genes like Bax and Bim (Harris and Johnson, 2001, Whitfield et al., 2001). Previous studies have reported the activation of JNK/c-jun signaling in RGCs in glaucoma and optic nerve injury models (Kwong and Caprioli, 2006, Levkovitch-Verbin et al., 2005, Wang et al., 2021, Yang et al., 2007). Furthermore, inactivation of Jun or inhibition of JNK signaling protects RGCs from degeneration in several glaucoma/ONI models (Fernandes et al., 2012, Sun et al., 2011, Syc-Mazurek et al., 2017a, Syc-Mazurek et al., 2017b).

Many reports using genetically modified mice models have implicated the intrinsic apoptotic pathway, which involves mitochondria dysfunction, in the pathogenesis of RGC degeneration. Members of the B-cell lymphoma 2 (Bcl2) family are known to mediate this process (Almasieh et al., 2012, Bahr, 2000, Maes et al., 2017). For example, overexpression of the anti-apoptotic proteins BCL2L1 (BCLx) and BCL-2 confers neuroprotection to RGCs during development, in response to axonal injury or in inherited glaucoma models (Bonfanti et al., 1996, Donahue et al., 2021, Harder et al., 2012). On the other hand, RGCs survive indefinitely in mice with deletion of the pro-apoptotic factor BCL2-associated X protein (BAX) following ONI.(Donahue et al., 2020, Libby et al., 2005). Collectively, different members of the Bcl2 family are key molecular checkpoints during RGC apoptosis in several acute and chronic glaucoma models.

3.2. Materials and methods

The resources used in the molecular study and their corresponding catalog numbers are listed in **Table 5.**

Table 5. List of resources used in the molecular study.

Name	Source or reference	Identifiers	Additional information
Mouse Zn5	ZIRC	ZDB-ATB-081002-19	1:50
Rabbit anti-p-Jun	Cell Signal	9164S	1:100
Rabbit anti-GFP	Thermo Fisher Scientific	A11122	1:500
Rabbit anti-Strn3	Thermo Fisher Scientific	PA5-31368	1:1000
Mouse anti-β-actin	MilliporeSigma	A5441	1:5000
Goat anti-rabbit Alexa 488 secondary antibody	Life Technologies	A11034	1:500
Goat anti-mouse Alexa 488 secondary antibody	Life Technologies	A11029	1:500
Goat anti-mouse Alexa 546 secondary antibody	Life Technologies	A11030	1:500
Goat anti-mouse Alexa 647 secondary antibody	Life Technologies	A21236	1:500
Hoechst 33342	Wako	346-07951	1:1000
Anti-rabbit IgG, HRP-linked Antibody	Cell Signaling	7074	1:5000
In Situ Cell Death Detection Kit, TMR Red	Roche	12156792910	
In Situ Cell Death Detection Kit, Fluorescein	Roche	11684795910	
Ethyl-3-aminobenzoate de methanesulfonate (Tricaine, MS-222)	Nacalai tesque	14805-82	
PTU (N-Phenylthiourea)	Nacalai tesque	27429-22	
GFP Trap Agarose	Chromotek	gta-20	
Arcturus PicoPure RNA Isolation Kit	Thermo Fisher Scientific	KIT0204	
NEB Next® Ultra™ II Directional RNA Library Prep Kit	New England BioLabs	E7760L	

Name	Source or reference	Identifiers	Additional information
Imaris	Bitplane	http://www.bitplane.com/imaris; RRID: SCR_007370	
Graphpad Prism v9.1.0.	Graphpad Prism	https://www.graphpad.com/scientific-software/prism/	
Proteome Discoverer	Thermo	https://www.thermofisher.com/store/products/OPTON-30945#/OPTON-30945	
STRING	(Szklarczyk et al., 2017)	https://string-db.org	
Metascape	(Zhou et al., 2019)	https://metascape.org	
R v3.4.2 , RStudio interface	(Team, 2016)	https://string-db.org	
BioVenn	(Hulsen et al., 2008)	http://www.biovenn.nl/	
Graphpad Prism v9.1.0.	Graphpad Prism	https://www.graphpad.com/scientific-software/prism/	

3.2.1. Transgenic fish lines

The transgenic lines used in the molecular study and the rationale for their use are described in **Table 6.**

Table 6. List of transgenic lines used in the molecular study.

Name	Description	Rationale	Reference
Tg[ath5:GFP]^{rw021}	GFP is expressed under control of the ath5 promoter.	To visualize RGCs	(Masai et al., 2003)
Tg[Ptf1a:mCherry-CAAX]^{oki067}	membrane-targeted mCherry is expressed under the control of ptf1a promoter	To visualize amacrine cells	This study
Tg[hsp:WT.Strip1-GFP]^{oki068}	GFP-tagged wild-type Strip1 at the C-terminus is expressed under control of the heat shock promoter.	To over express wild-type Strip1 for IP/MS experiment	This study
Tg[hsp:Mut.Strip1:GFP]^{oki069}	GFP-tagged *rw147* mutant form of Strip1 at the C-terminus is expressed under control of the heat shock promoter.	To over express mutant Strip1 as a negative control for IP/MS experiment	This study
Tg[hsp:Gal4;UAS:EGFP]	Generated by combining *Tg[hsp:gal4]^{kca4}* with *Tg[UAS:EGFP]* to express EGFP under control of the heat shock promoter	To over express GFP to be used as a negative control in IP/MS experiments	(Scheer et al., 2002) (Koster and Fraser, 2001)
Tg[hs:mCherry-tagged Bcl2]^{oki029}	mCherry-tagged Bcl2 at the N-terminal is overexpressed under control of the heat shock promoter	For Bcl2 overexpression in rescue experiments	ZDB-ALT-210524-5 (Nishiwaki and Masai, 2020)

3.2.2. Overexpression experiments

To generate samples for co-immunoprecipitation experiments, heat shock was applied to embryos from intercrosses of wild-type zebrafish combined with *Tg[hsp:WT.Strip1-GFP], Tg[hsp:Mut.Strip1:GFP]* or *Tg[hsp:Gal4;UAS:EGFP]*. To perform heat shock, embryos were incubated for 1 h at 39°C starting from 27-30 hpf and applied every 12 hours until 48 hpf. After screening for transgenic embryos based on GFP expression, embryos were processed for protein extraction. For Bcl2 rescue experiment, *Tg[hs:mCherry-tagged Bcl2]* was combined with *strip1^{rw147}* mutant line. Embryos from heterozygous intercross were subjected to heat shock treatment as described above to overexpress Bcl2. After screening for transgenic embryos, embryos were fixed in 4% PFA for histological assays.

3.2.3. Co-immunoprecipitation (CO-IP)

For co-immunoprecipitation, wild-type embryos carrying the transgenes *Tg[hsp:WT.Strip1-GFP], Tg[hsp:Mut.Strip1-GFP]* or *Tg[hsp:Gal4;UAS:GFP]* were exposed to 12-hr interval heat shocks starting at 27 hpf. At 2 dpf, embryo heads were dissected in Leibovitz's L-15 (L-15) medium. Lysates for each biological replicate were prepared from a pool of around 150 embryo heads in NP-40-based lysis buffer (150mM NaCl, 10 mM Tris (pH 7.5), 0.5 mM EDTA (pH 8), 0.5% NP-40 and 1× cocktail protease inhibitors), lysates were clarified by centrifugation at 10,000 g for 10 min at 4°C. Immunoprecipitation was performed on clarified lysates

using anti-GFP (GFP-Trap agarose beads, Chromotek) according to the manufacturer's protocol. Briefly, lysates were diluted in wash buffer (150mM NaCl, 10 mM Tris (pH 7.5), 0.5 mM EDTA (pH 8) and 1× cocktail protease inhibitors) to reach 0.1% NP-40. Then, incubated with pre-equilibrated GFP-Trap beads for 1 h at 4°C. Afterwards, beads were collected by centrifugation, washed in wash buffer 5 times, and processed for mass spectrometry analysis.

3.2.4. Mass spectrometry (MS) and data analysis

To prepare protein samples for MS analysis, immunoprecipitated protein complexes were eluted from GFP-Trap beads using an on-bead trypsin-based digestion protocol according to manufacturer's protocol. Digestion was performed overnight at 32°C and under rotation at 400 rpm. Afterwards, digested peptides were cleaned and desalted using C18 stage tips, as previously described (Rappsilber et al., 2007). Eluted peptides were vacuum-dried and re-constituted in 1% acetic acid, 0.5% formic acid for MS analysis using an Orbitrap-Fusion Lumos mass spectrometer coupled to a Waters nanoACQUITY Liquid Chromatography System. Samples were trapped on a nanoACQUITY UPLC 2G-V/M Trap 5 µm Symmetry C18, 180 µm × 20 mm column and analytical separation was performed on a nanoACQUITY UPLC HSS T3 1.8 µm, 75 µm × 150 mm column. Peptides were fractionated over a 60-min gradient from 1-32% acetonitrile with 0.1% formic acid. Solvent flow rate was 500 nL/min, and column temperature was 40°C.

Raw data files were analyzed using Proteome Discoverer (PD, v.2.2, Thermo Fisher Scientific). The SEQUEST algorithm was used to match MS data to the *Danio rerio* (zebrafish) database downloaded from UniProt (July 2021) and the common Repository of Adventitious Protein (cRAP, https://www.thegpm.org/crap). Database search parameters included carbamidomethylation of cysteine as fixed modification and oxidation of methionine, deamidation of glutamine and asparagine as dynamic modifications. Trypsin was specified as a cleavage enzyme with up to 2 missed cleavages. Normalization was performed based on specific protein amount (Trypsin) and proteins were filtered based on a false discovery rate of $q < 0.05$. Abundance ratios were generated for wild-type compared to mutant and wild-type compared to GFP control. Enriched proteins with an abundance ratio ≥ 2 and adjusted p-value <0.05 were considered statistically significant. Search Tool for the Retrieval of Interacting Genes/Proteins (STRING, v11.0) was used to visualize the Strip1-interaction network with the enriched proteins and calculate protein-protein interaction (PPI) value (Szklarczyk et al., 2017).

3.2.5. Western Blotting

To confirm that GFP-fused proteins were successfully pulled down after CO-IP, proteins were eluted from beads by boiling in 1x sample buffer for 5 mins. Then, 5% of pre-pulldown lysate (input) and 10% of the pulled-down proteins were run for western blotting using anti-GFP (1:500), as described in **2.2.7.**

To validate the specificity and efficiency of the newly designed MO-strn3, protein lysates were prepared from 2-dpf heads of standard morpholino-injected or

MO-strn3-injected wild-type embryos. Western blotting was performed as described in 2.2.7 using anti-Strn3 (1:1000) and anti- β-actin (1:5000).

3.2.6. RNA sequencing and analysis

Total RNA was isolated from 4 independent biological replicates of 60-64 hpf wild-type siblings and *strip1*^{rw147} mutant eye cups using a PicoPure RNA Isolation Kit (Thermo Fisher Scientific) according to the manufacturer's instructions. Each biological replicate represented a pool of eye lysates from 20-30 embryos. All samples had RNA integrity number (RIN) values greater than 8.5. The purified RNA was used for Poly(A)-selected mRNA library preparation with a NEBNext® Ultra™ II Directional RNA Library Prep Kit for Illumina and sequenced on a NovaSeq6000 SP to generate 150 bp paired-end reads. Sequencing reads were quality checked using FastQC (Andrews, 2010) and trimmed with FastP (Chen et al., 2018b). The resulting reads were mapped using hisat v2.1.0 (Kim et al., 2015). to the zebrafish reference genome (GRCz11). Mapped reads were counted using featureCounts, v1.6.2 (Liao et al., 2014) and differential gene expression analysis (Mutant vrs. Wild type) was carried out on the counts files using the EdgeR package, v3.32.1(Robinson et al., 2010) in RStudio, v1.4.1106 (Team, 2016). Genes with FDR <0.05 and Log2FC > |1| were considered statistically significant. EnhancedVolcano, v1.8.0 (Blighe et al., 2019) and pheatmap, v 1.0.12 (Kolde, 2012) packages were used to generate the volcano plot and heatmap, respectively. Gene Ontology analyses were performed using Metascape with *D. Rerio* as the input species and *M. Musculus* as the analysis species (Zhou et al., 2019). To analyze published scRNA sequencing data of zebrafish retina at 48 hpf, raw count matrices were analyzed with the Seurat package, v4.0.1(Satija et al., 2015) , as previously described (Xu et al., 2020). Clustering results were visualized using Uniform Manifold Approximation and Projection (UMAP). The BioVenn web application was used to generate Venn diagrams to compare Upregulated DEGs in this study with published upregulated DEGs in optic nerve injury models (Hulsen et al., 2008).

3.2.7. Morpholino knockdown assay

The embryos produced by intercrosses of wild-type or *strip1*^{rw147} heterozygous fish were injected with antisense morpholino oligonucleotides at 1-cell stage. Striatin3 morpholino (MO-strn3) was injected at a concentration of 250 µM, whereas MO-jun (Gan et al., 2008, Han et al., 2016). was injected at a concentration of 125 µM. For each morpholino experiment, the same concentration of the standard control morpholino (STD-MO) was used as a negative control. Detailed morpholino sequences are listed in **Table 7**.

Table 7. Sequences of morpholinos used in the molecular study.

Name	Sequence	Reference	Source/Identifier
STD-MO	5′-CCTCTTACCTCAGTTACAATTTATA-3′		Gene Tools
MO-strn3	5′- CCTGCTAGAAGTCGCCGATTGTTAC -3′	This study	Gene Tools
MO-jun	5' - CTTGGTAGACATAGAAGGCAAAGCG - 3'	ZDB-MRPHLNO-080908-1 (Han et al., 2016)	Gene Tools

3.2.8. Immunohistochemistry

Immunolabeling using cryosections was performed as previously described in **2.2.9.** Whole-mount immunostaining against p-Jun was performed following standard protocols (Ungos et al., 2003). To facilitate permeabilization, embryos were washed in distilled water three times for 30 mins each. Afterwards, blocking was done for 1 h at room temperature using the blocking solution (2% goat serum, 1% bovine serum albumin (BSA), 1% dimethylsulfoxide in BPTr buffer). Primary and secondary antibodies were incubated in blocking solution for 2-3 days at 4°C, with extensive washing in between with PBTr. After staining, embryos were washed in PBTr and mounted in 75% glycerol for confocal imaging. Details of antibodies used are described in **Table 5.**

3.2.9. Microscopy

Imaging of live, immunolabelled retinas and immunolabelled cryosections was performed as previously described in section **2.2.13.**

3.2.10. Quantification and statistical analysis

Quantification of ath5+ signal and the number of TUNEL+ cells was performed as previously described in **2.2.14**. To calculate the area of p-Jun signal in RGCs, an ROI containing the GCL was defined based on zn5 antibody signal (antigen: alcama, previously referred to as DM-GRASP) to exclude noise at the retina boundary. Masks were generated for the areas of p-Jun and zn5 signals and areas were quantified using Color Threshold tool in ImageJ. Signals from the lens were excluded from quantification. Data were represented as the percentage of p-Jun+ area to zn5+ area. Statistical analysis was performed as previously described in **2.2.14.**

3.3. Results

3.3.1. *rw147* mutant form of Strip1 fails to recruit the STRIPAK complex

Previous reports on Strip1 established that it functions as an adaptor molecule which gets recruited within different protein complexes to elicit different functions. To identify which molecules interact with Strip1 to regulate RGC survival, I conducted a co-immunoprecipitation experiment coupled with mass spectrometry (Co-IP/MS). Head lysates of wild-type embryos combined with the transgenic line *Tg[hsp:WT.Strip1-GFP]* were used to pull-down wild-type Strip1 and its interacting partners. As a negative control, I used lysates from 2 other lines; *Tg[hsp:Mut.Strip1-GFP]* and *Tg[hsp:Gal4;UAS:GFP]*, to rule out proteins enriched by the mutant form of Strip1 or by GFP alone (**Figure** 3.1 **A and B**).

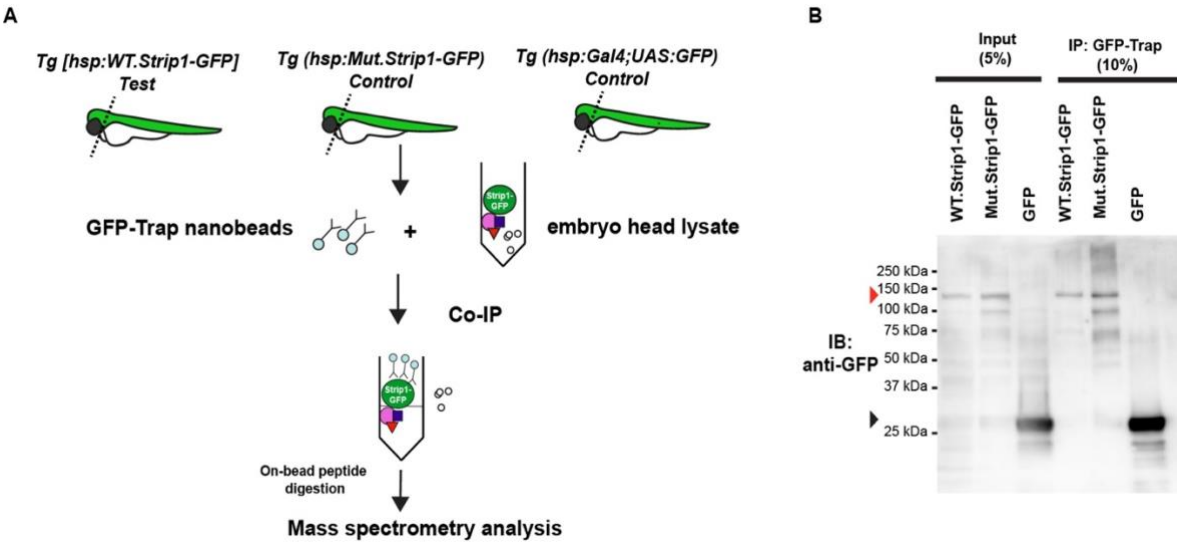

Figure 3.1. Design of Co-IP/MS experiment.

(A) Design of co-immunoprecipitation coupled with mass spectrometry (Co-IP/MS) to identify zebrafish Strip1-interacting partners. Embryos carrying the transgenes *Tg[hsp:WT.Strip1-GFP], Tg[hsp:Mut.Strip1-GFP] or Tg[hsp:Gal4;UAS:GFP]* were used to pull down wild-type GFP-tagged Strip1, mutant GFP-tagged Strip1 or only GFP, respectively. Head lysates from 2-dpf zebrafish embryos were subjected to immunoprecipitation using GFP-Trap beads. Immunoprecipitates were digested and analyzed by mass spectrometry. (B) Western blotting of whole head lysates (input) and immunoprecipitates (IP) using anti-GFP antibody. Red and black arrowheads indicate the expected band sizes for Strip1-GFP (~120 kDa) and GFP only (26 kDa), respectively.

Six proteins were enriched only by the wild-type Strip1, 5 of which are known components of the STRIPAK complex (**Figure** 3.2**. A-C**). Since none of these components has been studied in zebrafish, we analyzed previously published single-cell RNA sequencing data on transcriptomes from zebrafish embryonic retinas at 2 dpf (Xu et al., 2020), and found that *strip1* and *striatin3 (strn3)* mRNA are abundantly expressed in retinal cells (**Figure** 3.3**. A-G**)

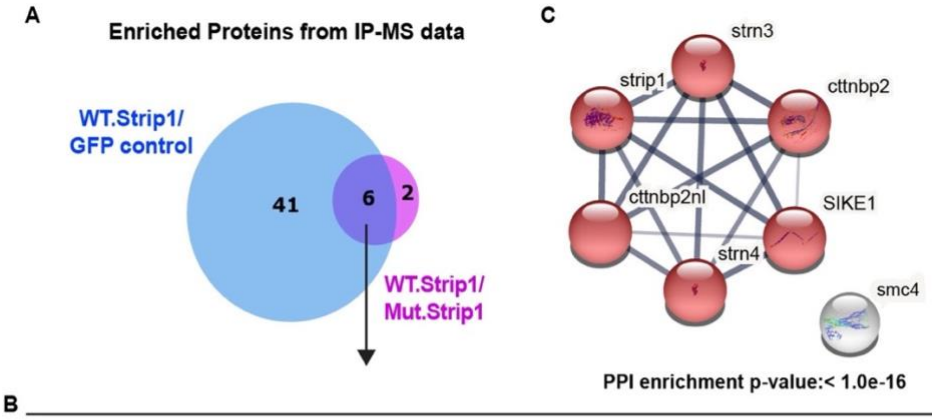

B

Uniprot accession	Gene name	Description	Abundance Ratio: (WT) / (CTRL)	Abundance Ratio: (WT) / (MUT)	Abundance Ratio Adj. P-Value: (WT) / (CTRL)	Abundance Ratio Adj. P-Value: (WT) / (MUT)
A0A2R8RT71	Cttnbp2nlb	CTTNBP2 N-terminal like b	14.103	3.698	2.7014E-13	4.3467E-08
F1QFV1	Cttnbp2	Cortactin binding protein 2	100	100	1.2157E-16	3.4667E-16
F1R1W1	Strn3	Striatin, calmodulin binding protein 3	27.748	7.824	1.2157E-16	3.4667E-16
A0A2R8QGU6	Strn4	Striatin, calmodulin binding protein 4	100	100	1.2157E-16	3.4667E-16
A0A0R4ISE8	Sike 1	Suppressor of IKBKE 1	5.575	2.952	1.632E-05	3.6751E-06

Figure 3.2. *rw147* mutant form of Strip1 fails to recruit STRIPAK components.

(A) Venn Diagram comparing proteins significantly enriched in WT.Strip1-GFP relative to control GFP (blue) and WT.Strip1-GFP relative to Mut.Strip1.GFP (magenta). Six proteins are commonly enriched in both groups, FC>2, $p < 0.05$. n=3 for WT.Strip1-GFP and Mut. Strip1-GFP and n=2 for GFP-control. (B) Five components of the STRIPAK complex found from six proteins commonly enriched in (A). (C) STRING protein-protein interaction (PPI) network analysis of six zebrafish Strip1 interacting partners significantly enriched from IP-MS analysis in (A). Network edges represent known and/or predicted functional interactions in the STRING database. Edge thickness reflects the combined STRING evidence score for each binary relationship. Thicker edges represent increased interaction evidence. PPI enrichment p-value <1.0e-16.

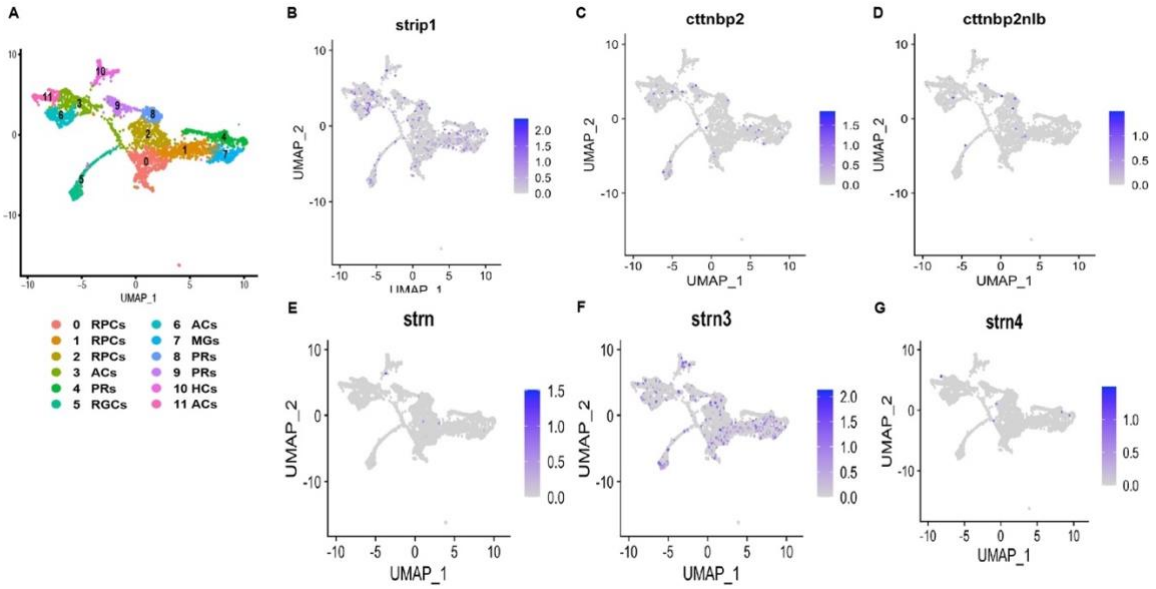

Figure 3.3. scRNA seq analysis of 2 dpf zebrafish retina showing expression of enriched STRIPAK components.

(A) UMAP plot showing different clusters of retinal cells at 48 hpf analyzed with Seuret R pipeline using data published by Xu B. et al, 2020. Twelve clusters are identified and categorized to different retinal cell types or sub-types. RPCs, retinal progenitor cells; RGCs, retinal ganglion cells; ACs, amacrine cells; BPs, bipolar cells; HCs, horizontal cells; PRs, photoreceptors; MGs, Müller glia. (B-G) UMAP plots showing retinal mRNA expression patterns of *strip1* (B), and its interacting STRIPAK components, identified from Co-IP/MS; *cttnbp2* (C), *cttnbp2nlb* (D), *strn* (E), *strn3* (F) and *strn4* (G), *strip1* and *strn3* show high retinal expression levels at 48 hpf compared to other partners.

3.3.2. Strip1 interacts with Strn3 to promote RGC survival

Striatins are core components of the STRIPAK complex, and they represent the regulatory subunit essential for complex assembly. Since Strn3 is the only striatin that shows retina-specific expression pattern, I knocked down Strn3 using morpholinos (MO-Strn3) to investigate its genetic interaction with Strip1 in RGC survival (**Figure** 3.4 **A-F**). I confirmed that MO-Strn3 can specifically and efficiently knock down zebrafish Strn3 (**Figure** 3.4 **A**). I observed a significant increase in apoptotic cells in the GCL of *strn3* morphants at 60 hpf (**Figure** 3.4 **B and C**). This leads to a significant reduction in RGCs at 60 and 76 hpf, as assessed by the ath5:GFP signal (**Figure** 3.4**. D-F**) Although *strn3* morphants showed similar RGC loss to *strip1* mutants, it was weaker. In addition, IPL defects were also milder in *strn3* morphants than in *strip1*^{rw147} mutants at 76 hpf (**Figure** 3.4 **D**). Taken together, this data suggests that Strip1 interacts with Strn3, probably in the context of STRIPAK complex. Such interaction most likely promotes RGC survival during development.

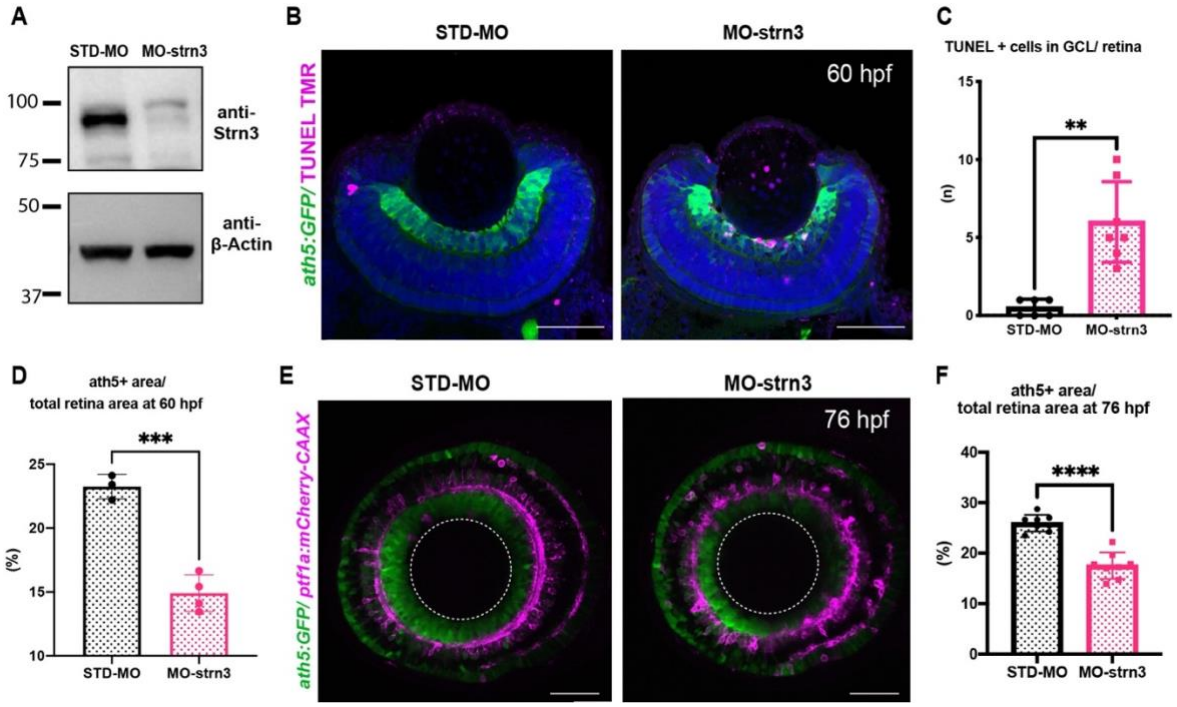

Figure 3.4. Strn3 knockdown leads to RGC death.

(A) Western blotting of 2-dpf head lysates from standard morpholino-injected and MO-strn3 injected wild-type embryos. (B) TUNEL of 60-hpf retinas of *Tg[ath5:GFP]* transgenic embryos injected with standard MO (STD-MO) and MO-Strn3. RGCs and apoptotic cells are labeled with *ath5:GFP* and TUNEL, respectively. Nuclei are stained with Hoechst (blue). (C) The number of TUNEL+ cells in GCL. Mann-Whitney U test, n≥6. (D) Percentage of ath5+ area relative to total retinal area at 60 hpf. Student's t test with Welch's correction, n≥3. (E) Confocal images of retinas of 76-hpf *Tg[ath5:GFP; ptf1a:mCherry-CAAX]* transgenic embryos injected with STD-MO and MO-Strn3. *ath5:GFP* and *ptf1a:mCherry-CAAX* label RGCs and ACs, respectively. (F) Percentage of ath5+ area relative to total retinal area at 76 hpf. Student's t test with Welch's correction, n=8.

3.3.3. Transcriptomic changes in *strip1* mutant eye cups

To determine what cell death mechanisms are activated in absence of Strip1 and the larger STRIPAK complex, I performed bulk RNA sequencing on transcriptomes from 62-hpf eye cups of *strip1*^{rw147} mutants. Compared to wild-type siblings, *strip1* mutants had 131 significantly upregulated genes and 75 downregulated genes (**Figure** 3.5 **A and B**, $\log_2$FC>|1|, and FDR<0.05). Most downregulated genes were markers of RGCs, like *isl2b*, *pou4f3* (also known as *brn3c*) and *tbr1b*, which reflects the reduction in RGCs. Genes related to synaptic development and transmission were also downregulated like glutamate receptors and potassium channels (**Figure** 3.5 **A-D**). On the other hand, many of the significantly upregulated genes were related to apoptosis, oxidative phosphorylation, cellular response to stress, and MAPK signaling pathway.

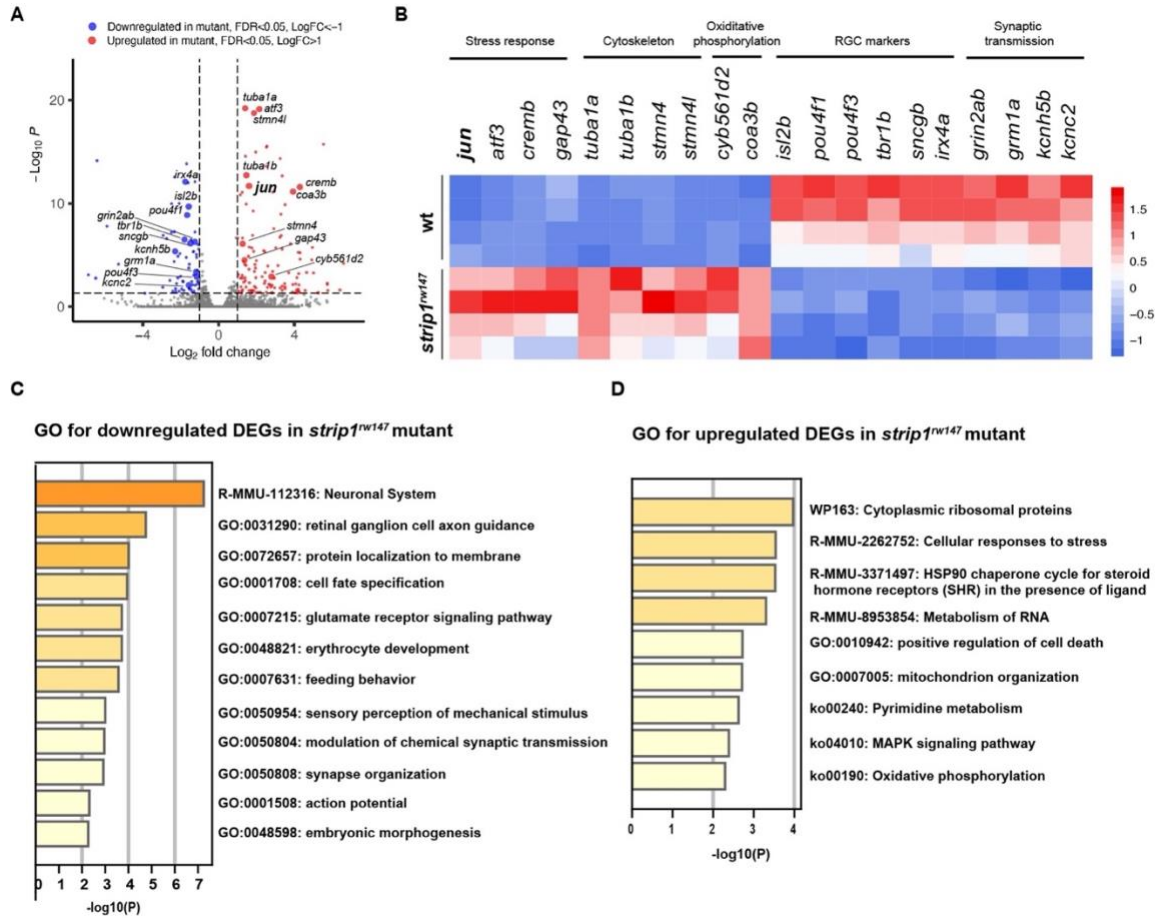

Figure 3.5. Transcriptomic changes in *strip1* mutant eyes.

(A) Volcano plot showing differentially expressed genes (DEGs) in *strip1*^{rw147} mutants compared to wild-type siblings. Colored points represent genes that are significantly upregulated (131 genes, red) or downregulated (75 genes, blue). Data are obtained from four independent collections of 62-hpf embryo eye cups. FDR<0.05, $Log_2FC > |1|$. (B) Heatmap of expression values (z-score) representing selected DEGs in *strip1*^{rw147} mutants compared to wild-type siblings. (C-D) List of enriched GO terms in DEGs downregulated (C) and upregulated (D) in *strip1*^{rw147} mutant relative to wild-type siblings as analyzed with Metascape, FDR<0.05 and $Log_2FC > |1|$.

Most reports on RGCs undergoing stress are in glaucoma and optic nerve injury models, where adult RGCs undergo cell death in response to injury (Bahr, 2000). Therefore, I compared the transcriptomic profiles of *strip1* mutant eyes to those of adult zebrafish RGCs following optic nerve injury (Veldman et al., 2007) or adult eyes after optic nerve crush (McCurley and Callard, 2010). Indeed, there were several genes commonly upregulated in all three models, namely, *jun*, *atf3*, *gap43*, *stmn4*, *sox11b*, and *adcyap1b* (**Figure** 3.6). These findings suggest that Strip1-deficient zebrafish RGCs share a similar stress response with adult RGCs following optic nerve injury.

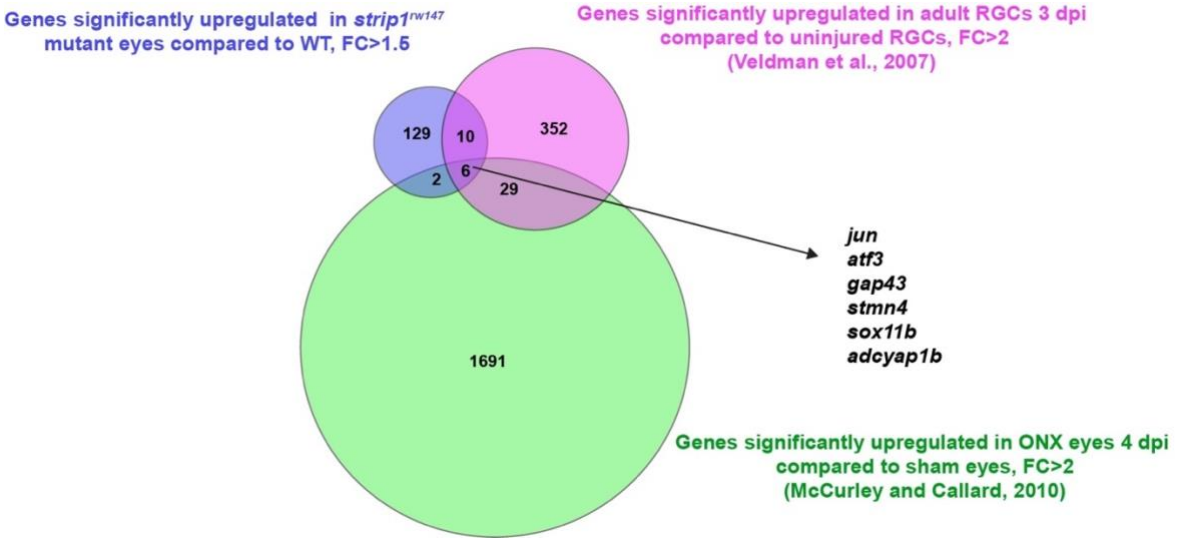

Figure 3.6. Comparison between transcriptomes of *strip1* mutant eyes and published optic nerve injury models.

Venn diagram showing overlap of upregulated DEGs in RNA sequencing datasets of *strip1*^{rw147} mutant relative to wild-type (FDR<0.05 and FC >1.5) in comparison with published upregulated DEGs in microarray data of adult zebrafish RGCs at 3 days post-optic nerve injury (ONI) (Veldman et al., 2007) and adult zebrafish eyes at 4 days-post optic nerve crush (ONX) (McCurley and Callard, 2010).

3.3.4. Jun is activated in RGCs of *strip1* mutants

In *strip1*^{rw147} mutants, *jun* was among the top upregulated stress response markers. Jun (the zebrafish homolog of mammalian c-Jun) is the canonical target of the Jun N-terminal kinase (JNK) pathway. Activation of the JNK pathway induces c-Jun phosphorylation and transactivation, which in turn activates *c-jun* gene expression (Eilers et al., 1998). To examine whether Jun signaling is activated in *strip1* mutants, I stained *strip1*^{rw147} mutant retinas with anti-phosphorylated c-Jun (p-Jun) antibody. At 54 hpf, *strip1*^{rw147} mutants showed significantly elevated levels of p-Jun compared to wild-type siblings. This elevation is specifically localized in RGCs visualized with zn5 antibody (**Figure** 3.7 **A and B**). Since Strip1 and Strn3 show overlapping function in RGC survival, I examined Jun activation in *strn3* morphants. Likewise, p-Jun was significantly elevated in RGCs of *strn3* morphants at 49 hpf compared to control injected embryos (**Figure** 3.7 **C and D**).

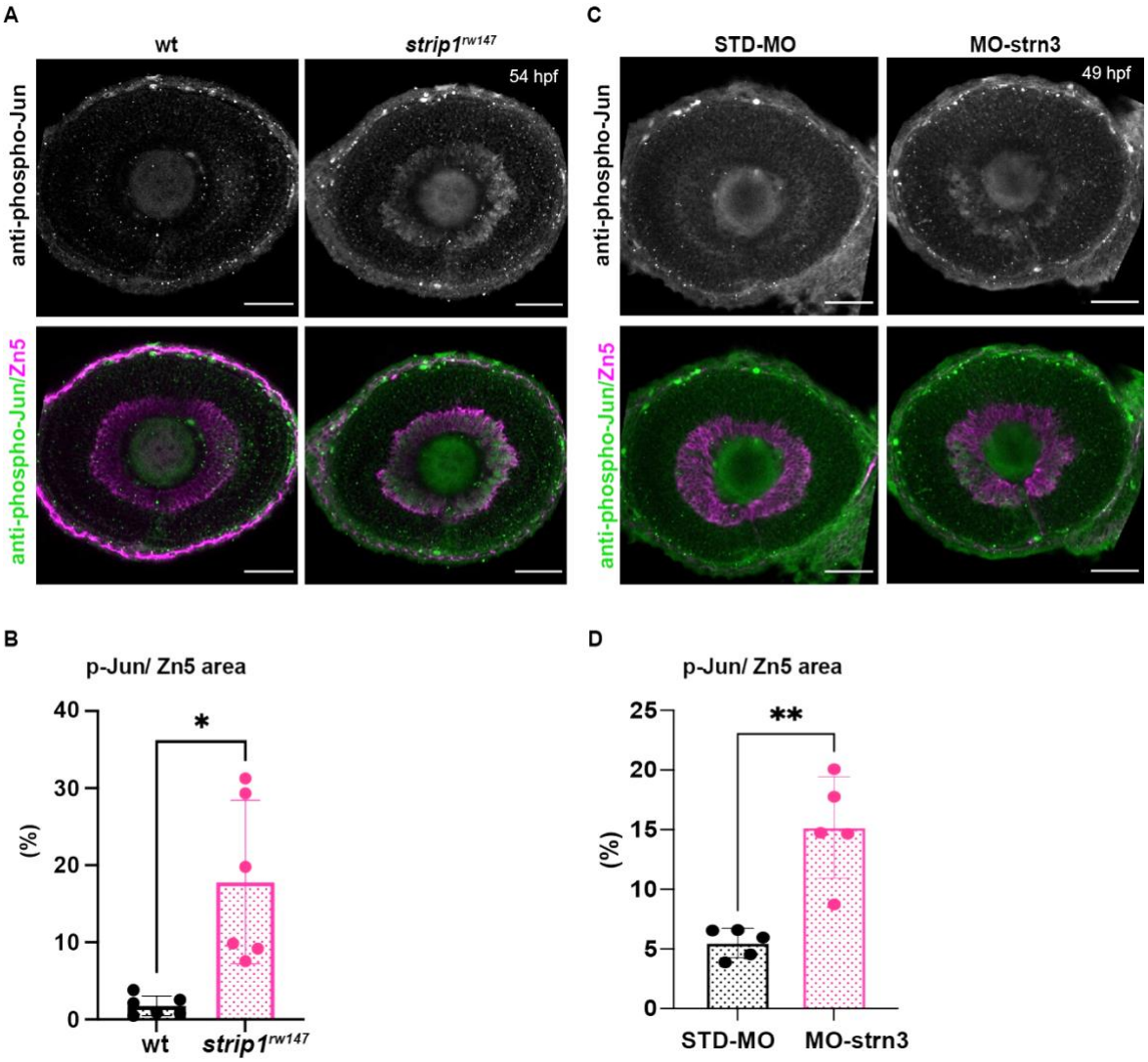

Figure 3.7. Jun is activated within RGCs of *strip1* mutants.

(A) Whole-mount labeling of 54-hpf wild-type and *strip1*^{rw147} mutant retinas with anti- phospho-Jun antibody and zn5 antibody, which label active Jun and RGCs, respectively. (B) Percentage of phospho-Jun area relative to zn5 area at 54-58 hpf. Student's t test with Welch's correction, n=6. (C) Whole-mount labeling of 49-hpf wild-type embryos injected with standard MO or MO-strn3 with anti-phospho-Jun antibody and zn5 antibody, respectively. (D) Percentage of phospho-Jun area relative to zn5 area at 49 hpf. Student's t test with Welch's correction, n=5.

3.3.5. Jun knock down rescues RGC death in *strip1* mutants

Next, I examined if Jun activation is related to RGC death in *strip1* mutants by performing Jun knock down using targeted morpholino (MO-jun) (Han et al., 2016). At 60 hpf, the number of apoptotic cells within the GCL of *strip1*^{rw147} mutants was significantly reduced upon Jun knockdown, when compared to *strip1*^{rw147} mutants injected with a standard control morpholino (**Figure** 3.8 **A and B**). This rescue was evident at 76 hpf as RGC population of *strip1*^{rw147} mutants was partially but significantly recovered to reach 18.29±1.5% of total retinal area compared to 25.78±0.57% in wild-type siblings, while RGCs of *strip1*^{rw147} mutants injected with a standard control morpholino were only 6.82±3.5% of total retinal area (**Figure** 3.8 **C and D**). Taken together, our findings show that Strip1, probably in the context of

the STRIPAK complex, suppresses Jun-mediated apoptotic signaling in RGCs during development.

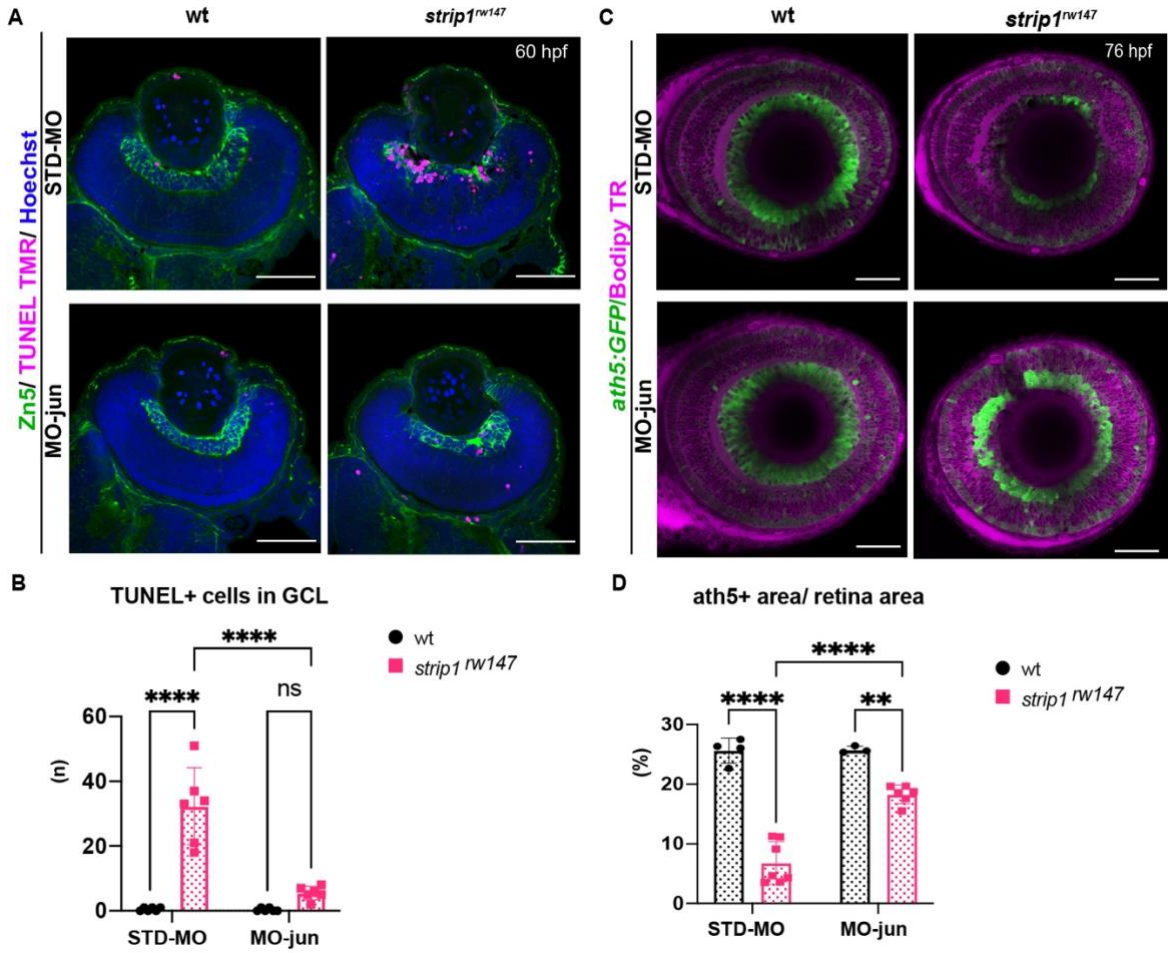

Figure 3.8. Jun knockdown rescues RGC death in *strip1* mutants.

(A) TUNEL and zn5 antibody labeling of 60-hpf wild-type and *strip1*^{rw147} mutant retinas injected with standard MO and MO-Jun. Nuclei are stained with Hoechst. (B) The number of TUNEL+ cells in GCL per retina. Two-way ANOVA with the Tukey multiple comparison test, n=6. (C) Confocal images of 76-hpf wild-type and *strip1*^{rw14} mutant retinas injected with standard-MO and MO-Jun. Embryos carry the transgene *Tg[ath5:GFP]* to label RGCs and are stained with bodipy TR methyl ester to visualize retinal layers. (D) Percentage of ath5+ area relative to total retinal area, Two-way ANOVA with the Tukey multiple comparison test, n≥3.

3.3.6. Bcl2 rescues RGC death in *strip1* mutants

The anti-apoptotic B-cell lymphoma 2 (Bcl2) is a key regulator of mitochondria-dependent apoptosis in neurons, both during survival and in response to injury (Anilkumar and Prehn, 2014). In addition, BCL-2 overexpression has demonstrated neuroprotective roles against RGC death in several models of optic nerve damage (Bahr, 2000, Bonfanti et al., 1996, Maes et al., 2017). Moreover, JNK/c-Jun activation induces neuronal apoptosis by modulating different members of the BCL2 family proteins (Guan et al., 2006, Hollville et al., 2019, Whitfield et al., 2001). To this end, I examined whether Bcl2 overexpression could rescue RGC death in absence of Strip1. Thus, I combined *strip1*^{rw147} mutants with the transgenic line *Tg[hsp:mCherry-Bcl2],* which overexpresses mCherry-tagged Bcl2 protein under control of a heat

shock promoter (Nishiwaki and Masai, 2020). Bcl2 overexpression significantly inhibited RGC apoptosis in *strip1*^{rw147} mutants (**Figure** 3.9 **A and B**). Accordingly, at 78 hpf, RGCs were partially but significantly recovered in *strip1*^{rw147} mutants overexpressing Bcl2 to reach 18.35±1.84% of total retinal area compared to 9.74±1.85% in non-transgenic mutants (**Figure** 3.10 **A and B**). Therefore, loss of RGCs in *strip1*^{rw147} mutants depends on the mitochondria-mediated apoptotic pathway.

Surprisingly, *strip1*^{rw147} mutants overexpressing Bcl2 still displayed IPL defects. In this case, the IPL was not formed at the interface between surviving RGCs and amacrine cells, but instead, a thin IPL-like neuropil was ectopically formed in the intermediate position of presumptive amacrines (Figure 3.10). Thus, a fraction of presumptive amacrine cells were abnormally located between surviving RGCs and IPL-like neuropil, although this amacrine cell fraction does not intermingle with surviving RGCs (**Figure** 3.10 **A**, bottom panels, asterisks). Consistent with previous observations from cell transplantation experiments, surviving RGCs in *strip1*^{rw147} mutants show defects in dendritic projection to the IPL-like thin neuropil. Upon closer examination, few surviving RGCs successfully innervate the IPL, and such areas show less infiltration of amacrine cells (**Figure** 3.10 **A**, bottom panels, arrow heads). These data further validate the importance of Strip1 in dendritic patterning of RGCs, which is likely to prevent ectopic IPL-like neuropil formation in the amacrine cell layer.

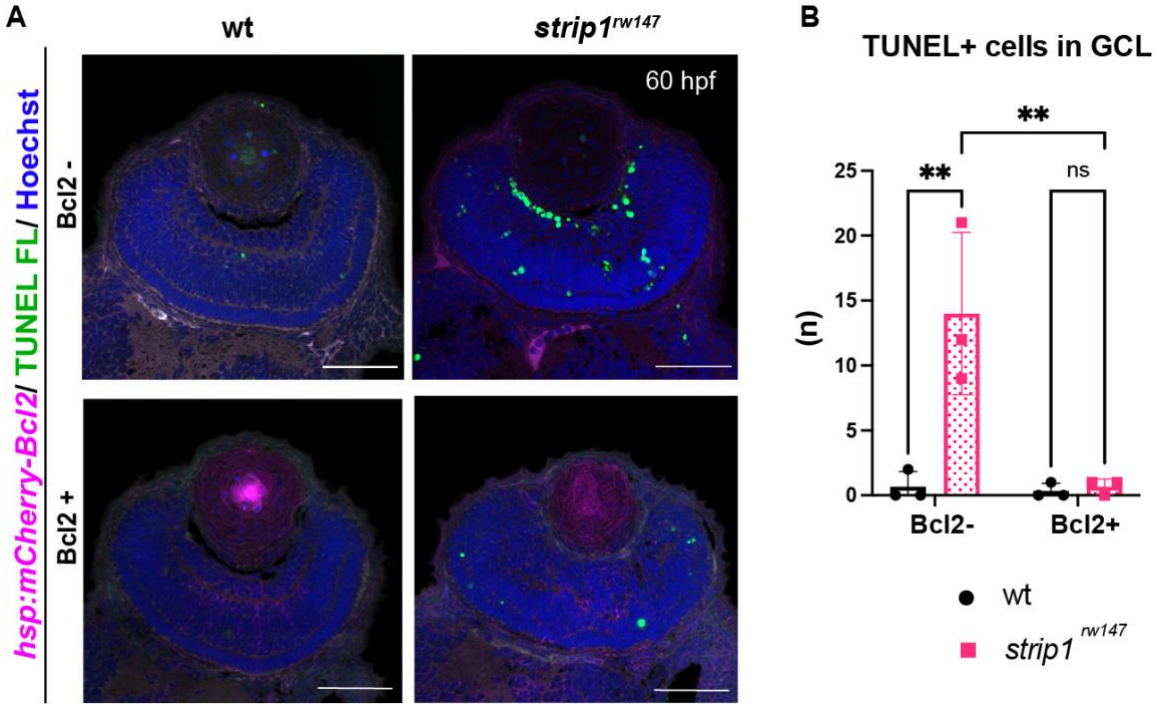

Figure 3.9. Bcl2 rescues apoptosis in the GCL of *strip1* mutants.

(A) 60-hpf wild-type and *strip1*^{rw147} mutants combined with the transgenic line *Tg[hsp:mCherry-Bcl2]*. Non-transgenic embryos (Bcl2-, top panels) are compared to transgenic embryos (Bcl2+, bottom panels) after heat-shock treatment. Apoptotic cells are visualized by TUNEL FL and fluorescent signals from mCherry-Bcl2 are shown. Nuclei are stained with Hoechst. (B) The number of TUNEL+ cells in GCL. Two-way ANOVA with the Tukey multiple comparison test, n=3.

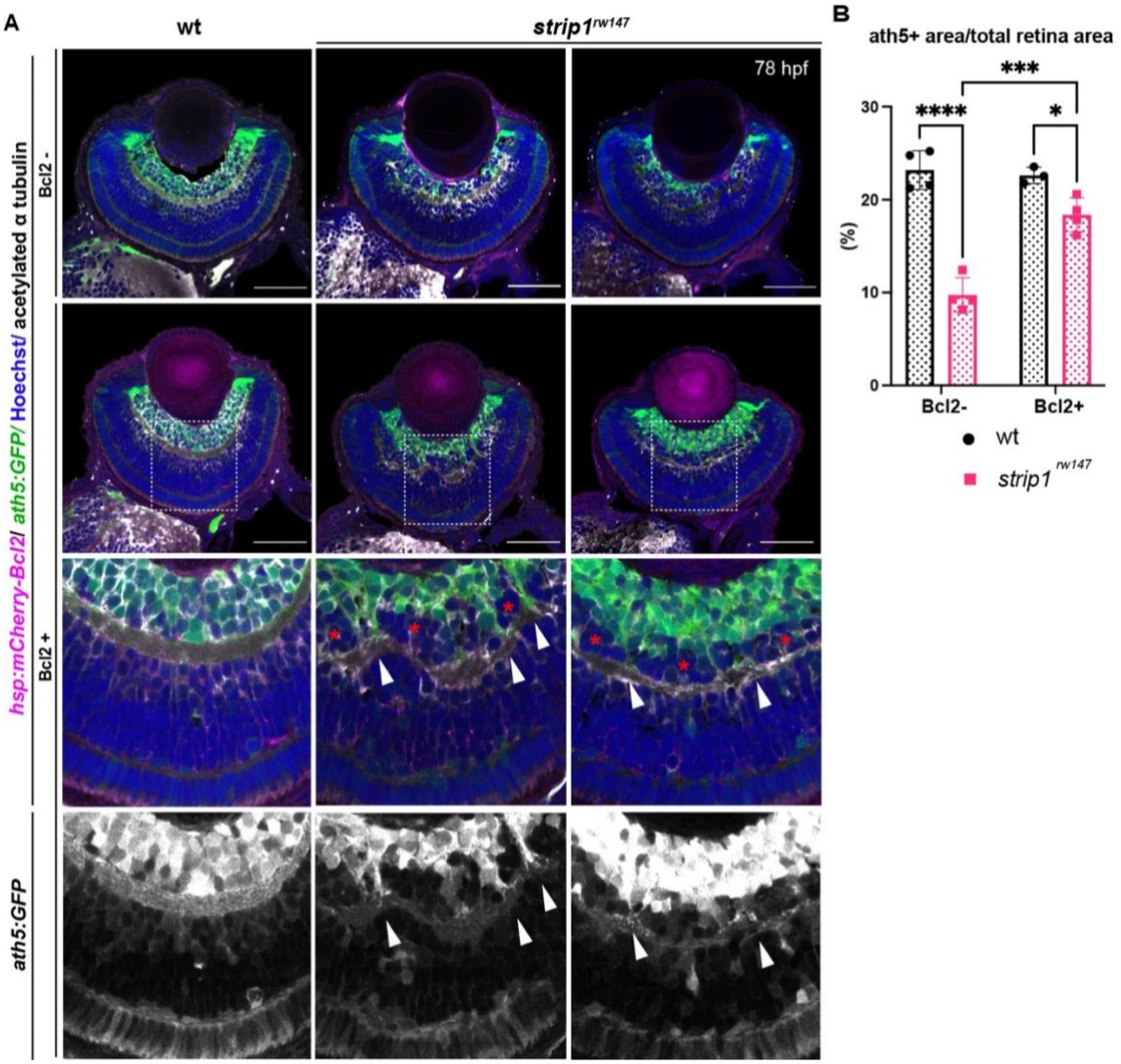

Figure 3.10. RGCs are recovered in Bcl2-rescued *strip1* mutants but an ectopic IPL is observed.

(A) 78-hpf wild-type and *strip1*^{rw147} mutant retinas combined with the transgenic lines, *Tg[ath5:GFP]* and *Tg[hsp:mCherry-Bcl2]*. Non-transgenic embryos (Bcl2-, top panels) are compared to transgenic embryos (Bcl2+, bottom panels) after heat-shock treatment. RGCs are labeled with *ath5:GFP* and fluorescent signals from mCherry-Bcl2 are shown. Anti-acetylated α-tubulin labels the IPL. Nuclei are stained with Hoechst. Arrowheads represent areas where RGC dendrites contribute to the IPL. Asterisks denote areas where RGC dendrites fails to project to the forming IPL and a fraction of presumptive amacrine cells is located in between. (B) Percentage of ath5+ area relative to retinal area. Two-way ANOVA with the Tukey multiple comparison test, n≥3.

3.4. Discussion

Zebrafish RGCs are more resistant to natural and injury-induced cell death, compared to mammalian RGCs. In zebrafish retina, only 1.06 % of RGCs die during development (Biehlmaier et al., 2001). However, around 50% of mammalian RGCs undergo apoptotic cell death (Bahr, 2000, Fawcett et al., 1984). Similarly, the survival rate of mouse RGCs following optic nerve injury (ONI) is only ~8% compared to ~75% survival rate of zebrafish RGCs (Li et al., 2020, Zou et al., 2013). This suggests the presence of RGC survival signals which are more active in zebrafish retina. Recently, many studies seek to identify such zebrafish-specific survival mechanisms with the aim that they could be therapeutically targeted to prevent death of mammalian RGCs (Chen et al., 2021). In this part of the study, I have demonstrated that zebrafish Strip1, and possibly the larger STRIPAK complex, is essential for RGC survival by suppressing Jun-mediated apoptotic signaling.

Loss of zebrafish Strip1 causes an elevated stress response profile within embryonic RGCs with a degree of overlap with adult RGCs post ONI. Interestingly, 5 out of the 6 overlapping upregulated markers (*jun, atf3, stmn4, sox11b* and *adcyap1b)* are commonly upregulated in many retinal transcriptomic studies of mammalian ONI models (Wang et al., 2021). Jun is the canonical target of JNK signaling and many studies have established that JNK/Jun activation is a major cause for axonal injury- or glaucoma-induced RGC death (Fernandes et al., 2012, Fernandes et al., 2013, Syc-Mazurek et al., 2017a). Taken together, JNK/Jun signaling appears to be a common mediator of RGC death across vertebrates and the findings of this study suggest that Strip1 and the larger STRIPAK complex might play a role in suppressing this signaling.

What is the molecular link between Strip1 and Jun suppression in RGCs? proteomic assays from this study revealed that the recruitment of many STRIPAK components is compromised in *strip1* mutants. At the genetic level, I demonstrated the functional interaction between Strip1 and Strn3 to regulate RGC survival. Recently, several mechanistic studies on human STRIPAK complex found that STRIP1 and STRN3 are organizing centers for STRIPAK complex, and their mutant forms compromise complex assembly and function (Jeong et al., 2021, Tang et al., 2019). The modulation of JNK/Jun signaling by STRIPAK complex is supported by several studies. MAP4 kinases are known to activate JNK signaling pathway and they are among the kinase family members which are recruited and dephosphorylated by STRIPAK complex (Fuller et al., 2021, Hwang and Pallas, 2014, Kim et al., 2020, Seo et al., 2020). Moreover, JNK signaling is activated in STRIP1/2 knockout human cell lines (Chen et al., 2019). Similarly, the interaction between Strip and CKa (*Drosophila* homologue of Striatins) suppresses JNK signaling in the developing *Drosophila* testis (La Marca et al., 2019). Thus, it is highly likely that Strip1 and Strn3 function in the context of STRIPAK complex to modulate JNK/Jun activity and thereby, promote RGC survival. So far, this study is the first to provide *in vivo* evidence for a functional interaction between STRIPAK components and Jun signaling in vertebrates.

Although Jun knock down rescues RGC death in *strip1* mutants, the involvement of other pro-apoptotic factors cannot be excluded. It is possible that Strip1/STRIPAK complex suppresses JNK-mediated apoptosis in both Jun-dependent and independent manners. Indeed, it was reported that JNK can directly modulate mitochondrial pro- and antiapoptotic proteins through phosphorylation events (Dhanasekaran and Reddy, 2008, Schroeter et al., 2003). I attempted to suppress JNK signaling using selective inhibitors to directly investigate its role. However, severe embryo toxicity due to global exposure made this investigation challenging. Another possibility is that STRIPAK suppresses other pathways together with JNK signaling to maintains RGCs, one strong candidate is the Hippo signaling pathway which plays important roles in organ size regulation by maintaining a balance between proliferation and cell death (Zhao et al., 2011). Suppression of Hippo causes over proliferation, while its activation leads to apoptosis (Huang et al., 2005, Wu et al., 2003). It was demonstrated that STRIPAK suppresses Hippo by dephosphorylating its upstream activator kinases MST1/2 or indirectly through the MAP4K which are also known to activate Hippo signaling (Chen et al., 2019, Kim et al., 2020, Meng et al., 2015, Seo et al., 2020, Tang et al., 2019). It will be of interest to see if STRIPAK plays dual roles through JNK and Hippo signaling to maintain RGCs.

One limitation of the study is the timepoint of transcriptome analysis. Since apoptosis starts at around 48 hpf in strip1 mutants, it would have been ideal to perform RNA sequencing prior or during this timepoint to get the best representation of molecular changes in intact RGCs. However, due to limitations of genotyping and the need to pool samples because of small sample size, RNA sequencing was performed at ~ 62 hpf. This explains that many of the downregulated genes in *strip1* mutants are known markers of RGCs, which coincides with ~ 50% reduction in RGC population at this time. In addition, this could explain the downregulation of markers related to synaptogenesis since many of them are specifically expressed in RGCs, like *grin2ab*, *chrnab*, and *kcnip3b* (Ackerman et al., 2009, Thisse and Thisse, 2004). On the other hand, the upregulation of microtubule-related factors in the transcriptome analysis is interesting, especially *stathmin-like 4/4l*. Stathmins are microtubule depolymerizing factors, which are highly expressed during brain development and perturbation in their expression are associated with defects in dendrite/axon outgrowth (Chauvin and Sobel, 2015). In zebrafish, Stmn4/4l are specifically expressed the GCL and the brain (Li et al., 2010, Thisse and Thisse, 2004). It will be of interest to examine the correlation between Stmn4/4l upregulation in *strip1* mutants and the observed neurite projection defects in RGCs, and the molecular signaling involved in this upregulation.

Chapter 4.

Conclusions and outlook

In this study, I have uncovered an essential and multifaceted role for Strip1 in neural circuit formation of zebrafish inner retina, the findings of this study are summarized in (**Figure** 4.1) .

First, zebrafish Strip1 is expressed in inner retinal neurons, mainly RGCs and amacrine cells. Upon the loss of Strip1, inner retinal neurons display severe and random neurite projection defects, which are associated with disruption in retinal lamination especially IPL formation.

Second, Strip1 is dispensable for RGC neurogenesis; however, loss of Strip1 causes dramatic RGC death shortly after birth. Subsequently, cells in the INL infiltrate the degenerating GCL, leading to a disorganized IPL.

Third, Cell transplantation experiments revealed that Strip1 cell-autonomously promotes RGC survival and dendritic morphogenesis; however, it is not required in INL cells for IPL formation. These findings suggest that Strip1-mediated RGC maintenance ensures proper positioning and neurite patterning of inner retinal neurons to establish an IPL.

Fourth, at the mechanistic level, Strip1 interacts with its STRIPAK partner, Strn3, to promote RGC survival through the suppression of the Jun-mediated apoptotic pathway. In addition, the rescue of RGC death in strip1 mutants by Bcl2 overexpression demonstrates that RGC death occurs through the mitochondria-mediated apoptotic pathway.

This work is expected to challenge the current consensus that RGCs do not play a major role in IPL formation by demonstrating a new instructive role for RGCs in this process. Strip1 promotes RGC survival which likely ensures the structural integrity of the IPL. This is in concert with similar phenotypes observed when RGCs aren't born in *ath5* mutants (Kay et al., 2004). Deciphering the impact of Strip1-mediated RGC dendritic patterning is more challenging due to the cell death phenotype. However, Bcl2-rescued *strip1* mutants provide valuable new insights on how RGC dendritic patterning might contribute to IPL development. Bcl2-rescued RGCs show defects in dendritic patterns, which are associated with an ectopic IPL formed within presumptive ACs. Thus, I propose that RGCs serve dual functions in IPL development (summarized in **Figure** 4.2); (1) RGCs act as a physical barrier

that prevents abnormal infiltration of amacrine cells into the GCL, and (2) RGCs show dendritic guidance cues that are likely to establish interactions between RGCs and amacrine cells for a proper IPL program. Future studies could help clarify what guidance clues are involved in this process.

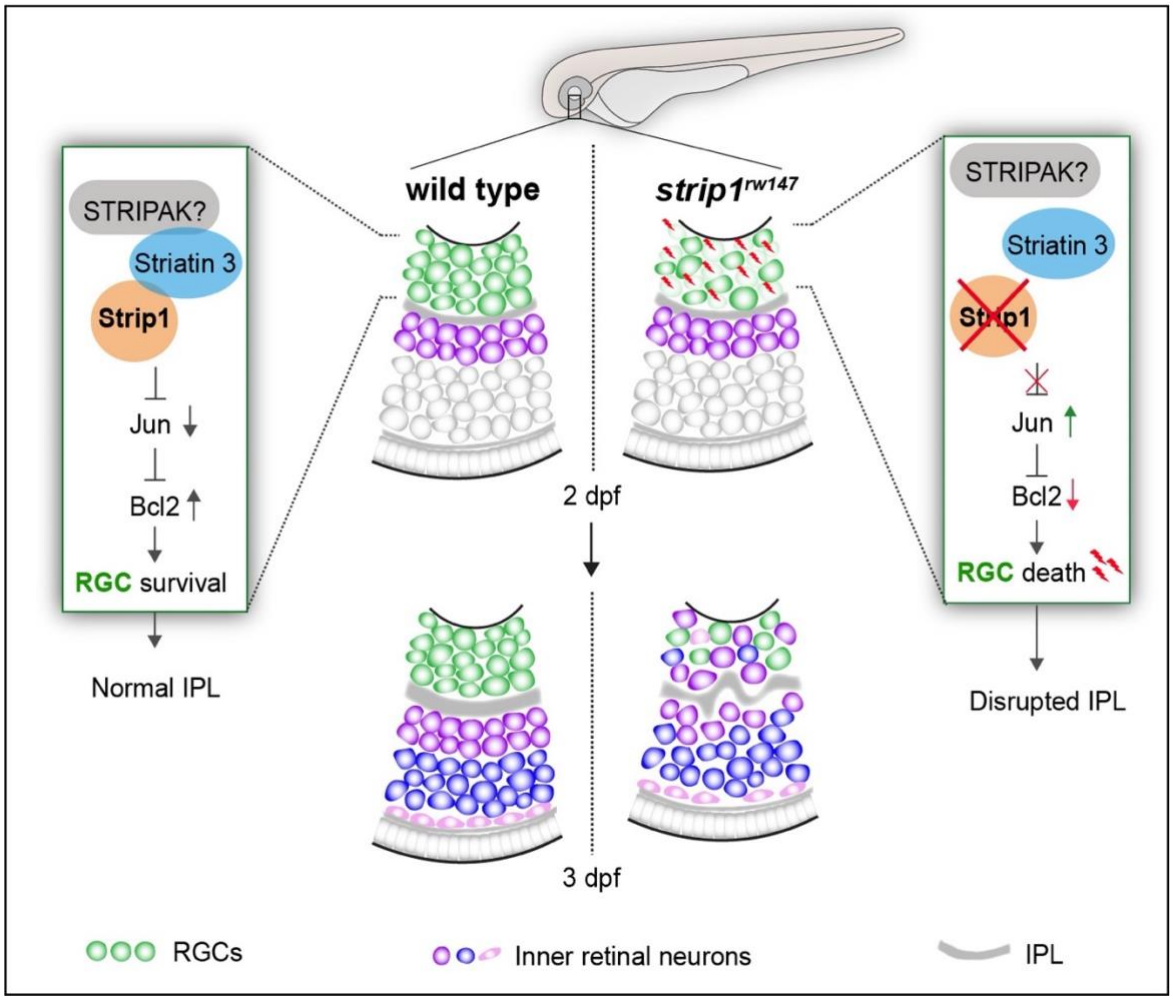

Figure 4.1. Summary of developmental and molecular events that underlie Strip1 function in inner retinal circuit formation.

In wild-type retina, Strip1 suppresses Jun-mediated pro-apoptotic signals, probably through the STIPAK complex, to maintain RGCs during development. In absence of Strip1, Jun is activated within RGCs leading to severe degeneration of RGCs as early as 2 dpf. Subsequently, cells in the INL abnormally infiltrate the GCL leading to a disrupted IPL at 3 dpf.

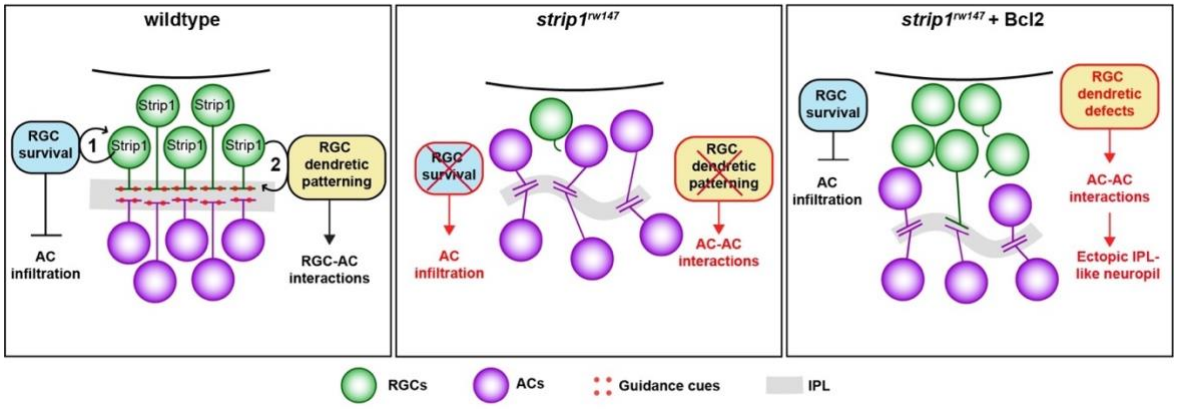

Figure 4.2. Proposed model for Strip1 role within RGCs to regulate AC positioning and IPL formation.

In wild type, Strip1 regulates (1) RGC survival to prevent AC infiltration, and (2) RGC dendritic patterning to promote RGC-AC interactions. In *strip1*^{rw147} mutants, both mechanisms are perturbed, leading to AC infiltration, increased AC-AC interactions, and IPL defects. In Bcl2-rescued *strip1*^{rw147}mutants, survived RGCs prevent AC infiltration. However, RGC dendritic defects lead to increased AC-AC interactions and ectopic IPL formation.

Since its initial identification in 2009, there has been an influx of crystallography, biochemical and functional studies on STRIPAK complex to identify its topological organization (Goudreault et al., 2009, Jeong et al., 2021, Kean et al., 2011, Tang et al., 2019). It is thought that STRIPAK complex can assemble into variable complexes with different subunits to regulate multiple cellular processes. However, our knowledge on the physiological functions of such different assemblies is limited to *in vitro* studies or invertebrate animal models (Madsen et al., 2015, Neal et al., 2020, Neisch et al., 2017, Sakuma et al., 2016). This work will open exciting new research avenues to determine if Strip1-mediated Jun suppression can modulate proapoptotic signaling in adult RGCs of both zebrafish and higher vertebrates, with the hope to find novel targets that could mitigate optic neuropathy-induced RGC degeneration.

This work raises exciting questions and new insights beyond the scope of visual research. lamination is a conserved feature of the vertebrate central nervous system. The presented data sheds the light on how interactions among synaptic partners during development can influence cellular positioning and synaptic layer formation. In addition, I reported the presence of significant apoptosis in the optic tectum, which raises questions on whether Strip1/Jun signaling regulates neuronal survival in the brain. Furthermore, the proteomics findings from whole head lysates shows that several components of the STRIPAK complex aren't recruited by the mutant form of Strip1. This raises questions on whether Strip1 is implicated in neurodevelopmental disorders associated with these STRIPAK complex components. One interesting candidate is CTTNBP2. Like Strip1, CTTNBP2 regulates microtubule stability (Sakuma et al., 2015, Shih et al., 2014). In addition, CTTNBP2 promotes dendritic spine formation and maintenance (Chen et al., 2012). It is also located in a high-risk locus linked to ASD and CTTNBP2-defficient mice have autism-like behavior (Cheung et al., 2001, Iossifov et al., 2012, Shih et al., 2020). It will be of interest to investigate whether Strip1 functions with CTTNBP2 to regulate such neurodevelopmental phenotypes.

In summary, this work unmasks a pivotal role for Strip1 in inner retinal neural circuit wiring by maintaining RGCs during development. Our findings pave the road for future studies in vertebrate animal models that aim to disentangle the function Strip1 signaling within and beyond visual research.

References

ACKERMAN, K. M., NAKKULA, R., ZIRGER, J. M., BEATTIE, C. E. & BOYD, R. T. 2009. Cloning and spatiotemporal expression of zebrafish neuronal nicotinic acetylcholine receptor alpha 6 and alpha 4 subunit RNAs. *Dev Dyn,* 238**,** 980-92.

AHMED, M., KOJIMA, Y. & MASAI, I. 2021. Strip1 regulates retinal ganglion cell survival by suppressing Jun-mediated apoptosis to promote retinal neural circuit formation. *bioRxiv*.

ALBRECHT, N. E., BURGER, C. A. & SAMUEL, M. A. 2020. Neuroscience in the blink of an eye: using the retina to understand the brain. *The Biochemist,* 42**,** 18-24.

ALMASIEH, M., WILSON, A. M., MORQUETTE, B., CUEVA VARGAS, J. L. & DI POLO, A. 2012. The molecular basis of retinal ganglion cell death in glaucoma. *Prog Retin Eye Res,* 31**,** 152-81.

AMINI, R., ROCHA-MARTINS, M. & NORDEN, C. 2018. Neuronal Migration and Lamination in the Vertebrate Retina. *Frontiers in Neuroscience,* 11.

ANDREWS, S. 2010. FastQC: A Quality Control Tool for High Throughput Sequence Data.

ANILKUMAR, U. & PREHN, J. H. 2014. Anti-apoptotic BCL-2 family proteins in acute neural injury. *Front Cell Neurosci,* 8**,** 281.

AUER, T. O., XIAO, T., BERCIER, V., GEBHARDT, C., DUROURE, K., CONCORDET, J. P., WYART, C., SUSTER, M., KAWAKAMI, K., WITTBRODT, J., BAIER, H. & DEL BENE, F. 2015. Deletion of a kinesin I motor unmasks a mechanism of homeostatic branching control by neurotrophin-3. *Elife,* 4.

AVANESOV, A. & MALICKI, J. 2010. Analysis of the retina in the zebrafish model. *Methods Cell Biol,* 100**,** 153-204.

BADEN, T., EULER, T. & BERENS, P. 2020. Understanding the retinal basis of vision across species. *Nat Rev Neurosci,* 21**,** 5-20.

BAHR, M. 2000. Live or let die - retinal ganglion cell death and survival during development and in the lesioned adult CNS. *Trends Neurosci,* 23**,** 483-90.

BAI, S. W., HERRERA-ABREU, M. T., ROHN, J. L., RACINE, V., TAJADURA, V., SURYAVANSHI, N., BECHTEL, S., WIEMANN, S., BAUM, B. & RIDLEY, A. J. 2011. Identification and characterization of a set of conserved and new regulators of cytoskeletal organization, cell morphology and migration. *BMC Biol,* 9**,** 54.

BAIER, H. 2013. Synaptic laminae in the visual system: molecular mechanisms forming layers of perception. *Annu Rev Cell Dev Biol,* 29**,** 385-416.

BARTOLI, M., TERNAUX, J. P., FORNI, C., PORTALIER, P., SALIN, P., AMALRIC, M. & MONNERON, A. 1999. Down-regulation of striatin, a neuronal calmodulin-

binding protein, impairs rat locomotor activity. *Journal of neurobiology,* 40**,** 234-243.

BAZZI, H., SOROKA, E., ALCORN, H. L. & ANDERSON, K. V. 2017. STRIP1, a core component of STRIPAK complexes, is essential for normal mesoderm migration in the mouse embryo. *Proc Natl Acad Sci U S A,* 114**,** E10928-E10936.

BENOIST, M., GAILLARD, S. & CASTETS, F. 2006. The striatin family: a new signaling platform in dendritic spines. *Journal of Physiology-Paris,* 99**,** 146-153.

BERNARDOS, R. L., LENTZ, S. I., WOLFE, M. S. & RAYMOND, P. A. 2005. Notch-Delta signaling is required for spatial patterning and Muller glia differentiation in the zebrafish retina. *Dev Biol,* 278**,** 381-95.

BEROS, J., RODGER, J. & HARVEY, A. R. 2018. Developmental retinal ganglion cell death and retinotopicity of the murine retinocollicular projection. *Dev Neurobiol,* 78**,** 51-60.

BIEHLMAIER, O., NEUHAUSS, S. C. & KOHLER, K. 2001. Onset and time course of apoptosis in the developing zebrafish retina. *Cell Tissue Res,* 306**,** 199-207.

BLIGHE, K., RANA, S. & LEWIS, M. 2019. EnhancedVolcano: Publication-ready volcano plots with enhanced colouring and labeling. *R package version,* 1.

BONFANTI, L., STRETTOI, E., CHIERZI, S., CENNI, M. C., LIU, X. H., MARTINOU, J. C., MAFFEI, L. & RABACCHI, S. A. 1996. Protection of retinal ganglion cells from natural and axotomy-induced cell death in neonatal transgenic mice overexpressing bcl-2. *J Neurosci,* 16**,** 4186-94.

BRUCE, F. M., BROWN, S., SMITH, J. N., FUERST, P. G. & ERSKINE, L. 2017. DSCAM promotes axon fasciculation and growth in the developing optic pathway. *Proceedings of the National Academy of Sciences***,** 201618606.

BURRILL, J. D. & EASTER JR, S. S. 1994. Development of the retinofugal projections in the embryonic and larval zebrafish (Brachydanio rerio). *Journal of Comparative Neurology,* 346**,** 583-600.

CASANO, A. M., ALBERT, M. & PERI, F. 2016. Developmental Apoptosis Mediates Entry and Positioning of Microglia in the Zebrafish Brain. *Cell Rep,* 16**,** 897-906.

CHAUVIN, S. & SOBEL, A. 2015. Neuronal stathmins: a family of phosphoproteins cooperating for neuronal development, plasticity and regeneration. *Prog Neurobiol,* 126**,** 1-18.

CHEN, M., ZHANG, H., SHI, Z., LI, Y., ZHANG, X., GAO, Z., ZHOU, L., MA, J., XU, Q., GUAN, J., CHENG, Y., JIAO, S. & ZHOU, Z. 2018a. The MST4-MOB4 complex disrupts the MST1-MOB1 complex in the Hippo-YAP pathway and plays a pro-oncogenic role in pancreatic cancer. *J Biol Chem,* 293**,** 14455-14469.

CHEN, R., XIE, R., MENG, Z., MA, S. & GUAN, K. L. 2019. STRIPAK integrates upstream signals to initiate the Hippo kinase cascade. *Nat Cell Biol,* 21**,** 1565-1577.

CHEN, S., LATHROP, K. L., KUWAJIMA, T. & GROSS, J. M. 2021. Retinal ganglion cell survival after severe optic nerve injury is modulated by crosstalk between JAK/STAT signaling and innate immune responses in the zebrafish retina. *bioRxiv***,** 2021.04.08.439090.

CHEN, S., ZHOU, Y., CHEN, Y. & GU, J. 2018b. fastp: an ultra-fast all-in-one FASTQ preprocessor. *Bioinformatics,* 34**,** i884-i890.

CHEN, Y.-K., CHEN, C.-Y., HU, H.-T. & HSUEH, Y.-P. 2012. CTTNBP2, but not CTTNBP2NL, regulates dendritic spinogenesis and synaptic distribution of the striatin–PP2A complex. *Molecular biology of the cell,* 23**,** 4383-4392.

CHENG, L., SAPIEHA, P., KITTLEROVA, P., HAUSWIRTH, W. W. & DI POLO, A. 2002. TrkB gene transfer protects retinal ganglion cells from axotomy-induced death in vivo. *J Neurosci,* 22**,** 3977-86.

CHEUNG, J., PETEK, E., NAKABAYASHI, K., TSUI, L.-C., VINCENT, J. B. & SCHERER, S. W. 2001. Identification of the human cortactin-binding protein-2 gene from the autism candidate region at 7q31. *Genomics,* 78**,** 7-11.

CHKLOVSKII, D. B. & KOULAKOV, A. A. 2004. Maps in the brain: what can we learn from them? *Annu Rev Neurosci,* 27**,** 369-92.

CHOI, J.-H., LAW, M.-Y., CHIEN, C.-B., LINK, B. A. & WONG, R. O. 2010. In vivo development of dendritic orientation in wild-type and mislocalized retinal ganglion cells. *Neural development,* 5**,** 29.

CHOW, R. W., ALMEIDA, A. D., RANDLETT, O., NORDEN, C. & HARRIS, W. A. 2015. Inhibitory neuron migration and IPL formation in the developing zebrafish retina. *Development,* 142**,** 2665-77.

CLAES, M., DE GROEF, L. & MOONS, L. 2019. Target-Derived Neurotrophic Factor Deprivation Puts Retinal Ganglion Cells on Death Row: Cold Hard Evidence and Caveats. *Int J Mol Sci,* 20.

CONNAUGHTON, V. 2011. Bipolar cells in the zebrafish retina. *Visual neuroscience,* 28**,** 77-93.

D'AGATI, G., BELTRE, R., SESSA, A., BURGER, A., ZHOU, Y., MOSIMANN, C. & WHITE, R. M. 2017. A defect in the mitochondrial protein Mpv17 underlies the transparent casper zebrafish. *Dev Biol,* 430**,** 11-17.

D'SOUZA, S. & LANG, R. A. 2020. Retinal ganglion cell interactions shape the developing mammalian visual system. *Development,* 147.

D'ORAZI, F. D., SUZUKI, S. C. & WONG, R. O. 2014. Neuronal remodeling in retinal circuit assembly, disassembly, and reassembly. *Trends in neurosciences,* 37**,** 594-603.

DEANS, M. R., KROL, A., ABRAIRA, V. E., COPLEY, C. O., TUCKER, A. F. & GOODRICH, L. V. 2011. Control of neuronal morphology by the atypical cadherin Fat3. *Neuron,* 71**,** 820-32.

DHANASEKARAN, D. N. & REDDY, E. P. 2008. JNK signaling in apoptosis. *Oncogene,* 27**,** 6245-51.

DI DONATO, V. 2016. *Axonal target specificity in the CRISPR/Cas9 era: a new role for Reelin in vertebrate visual sytem development.* Université Pierre et Marie Curie-Paris VI.

DI DONATO, V., DE SANTIS, F., ALBADRI, S., AUER, T. O., DUROURE, K., CHARPENTIER, M., CONCORDET, J.-P., GEBHARDT, C. & DEL BENE, F. 2018. An Attractive Reelin Gradient Establishes Synaptic Lamination in the Vertebrate Visual System. *Neuron,* 97**,** 1049-1062. e6.

DING, H., HOWARTH, A. G., PANNIRSELVAM, M., ANDERSON, T. J., SEVERSON, D. L., WIEHLER, W. B., TRIGGLE, C. R. & TUANA, B. S. 2005. Endothelial

dysfunction in Type 2 diabetes correlates with deregulated expression of the tail-anchored membrane protein SLMAP. *American Journal of Physiology-Heart and Circulatory Physiology,* 289**,** H206-H211.

DONAHUE, R. J., FEHRMAN, R. L., GUSTAFSON, J. R. & NICKELLS, R. W. 2021. BCLXL gene therapy moderates neuropathology in the DBA/2J mouse model of inherited glaucoma. *Cell Death Dis,* 12**,** 781.

DONAHUE, R. J., MAES, M. E., GROSSER, J. A. & NICKELLS, R. W. 2020. BAX-Depleted Retinal Ganglion Cells Survive and Become Quiescent Following Optic Nerve Damage. *Mol Neurobiol,* 57**,** 1070-1084.

DOWLING, J. E. 1987. *The retina: an approachable part of the brain*, Harvard University Press.

EILERS, A., WHITFIELD, J., BABIJ, C., RUBIN, L. L. & HAM, J. 1998. Role of the Jun kinase pathway in the regulation of c-Jun expression and apoptosis in sympathetic neurons. *J Neurosci,* 18**,** 1713-24.

ELDRED, M. K., CHARLTON-PERKINS, M., MURESAN, L. & HARRIS, W. A. 2017. Self-organising aggregates of zebrafish retinal cells for investigating mechanisms of neural lamination. *Development,* 144**,** 1097-1106.

ENGERER, P., SUZUKI, S. C., YOSHIMATSU, T., CHAPOUTON, P., OBENG, N., ODERMATT, B., WILLIAMS, P. R., MISGELD, T. & GODINHO, L. 2017. Uncoupling of neurogenesis and differentiation during retinal development. *The EMBO journal***,** e201694230.

FADOOL, J. M. & DOWLING, J. E. 2008. Zebrafish: a model system for the study of eye genetics. *Progress in retinal and eye research,* 27**,** 89-110.

FALK, J., KONOPACKI, F. A., ZIVRAJ, K. H. & HOLT, C. E. 2014. Rab5 and Rab4 regulate axon elongation in the Xenopus visual system. *Journal of Neuroscience,* 34**,** 373-391.

FAWCETT, J. W., O'LEARY, D. D. & COWAN, W. M. 1984. Activity and the control of ganglion cell death in the rat retina. *Proc Natl Acad Sci U S A,* 81**,** 5589-93.

FENG, L., CHEN, H., YI, J., TROY, J. B., ZHANG, H. F. & LIU, X. 2016. Long-Term Protection of Retinal Ganglion Cells and Visual Function by Brain-Derived Neurotrophic Factor in Mice With Ocular Hypertension. *Invest Ophthalmol Vis Sci,* 57**,** 3793-802.

FERNANDES, K. A., HARDER, J. M., FORNAROLA, L. B., FREEMAN, R. S., CLARK, A. F., PANG, I. H., JOHN, S. W. & LIBBY, R. T. 2012. JNK2 and JNK3 are major regulators of axonal injury-induced retinal ganglion cell death. *Neurobiol Dis,* 46**,** 393-401.

FERNANDES, K. A., HARDER, J. M., KIM, J. & LIBBY, R. T. 2013. JUN regulates early transcriptional responses to axonal injury in retinal ganglion cells. *Exp Eye Res,* 112**,** 106-17.

FIDALGO, M., FRAILE, M., PIRES, A., FORCE, T., POMBO, C. & ZALVIDE, J. 2010. CCM3/PDCD10 stabilizes GCKIII proteins to promote Golgi assembly and cell orientation. *J Cell Sci,* 123**,** 1274-84.

FLYNN, K., STIESS, M. & BRADKE, F. 2013. Role of the Cytoskeleton and Membrane Trafficking in Axon–Dendrite Morphogenesis. *Cellular Migration and Formation of*

Neuronal Connections. Elsevier.

FRICKER, M., TOLKOVSKY, A. M., BORUTAITE, V., COLEMAN, M. & BROWN, G. C. 2018. Neuronal Cell Death. *Physiol Rev,* 98**,** 813-880.

FULLER, S. J., EDMUNDS, N. S., MCGUFFIN, L. J., HARDYMAN, M. A., CULL, J. J., ALHARBI, H. O., MEIJLES, D. N., SUGDEN, P. H. & CLERK, A. 2021. MAP4K4 expression in cardiomyocytes: multiple isoforms, multiple phosphorylations and interactions with striatins. *Biochem J,* 478**,** 2121-2143.

GAN, X. Q., WANG, J. Y., XI, Y., WU, Z. L., LI, Y. P. & LI, L. 2008. Nuclear Dvl, c-Jun, beta-catenin, and TCF form a complex leading to stabilization of beta-catenin-TCF interaction. *J Cell Biol,* 180**,** 1087-100.

GODINHO, L., MUMM, J. S., WILLIAMS, P. R., SCHROETER, E. H., KOERBER, A., PARK, S. W., LEACH, S. D. & WONG, R. O. 2005. Targeting of amacrine cell neurites to appropriate synaptic laminae in the developing zebrafish retina. *Development,* 132**,** 5069-79.

GOUDREAULT, M., D'AMBROSIO, L. M., KEAN, M. J., MULLIN, M. J., LARSEN, B. G., SANCHEZ, A., CHAUDHRY, S., CHEN, G. I., SICHERI, F. & NESVIZHSKII, A. I. 2009. A PP2A phosphatase high density interaction network identifies a novel striatin-interacting phosphatase and kinase complex linked to the cerebral cavernous malformation 3 (CCM3) protein. *Molecular & Cellular Proteomics,* 8**,** 157-171.

GUAN, Q. H., PEI, D. S., ZONG, Y. Y., XU, T. L. & ZHANG, G. Y. 2006. Neuroprotection against ischemic brain injury by a small peptide inhibitor of c-Jun N-terminal kinase (JNK) via nuclear and non-nuclear pathways. *Neuroscience,* 139**,** 609-27.

HALLORAN, M. C., SATO-MAEDA, M., WARREN, J. T., SU, F., LELE, Z., KRONE, P. H., KUWADA, J. Y. & SHOJI, W. 2000. Laser-induced gene expression in specific cells of transgenic zebrafish. *Development,* 127**,** 1953-60.

HAM, J., EILERS, A., WHITFIELD, J., NEAME, S. J. & SHAH, B. 2000. c-Jun and the transcriptional control of neuronal apoptosis. *Biochem Pharmacol,* 60**,** 1015-21.

HAN, R., WANG, R., ZHAO, Q., HAN, Y., ZONG, S., MIAO, S., SONG, W. & WANG, L. 2016. Trim69 regulates zebrafish brain development by ap-1 pathway. *Sci Rep,* 6**,** 24034.

HARDER, J. M., DING, Q., FERNANDES, K. A., CHERRY, J. D., GAN, L. & LIBBY, R. T. 2012. BCL2L1 (BCL-X) promotes survival of adult and developing retinal ganglion cells. *Mol Cell Neurosci,* 51**,** 53-9.

HARRIS, C. A. & JOHNSON, E. M., JR. 2001. BH3-only Bcl-2 family members are coordinately regulated by the JNK pathway and require Bax to induce apoptosis in neurons. *J Biol Chem,* 276**,** 37754-60.

HARVEY, A. R. & ROBERTSON, D. 1992. Time-course and extent of retinal ganglion cell death following ablation of the superior colliculus in neonatal rats. *J Comp Neurol,* 325**,** 83-94.

HARVEY, B. M., BAXTER, M. & GRANATO, M. 2019. Optic nerve regeneration in larval zebrafish exhibits spontaneous capacity for retinotopic but not tectum specific axon targeting. *PLoS One,* 14**,** e0218667.

HOLLVILLE, E., ROMERO, S. E. & DESHMUKH, M. 2019. Apoptotic cell death regulation in neurons. *FEBS J,* 286**,** 3276-3298.

HOON, M., OKAWA, H., DELLA SANTINA, L. & WONG, R. O. 2014. Functional architecture of the retina: development and disease. *Progress in retinal and eye research,* 42**,** 44-84.

HORNE-BADOVINAC, S., LIN, D., WALDRON, S., SCHWARZ, M., MBAMALU, G., PAWSON, T., JAN, Y., STAINIER, D. Y. & ABDELILAH-SEYFRIED, S. 2001. Positional cloning of heart and soul reveals multiple roles for PKC lambda in zebrafish organogenesis. *Curr Biol,* 11**,** 1492-502.

HU, M. & EASTER JR, S. S. 1999. Retinal neurogenesis: the formation of the initial central patch of postmitotic cells. *Developmental biology,* 207**,** 309-321.

HUANG, J., WU, S., BARRERA, J., MATTHEWS, K. & PAN, D. 2005. The Hippo signaling pathway coordinately regulates cell proliferation and apoptosis by inactivating Yorkie, the Drosophila Homolog of YAP. *Cell,* 122**,** 421-34.

HUBERMAN, A. D., CLANDININ, T. R. & BAIER, H. 2010. Molecular and cellular mechanisms of lamina-specific axon targeting. *Cold Spring Harb Perspect Biol,* 2**,** a001743.

HULSEN, T., DE VLIEG, J. & ALKEMA, W. 2008. BioVenn–a web application for the comparison and visualization of biological lists using area-proportional Venn diagrams. *BMC genomics,* 9**,** 1-6.

HWANG, J. & PALLAS, D. C. 2014. STRIPAK complexes: structure, biological function, and involvement in human diseases. *The international journal of biochemistry & cell biology,* 47**,** 118-148.

ICHA, J., KUNATH, C., ROCHA-MARTINS, M. & NORDEN, C. 2016. Independent modes of ganglion cell translocation ensure correct lamination of the zebrafish retina. *J Cell Biol,* 215**,** 259-275.

IMAI, F., YOSHIZAWA, A., FUJIMORI-TONOU, N., KAWAKAMI, K. & MASAI, I. 2010. The ubiquitin proteasome system is required for cell proliferation of the lens epithelium and for differentiation of lens fiber cells in zebrafish. *Development,* 137**,** 3257-68.

IOSSIFOV, I., RONEMUS, M., LEVY, D., WANG, Z., HAKKER, I., ROSENBAUM, J., YAMROM, B., LEE, Y. H., NARZISI, G., LEOTTA, A., KENDALL, J., GRABOWSKA, E., MA, B., MARKS, S., RODGERS, L., STEPANSKY, A., TROGE, J., ANDREWS, P., BEKRITSKY, M., PRADHAN, K., GHIBAN, E., KRAMER, M., PARLA, J., DEMETER, R., FULTON, L. L., FULTON, R. S., MAGRINI, V. J., YE, K., DARNELL, J. C., DARNELL, R. B., MARDIS, E. R., WILSON, R. K., SCHATZ, M. C., MCCOMBIE, W. R. & WIGLER, M. 2012. De novo gene disruptions in children on the autistic spectrum. *Neuron,* 74**,** 285-99.

JACOBSON, S. G., CIDECIYAN, A. V., ALEMAN, T. S., PIANTA, M. J., SUMAROKA, A., SCHWARTZ, S. B., SMILKO, E. E., MILAM, A. H., SHEFFIELD, V. C. & STONE, E. M. 2003. Crumbs homolog 1 (CRB1) mutations result in a thick human retina with abnormal lamination. *Hum Mol Genet,* 12**,** 1073-8.

JENSEN, A. M. & WESTERFIELD, M. 2004. Zebrafish mosaic eyes is a novel FERM protein required for retinal lamination and retinal pigmented epithelial tight junction formation. *Current biology,* 14**,** 711-717.

JEONG, B. C., BAE, S. J., NI, L., ZHANG, X., BAI, X. C. & LUO, X. 2021. Cryo-EM structure of the Hippo signaling integrator human STRIPAK. *Nat Struct Mol Biol,*

28**,** 290-299.

JOHNSON, E. C., GUO, Y., CEPURNA, W. O. & MORRISON, J. C. 2009. Neurotrophin roles in retinal ganglion cell survival: lessons from rat glaucoma models. *Exp Eye Res,* 88**,** 808-15.

JOVIC, M., SHARMA, M., RAHAJENG, J. & CAPLAN, S. 2010. The early endosome: a busy sorting station for proteins at the crossroads. *Histology and histopathology,* 25**,** 99.

JUSUF, P. R., ALBADRI, S., PAOLINI, A., CURRIE, P. D., ARGENTON, F., HIGASHIJIMA, S., HARRIS, W. A. & POGGI, L. 2012. Biasing amacrine subtypes in the Atoh7 lineage through expression of Barhl2. *J Neurosci,* 32**,** 13929-44.

JUSUF, P. R. & HARRIS, W. A. 2009. Ptf1a is expressed transiently in all types of amacrine cells in the embryonic zebrafish retina. *Neural Dev,* 4**,** 34.

KAY, J. N., FINGER-BAIER, K. C., ROESER, T., STAUB, W. & BAIER, H. 2001. Retinal ganglion cell genesis requires lakritz, a Zebrafish atonal Homolog. *Neuron,* 30**,** 725-36.

KAY, J. N., ROESER, T., MUMM, J. S., GODINHO, L., MREJERU, A., WONG, R. O. & BAIER, H. 2004. Transient requirement for ganglion cells during assembly of retinal synaptic layers. *Development,* 131**,** 1331-42.

KEAN, M. J., CECCARELLI, D. F., GOUDREAULT, M., SANCHES, M., TATE, S., LARSEN, B., GIBSON, L. C., DERRY, W. B., SCOTT, I. C., PELLETIER, L., BAILLIE, G. S., SICHERI, F. & GINGRAS, A. C. 2011. Structure-function analysis of core STRIPAK Proteins: a signaling complex implicated in Golgi polarization. *J Biol Chem,* 286**,** 25065-75.

KEMP, H. A., CARMANY-RAMPEY, A. & MOENS, C. 2009. Generating chimeric zebrafish embryos by transplantation. *J Vis Exp*.

KHATIB, T. Z. & MARTIN, K. R. 2017. Protecting retinal ganglion cells. *Eye,* 31**,** 218-224.

KIM, D., LANGMEAD, B. & SALZBERG, S. L. 2015. HISAT: a fast spliced aligner with low memory requirements. *Nat Methods,* 12**,** 357-60.

KIM, J. W., BERRIOS, C., KIM, M., SCHADE, A. E., ADELMANT, G., YEERNA, H., DAMATO, E., INIGUEZ, A. B., FLORENS, L., WASHBURN, M. P., STEGMAIER, K., GRAY, N. S., TAMAYO, P., GJOERUP, O., MARTO, J. A., DECAPRIO, J. & HAHN, W. C. 2020. STRIPAK directs PP2A activity toward MAP4K4 to promote oncogenic transformation of human cells. *Elife,* 9.

KOIKE, C., NISHIDA, A., AKIMOTO, K., NAKAYA, M. A., NODA, T., OHNO, S. & FURUKAWA, T. 2005. Function of atypical protein kinase C lambda in differentiating photoreceptors is required for proper lamination of mouse retina. *J Neurosci,* 25**,** 10290-8.

KOLDE, R. 2012. Pheatmap: pretty heatmaps. *R package version,* 1**,** 726.

KOLSCH, Y., HAHN, J., SAPPINGTON, A., STEMMER, M., FERNANDES, A. M., HELMBRECHT, T. O., LELE, S., BUTRUS, S., LAURELL, E., ARNOLD-AMMER, I., SHEKHAR, K., SANES, J. R. & BAIER, H. 2021. Molecular classification of zebrafish retinal ganglion cells links genes to cell types to behavior. *Neuron,* 109**,** 645-662 e9.

KOSTER, R. W. & FRASER, S. E. 2001. Tracing transgene expression in living zebrafish embryos. *Dev Biol,* 233**,** 329-46.

KWONG, J. M. & CAPRIOLI, J. 2006. Expression of phosphorylated c-Jun N-terminal protein kinase (JNK) in experimental glaucoma in rats. *Exp Eye Res,* 82**,** 576-82.

LA MARCA, J. E., DIEPSTRATEN, S. T., HODGE, A. L., WANG, H., HART, A. H., RICHARDSON, H. E. & SOMERS, W. G. 2019. Strip and Cka negatively regulate JNK signalling during Drosophila spermatogenesis. *Development,* 146.

LEVKOVITCH-VERBIN, H., QUIGLEY, H. A., MARTIN, K. R., HARIZMAN, N., VALENTA, D. F., PEASE, M. E. & MELAMED, S. 2005. The transcription factor c-jun is activated in retinal ganglion cells in experimental rat glaucoma. *Exp Eye Res,* 80**,** 663-70.

LI, D., MUSANTE, V., ZHOU, W.-L., PICCIOTTO, M. R. & NAIRN, A. C. 2018. Striatin-1 is a B subunit of protein phosphatase PP2A that regulates dendritic arborization and spine development in striatal neurons. *Journal of Biological Chemistry***,** jbc. RA117. 001519.

LI, L., HUANG, H., FANG, F., LIU, L., SUN, Y. & HU, Y. 2020. Longitudinal Morphological and Functional Assessment of RGC Neurodegeneration After Optic Nerve Crush in Mouse. *Front Cell Neurosci,* 14**,** 109.

LI, S., YIN, M., LIU, S., CHEN, Y., YIN, Y., LIU, T. & ZHOU, J. 2010. Expression of ventral diencephalon-enriched genes in zebrafish. *Dev Dyn,* 239**,** 3368-79.

LIAO, Y., SMYTH, G. K. & SHI, W. 2014. featureCounts: an efficient general purpose program for assigning sequence reads to genomic features. *Bioinformatics,* 30**,** 923-30.

LIBBY, R. T., LI, Y., SAVINOVA, O. V., BARTER, J., SMITH, R. S., NICKELLS, R. W. & JOHN, S. W. 2005. Susceptibility to neurodegeneration in a glaucoma is modified by Bax gene dosage. *PLoS Genet,* 1**,** 17-26.

MA, Y. T., HSIEH, T., FORBES, M. E., JOHNSON, J. E. & FROST, D. O. 1998. BDNF injected into the superior colliculus reduces developmental retinal ganglion cell death. *J Neurosci,* 18**,** 2097-107.

MACDONALD, R. & WILSON, S. W. 1997. Distribution of Pax6 protein during eye development suggests discrete roles in proliferative and differentiated visual cells. *Dev Genes Evol,* 206**,** 363-369.

MACDONALD, R. B., RANDLETT, O., OSWALD, J., YOSHIMATSU, T., FRANZE, K. & HARRIS, W. A. 2015. Muller glia provide essential tensile strength to the developing retina. *J Cell Biol,* 210**,** 1075-83.

MADSEN, C. D., HOOPER, S., TOZLUOGLU, M., BRUCKBAUER, A., FLETCHER, G., ERLER, J. T., BATES, P. A., THOMPSON, B. & SAHAI, E. 2015. STRIPAK components determine mode of cancer cell migration and metastasis. *Nat Cell Biol,* 17**,** 68-80.

MAES, M. E., SCHLAMP, C. L. & NICKELLS, R. W. 2017. BAX to basics: How the BCL2 gene family controls the death of retinal ganglion cells. *Prog Retin Eye Res,* 57**,** 1-25.

MALICKI, J., JO, H. & PUJIC, Z. 2003. Zebrafish N-cadherin, encoded by the glass onion locus, plays an essential role in retinal patterning. *Developmental biology,* 259**,** 95-

108.

MARCHLER-BAUER, A., DERBYSHIRE, M. K., GONZALES, N. R., LU, S., CHITSAZ, F., GEER, L. Y., GEER, R. C., HE, J., GWADZ, M. & HURWITZ, D. I. 2014. CDD: NCBI's conserved domain database. *Nucleic acids research,* 43**,** D222-D226.

MARTIN, K. R., QUIGLEY, H. A., ZACK, D. J., LEVKOVITCH-VERBIN, H., KIELCZEWSKI, J., VALENTA, D., BAUMRIND, L., PEASE, M. E., KLEIN, R. L. & HAUSWIRTH, W. W. 2003. Gene therapy with brain-derived neurotrophic factor as a protection: retinal ganglion cells in a rat glaucoma model. *Invest Ophthalmol Vis Sci,* 44**,** 4357-65.

MASAI, I., LELE, Z., YAMAGUCHI, M., KOMORI, A., NAKATA, A., NISHIWAKI, Y., WADA, H., TANAKA, H., NOJIMA, Y. & HAMMERSCHMIDT, M. 2003. N-cadherin mediates retinal lamination, maintenance of forebrain compartments and patterning of retinal neurites. *Development,* 130**,** 2479-2494.

MASAI, I., STEMPLE, D. L., OKAMOTO, H. & WILSON, S. W. 2000. Midline signals regulate retinal neurogenesis in zebrafish. *Neuron,* 27**,** 251-263.

MATSUOKA, R. L., CHIVATAKARN, O., BADEA, T. C., SAMUELS, I. S., CAHILL, H., KATAYAMA, K., KUMAR, S. R., SUTO, F., CHEDOTAL, A., PEACHEY, N. S., NATHANS, J., YOSHIDA, Y., GIGER, R. J. & KOLODKIN, A. L. 2011a. Class 5 transmembrane semaphorins control selective Mammalian retinal lamination and function. *Neuron,* 71**,** 460-73.

MATSUOKA, R. L., NGUYEN-BA-CHARVET, K. T., PARRAY, A., BADEA, T. C., CHEDOTAL, A. & KOLODKIN, A. L. 2011b. Transmembrane semaphorin signalling controls laminar stratification in the mammalian retina. *Nature,* 470**,** 259-63.

MCCURLEY, A. T. & CALLARD, G. V. 2010. Time Course Analysis of Gene Expression Patterns in Zebrafish Eye During Optic Nerve Regeneration. *J Exp Neurosci,* 2010**,** 17-33.

MENG, Z., MOROISHI, T., MOTTIER-PAVIE, V., PLOUFFE, S. W., HANSEN, C. G., HONG, A. W., PARK, H. W., MO, J. S., LU, W., LU, S., FLORES, F., YU, F. X., HALDER, G. & GUAN, K. L. 2015. MAP4K family kinases act in parallel to MST1/2 to activate LATS1/2 in the Hippo pathway. *Nat Commun,* 6**,** 8357.

MORGAN, J. L., DHINGRA, A., VARDI, N. & WONG, R. O. 2006. Axons and dendrites originate from neuroepithelial-like processes of retinal bipolar cells. *Nature neuroscience,* 9**,** 85.

MORRIS, A. & FADOOL, J. 2005. Studying rod photoreceptor development in zebrafish. *Physiology & behavior,* 86**,** 306-313.

MOSHIRI, A., GONZALEZ, E., TAGAWA, K., MAEDA, H., WANG, M., FRISHMAN, L. J. & WANG, S. W. 2008. Near complete loss of retinal ganglion cells in the math5/brn3b double knockout elicits severe reductions of other cell types during retinal development. *Dev Biol,* 316**,** 214-27.

MUMM, J. S., WILLIAMS, P. R., GODINHO, L., KOERBER, A., PITTMAN, A. J., ROESER, T., CHIEN, C.-B., BAIER, H. & WONG, R. O. 2006. In vivo imaging reveals dendritic targeting of laminated afferents by zebrafish retinal ganglion cells. *Neuron,* 52**,** 609-621.

MUNEMASA, Y. & KITAOKA, Y. 2012. Molecular mechanisms of retinal ganglion cell

degeneration in glaucoma and future prospects for cell body and axonal protection. *Front Cell Neurosci,* 6**,** 60.

NADER, M., WESTENDORP, B., HAWARI, O., SALIH, M., STEWART, A. F., LEENEN, F. H. & TUANA, B. S. 2012. Tail-anchored membrane protein SLMAP is a novel regulator of cardiac function at the sarcoplasmic reticulum. *American Journal of Physiology-Heart and Circulatory Physiology,* 302**,** H1138-H1145.

NASSI, J. J. & CALLAWAY, E. M. 2009. Parallel processing strategies of the primate visual system. *Nat Rev Neurosci,* 10**,** 360-72.

NEAL, S. J., ZHOU, Q. & PIGNONI, F. 2020. STRIPAK-PP2A regulates Hippo-Yorkie signaling to suppress retinal fate in the Drosophila eye disc peripodial epithelium. *J Cell Sci,* 133.

NEISCH, A. L., NEUFELD, T. P. & HAYS, T. S. 2017. A STRIPAK complex mediates axonal transport of autophagosomes and dense core vesicles through PP2A regulation. *J Cell Biol,* 216**,** 441-461.

NIKOLAOU, N. & MEYER, M. P. 2015. Lamination Speeds the Functional Development of Visual Circuits. *Neuron,* 88**,** 999-1013.

NISHIWAKI, Y., KOMORI, A., SAGARA, H., SUZUKI, E., MANABE, T., HOSOYA, T., NOJIMA, Y., WADA, H., TANAKA, H., OKAMOTO, H. & MASAI, I. 2008. Mutation of cGMP phosphodiesterase 6alpha'-subunit gene causes progressive degeneration of cone photoreceptors in zebrafish. *Mech Dev,* 125**,** 932-46.

NISHIWAKI, Y. & MASAI, I. 2020. beta-SNAP activity in the outer segment growth period is critical for preventing BNip1-dependent apoptosis in zebrafish photoreceptors. *Sci Rep,* 10**,** 17379.

OHNO, S. 2001. Intercellular junctions and cellular polarity: the PAR-aPKC complex, a conserved core cassette playing fundamental roles in cell polarity. *Curr Opin Cell Biol,* 13**,** 641-8.

OKUMURA, M., SAKUMA, C., MIURA, M. & CHIHARA, T. 2015. Linking cell surface receptors to microtubules: tubulin folding cofactor D mediates Dscam functions during neuronal morphogenesis. *Journal of Neuroscience,* 35**,** 1979-1990.

OMORI, Y. & MALICKI, J. 2006. Oko meduzy and related crumbs genes are determinants of apical cell features in the vertebrate embryo. *Current biology,* 16**,** 945-957.

OSBORNE, A., KHATIB, T. Z., SONGRA, L., BARBER, A. C., HALL, K., KONG, G. Y. X., WIDDOWSON, P. S. & MARTIN, K. R. 2018. Neuroprotection of retinal ganglion cells by a novel gene therapy construct that achieves sustained enhancement of brain-derived neurotrophic factor/tropomyosin-related kinase receptor-B signaling. *Cell Death Dis,* 9**,** 1007.

PERKINS, B. D. & FADOOL, J. M. 2010. Photoreceptor structure and development: analyses using GFP transgenes. *Methods in cell biology.* Elsevier.

PETERSON, R. E., FADOOL, J. M., MCCLINTOCK, J. & LINSER, P. J. 2001. Muller cell differentiation in the zebrafish neural retina: evidence of distinct early and late stages in cell maturation. *J Comp Neurol,* 429**,** 530-40.

PITTMAN, A. J., LAW, M. Y. & CHIEN, C. B. 2008. Pathfinding in a large vertebrate axon tract: isotypic interactions guide retinotectal axons at multiple choice points. *Development,* 135**,** 2865-71.

POGGI, L., VITORINO, M., MASAI, I. & HARRIS, W. A. 2005. Influences on neural lineage and mode of division in the zebrafish retina in vivo. *The Journal of cell biology,* 171**,** 991-999.

QU, J., WANG, D. & GROSSKREUTZ, C. L. 2010. Mechanisms of retinal ganglion cell injury and defense in glaucoma. *Exp Eye Res,* 91**,** 48-53.

RANAWAT, N. & MASAI, I. 2021. Mechanisms underlying microglial colonization of developing neural retina in zebrafish. *bioRxiv***,** 2021.05.20.444912.

RANDLETT, O., MACDONALD, R. B., YOSHIMATSU, T., ALMEIDA, A. D., SUZUKI, S. C., WONG, R. O. & HARRIS, W. A. 2013. Cellular requirements for building a retinal neuropil. *Cell Rep,* 3**,** 282-90.

RAPPSILBER, J., MANN, M. & ISHIHAMA, Y. 2007. Protocol for micro-purification, enrichment, pre-fractionation and storage of peptides for proteomics using StageTips. *Nat Protoc,* 2**,** 1896-906.

RAYMOND, P. A., BARTHEL, L. K., BERNARDOS, R. L. & PERKOWSKI, J. J. 2006. Molecular characterization of retinal stem cells and their niches in adult zebrafish. *BMC developmental biology,* 6**,** 36.

RICE, D. S., NUSINOWITZ, S., AZIMI, A. M., MARTÍNEZ, A., SORIANO, E. & CURRAN, T. 2001. The reelin pathway modulates the structure and function of retinal synaptic circuitry. *Neuron,* 31**,** 929-941.

RICHARD, M., ROEPMAN, R., AARTSEN, W. M., VAN ROSSUM, A. G., DEN HOLLANDER, A. I., KNUST, E., WIJNHOLDS, J. & CREMERS, F. P. 2006. Towards understanding CRUMBS function in retinal dystrophies. *Hum Mol Genet,* 15 Spec No 2**,** R235-43.

RICHARDSON, R., TRACEY-WHITE, D., WEBSTER, A. & MOOSAJEE, M. 2017. The zebrafish eye-a paradigm for investigating human ocular genetics. *Eye (Lond),* 31**,** 68-86.

RICK, J. M., HORSCHKE, I. & NEUHAUSS, S. C. 2000. Optokinetic behavior is reversed in achiasmatic mutant zebrafish larvae. *Curr Biol,* 10**,** 595-8.

ROBINSON, M. D., MCCARTHY, D. J. & SMYTH, G. K. 2010. edgeR: a Bioconductor package for differential expression analysis of digital gene expression data. *Bioinformatics,* 26**,** 139-40.

ROBLES, E., LAURELL, E. & BAIER, H. 2014. The retinal projectome reveals brain-area-specific visual representations generated by ganglion cell diversity. *Current Biology,* 24**,** 2085-2096.

RODRIGUEZ-CUPELLO, C., DAM, M., SERINI, L., WANG, S., LINDGREN, D., ENGLUND, E., KJELLMAN, P., AXELSON, H., GARCIA-MARISCAL, A. & MADSEN, C. D. 2020. The STRIPAK Complex Regulates Response to Chemotherapy Through p21 and p27. *Front Cell Dev Biol,* 8**,** 146.

SAKUMA, C., KAWAUCHI, T., HARAGUCHI, S., SHIKANAI, M., YAMAGUCHI, Y., GELFAND, V. I., LUO, L., MIURA, M. & CHIHARA, T. 2014. Drosophila Strip serves as a platform for early endosome organization during axon elongation. *Nat Commun,* 5**,** 5180.

SAKUMA, C., OKUMURA, M., UMEHARA, T., MIURA, M. & CHIHARA, T. 2015. A STRIPAK component Strip regulates neuronal morphogenesis by affecting

microtubule stability. *Sci Rep,* 5**,** 17769.

SAKUMA, C., SAITO, Y., UMEHARA, T., KAMIMURA, K., MAEDA, N., MOSCA, T. J., MIURA, M. & CHIHARA, T. 2016. The Strip-Hippo Pathway Regulates Synaptic Terminal Formation by Modulating Actin Organization at the Drosophila Neuromuscular Synapses. *Cell Rep,* 16**,** 2289-97.

SATIJA, R., FARRELL, J. A., GENNERT, D., SCHIER, A. F. & REGEV, A. 2015. Spatial reconstruction of single-cell gene expression data. *Nature biotechnology,* 33**,** 495-502.

SCHEER, N., RIEDL, I., WARREN, J. T., KUWADA, J. Y. & CAMPOS-ORTEGA, J. A. 2002. A quantitative analysis of the kinetics of Gal4 activator and effector gene expression in the zebrafish. *Mech Dev,* 112**,** 9-14.

SCHMITT, E. A. & DOWLING, J. E. 1994. Early-eye morphogenesis in the zebrafish, Brachydanio rerio. *Journal of Comparative Neurology,* 344**,** 532-542.

SCHMITT, E. A. & DOWLING, J. E. 1999. Early retinal development in the zebrafish, Danio rerio: light and electron microscopic analyses. *J Comp Neurol,* 404**,** 515-36.

SCHNEIDER, C. A., RASBAND, W. S. & ELICEIRI, K. W. 2012. NIH Image to ImageJ: 25 years of image analysis. *Nat Methods,* 9**,** 671-5.

SCHROETER, E. H., WONG, R. O. & GREGG, R. G. 2006. In vivo development of retinal ON-bipolar cell axonal terminals visualized in nyx:: MYFP transgenic zebrafish. *Visual neuroscience,* 23**,** 833-843.

SCHROETER, H., BOYD, C. S., AHMED, R., SPENCER, J. P., DUNCAN, R. F., RICE-EVANS, C. & CADENAS, E. 2003. c-Jun N-terminal kinase (JNK)-mediated modulation of brain mitochondria function: new target proteins for JNK signalling in mitochondrion-dependent apoptosis. *Biochem J,* 372**,** 359-69.

SCHULTE, J., SEPP, K. J., JORQUERA, R. A., WU, C., SONG, Y., HONG, P. & LITTLETON, J. T. 2010. DMob4/Phocein regulates synapse formation, axonal transport, and microtubule organization. *Journal of Neuroscience,* 30**,** 5189-5203.

SEO, G., HAN, H., VARGAS, R. E., YANG, B., LI, X. & WANG, W. 2020. MAP4K Interactome Reveals STRN4 as a Key STRIPAK Complex Component in Hippo Pathway Regulation. *Cell Rep,* 32**,** 107860.

SHI, Z., JIAO, S. & ZHOU, Z. 2016. STRIPAK complexes in cell signaling and cancer. *Oncogene,* 35**,** 4549.

SHIELDS, C. R., KLOOSTER, J., CLAASSEN, Y., UL-HUSSAIN, M., ZOIDL, G., DERMIETZEL, R. & KAMERMANS, M. 2007. Retinal horizontal cell-specific promoter activity and protein expression of zebrafish connexin 52.6 and connexin 55.5. *Journal of Comparative Neurology,* 501**,** 765-779.

SHIH, P. Y., HSIEH, B. Y., LIN, M. H., HUANG, T. N., TSAI, C. Y., PONG, W. L., LEE, S. P. & HSUEH, Y. P. 2020. CTTNBP2 Controls Synaptic Expression of Zinc-Related Autism-Associated Proteins and Regulates Synapse Formation and Autism-like Behaviors. *Cell Rep,* 31**,** 107700.

SHIH, P. Y., LEE, S. P., CHEN, Y. K. & HSUEH, Y. P. 2014. Cortactin-binding protein 2 increases microtubule stability and regulates dendritic arborization. *J Cell Sci,* 127**,** 3521-34.

SPENCE, E. F., KANAK, D. J., CARLSON, B. R. & SODERLING, S. H. 2016. The Arp2/3

complex is essential for distinct stages of spine synapse maturation, including synapse unsilencing. *Journal of Neuroscience,* 36**,** 9696-9709.

STUERMER, C. A. 1988. Retinotopic organization of the developing retinotectal projection in the zebrafish embryo. *J Neurosci,* 8**,** 4513-30.

SULLIVAN-BROWN, J., BISHER, M. E. & BURDINE, R. D. 2011. Embedding, serial sectioning and staining of zebrafish embryos using JB-4 resin. *Nat Protoc,* 6**,** 46-55.

SUN, H., WANG, Y., PANG, I. H., SHEN, J., TANG, X., LI, Y., LIU, C. & LI, B. 2011. Protective effect of a JNK inhibitor against retinal ganglion cell loss induced by acute moderate ocular hypertension. *Mol Vis,* 17**,** 864-75.

SUZUKI, S. C., BLECKERT, A., WILLIAMS, P. R., TAKECHI, M., KAWAMURA, S. & WONG, R. O. 2013. Cone photoreceptor types in zebrafish are generated by symmetric terminal divisions of dedicated precursors. *Proceedings of the National Academy of Sciences***,** 201303551.

SYC-MAZUREK, S. B., FERNANDES, K. A. & LIBBY, R. T. 2017a. JUN is important for ocular hypertension-induced retinal ganglion cell degeneration. *Cell Death Dis,* 8**,** e2945.

SYC-MAZUREK, S. B., FERNANDES, K. A., WILSON, M. P., SHRAGER, P. & LIBBY, R. T. 2017b. Together JUN and DDIT3 (CHOP) control retinal ganglion cell death after axonal injury. *Mol Neurodegener,* 12**,** 71.

SZKLARCZYK, D., MORRIS, J. H., COOK, H., KUHN, M., WYDER, S., SIMONOVIC, M., SANTOS, A., DONCHEVA, N. T., ROTH, A., BORK, P., JENSEN, L. J. & VON MERING, C. 2017. The STRING database in 2017: quality-controlled protein-protein association networks, made broadly accessible. *Nucleic Acids Res,* 45**,** D362-D368.

TANG, Y., CHEN, M., ZHOU, L., MA, J., LI, Y., ZHANG, H., SHI, Z., XU, Q., ZHANG, X., GAO, Z., ZHAO, Y., CHENG, Y., JIAO, S. & ZHOU, Z. 2019. Architecture, substructures, and dynamic assembly of STRIPAK complexes in Hippo signaling. *Cell Discov,* 5**,** 3.

TEAM, R. 2016. RStudio: Integrated development environment for R. Boston, MA.

THISSE, B. & THISSE, C. 2004. Fast release clones: A high throughput expression analysis. ZFIN Direct Data Submission https://zfin. org. ZDB-PUB-040907-1 (accessed 13 February 2013).

THISSE, C. & THISSE, B. 2008. High-resolution in situ hybridization to whole-mount zebrafish embryos. *Nat Protoc,* 3**,** 59-69.

UNGOS, J. M., KARLSTROM, R. O. & RAIBLE, D. W. 2003. Hedgehog signaling is directly required for the development of zebrafish dorsal root ganglia neurons. *Development,* 130**,** 5351-62.

URASAKI, A., MORVAN, G. & KAWAKAMI, K. 2006. Functional dissection of the Tol2 transposable element identified the minimal cis-sequence and a highly repetitive sequence in the subterminal region essential for transposition. *Genetics,* 174**,** 639-49.

VELDMAN, M. B., BEMBEN, M. A., THOMPSON, R. C. & GOLDMAN, D. 2007. Gene expression analysis of zebrafish retinal ganglion cells during optic nerve regeneration identifies KLF6a and KLF7a as important regulators of axon regeneration. *Dev Biol,*

312**,** 596-612.

WANG, J., STRUEBING, F. L. & GEISERT, E. E. 2021. Commonalities of optic nerve injury and glaucoma-induced neurodegeneration: Insights from transcriptome-wide studies. *Exp Eye Res,* 207**,** 108571.

WEI, X. & MALICKI, J. 2002. nagie oko, encoding a MAGUK-family protein, is essential for cellular patterning of the retina. *Nature genetics,* 31**,** 150.

WESTERFIELD, M. 1995. *The zebrafish book: a guide for the laboratory use of zebrafish (Brachydanio rerio)*, University of Oregon press.

WHITFIELD, J., NEAME, S. J., PAQUET, L., BERNARD, O. & HAM, J. 2001. Dominant-negative c-Jun promotes neuronal survival by reducing BIM expression and inhibiting mitochondrial cytochrome c release. *Neuron,* 29**,** 629-43.

WU, S., HUANG, J., DONG, J. & PAN, D. 2003. hippo encodes a Ste-20 family protein kinase that restricts cell proliferation and promotes apoptosis in conjunction with salvador and warts. *Cell,* 114**,** 445-56.

XU, B., TANG, X., JIN, M., ZHANG, H., DU, L., YU, S. & HE, J. 2020. Unifying developmental programs for embryonic and postembryonic neurogenesis in the zebrafish retina. *Development,* 147.

XU, Q., HOLDER, N., PATIENT, R. & WILSON, S. W. 1994. Spatially regulated expression of three receptor tyrosine kinase genes during gastrulation in the zebrafish. *Development,* 120**,** 287-99.

Y CAJAL, S. R. 1972. *The structure of the retina*, Charles C. Thomas Publisher.

YAMAGATA, M. & SANES, J. R. 2008. Dscam and Sidekick proteins direct lamina-specific synaptic connections in vertebrate retina. *Nature,* 451**,** 465.

YAMAGATA, M., WEINER, J. A. & SANES, J. R. 2002. Sidekicks: synaptic adhesion molecules that promote lamina-specific connectivity in the retina. *Cell,* 110**,** 649-60.

YANG, Z., QUIGLEY, H. A., PEASE, M. E., YANG, Y., QIAN, J., VALENTA, D. & ZACK, D. J. 2007. Changes in gene expression in experimental glaucoma and optic nerve transection: the equilibrium between protective and detrimental mechanisms. *Invest Ophthalmol Vis Sci,* 48**,** 5539-48.

YOSHIMATSU, T., SUZUKI, S. & WONG, R. 2013. Circuit assembly in the developing vertebrate retina. *Cellular Migration and Formation of Neuronal Connections.* Elsevier.

ZHANG, S., DONG, Y., QIANG, R., ZHANG, Y., ZHANG, X., CHEN, Y., JIANG, P., MA, X., WU, L., AI, J., GAO, X., WANG, P., CHEN, J. & CHAI, R. 2021. Characterization of Strip1 Expression in Mouse Cochlear Hair Cells. *Front Genet,* 12**,** 625867.

ZHAO, B., TUMANENG, K. & GUAN, K. L. 2011. The Hippo pathway in organ size control, tissue regeneration and stem cell self-renewal. *Nat Cell Biol,* 13**,** 877-83.

ZHAO, X.-F., ELLINGSEN, S. & FJOSE, A. 2009. Labelling and targeted ablation of specific bipolar cell types in the zebrafish retina. *BMC neuroscience,* 10**,** 107.

ZHOU, Y., PERNET, V., HAUSWIRTH, W. W. & DI POLO, A. 2005. Activation of the extracellular signal-regulated kinase 1/2 pathway by AAV gene transfer protects retinal ganglion cells in glaucoma. *Mol Ther,* 12**,** 402-12.

ZHOU, Y., ZHOU, B., PACHE, L., CHANG, M., KHODABAKHSHI, A. H., TANASEICHUK, O., BENNER, C. & CHANDA, S. K. 2019. Metascape provides a biologist-oriented resource for the analysis of systems-level datasets. *Nat Commun,* 10**,** 1523.

ZOU, S., TIAN, C., GE, S. & HU, B. 2013. Neurogenesis of retinal ganglion cells is not essential to visual functional recovery after optic nerve injury in adult zebrafish. *PLoS One,* 8**,** e57280.

Appendix

Table 8. Selected 15 genes significantly downregulated in transcriptome of *strip1* mutant eyes.

Gene stable ID	Gene description	Gene name	Log_2FC	PValue	FDR
ENSDARG00000069737	POU class 4 homeobox 2	pou4f2	-1.684053641	9.82E-18	1.44E-14
ENSDARG00000035648	iroquois homeobox 4a	irx4a	-1.758071037	7.64E-16	8.01E-13
ENSDARG00000053499	ISL LIM homeobox 2b	isl2b	-1.578818516	3.02E-13	2.05E-10
ENSDARG00000005559	POU class 4 homeobox 1	pou4f1	-1.662408296	2.14E-12	1.35E-09
ENSDARG00000004712	T-box brain transcription factor 1b	tbr1b	-1.798201702	6.72E-10	3.22E-07
ENSDARG00000055559	cholinergic receptor, nicotinic, alpha 6	chrna6	-1.456669842	7.19E-10	3.39E-07
ENSDARG00000070543	glutamate receptor, ionotropic, N-methyl D-aspartate 2A, b	grin2ab	-1.246284746	1.12E-09	5.17E-07
ENSDARG00000109715	synuclein, gamma b (breast cancer-specific protein 1)	sncgb	-1.484010355	1.59E-09	7.25E-07
ENSDARG00000069117	potassium voltage-gated channel, subfamily H (eag-related), member 5b	kcnh5b	-2.290882655	1.18E-08	4.49E-06
ENSDARG00000017880	Kv channel interacting protein 3b, calsenilin	kcnip3b	-2.342018452	1.43E-07	4.28E-05
ENSDARG00000026796	glutamate receptor, metabotropic 1a	grm1a	-1.19183933	1.65E-06	0.000420785
ENSDARG00000006206	POU class 4 homeobox 3	pou4f3	-1.15249828	5.54E-06	0.001250167

Gene stable ID	Gene description	Gene name	Log_2FC	PValue	FDR
ENSDARG00000001785	iroquois homeobox 2a	irx2a	-1.02849215	1.61E-05	0.003236797
ENSDARG00000057468	potassium voltage-gated channel, Shaw-related subfamily, member 2	kcnc2	-1.572337622	4.97E-05	0.00841739
ENSDARG00000051852	potassium voltage-gated channel, Shaw-related subfamily, member 1a	kcnc1a	-1.046055885	0.000133123	0.019155177

Table 9. Selected 15 genes significantly upregulated in transcriptome of *strip1* mutant eyes.

Gene stable ID	Gene description	Gene name	Log_2FC	PValue	FDR
ENSDARG00000076891	regulatory factor X-associated protein	rfxap	8.667492494	7.67E-29	3.04E-25
ENSDARG00000001889	tubulin, alpha 1a	tuba1a	1.405749802	1.70E-23	5.91E-20
ENSDARG00000007823	activating transcription factor 3	atf3	2.14952789	2.34E-23	7.21E-20
ENSDARG00000043932	stathmin-like 4, like	stmn4l	1.867895419	6.52E-23	1.81E-19
ENSDARG00000043467	NADH:ubiquinone oxidoreductase subunit B11	ndufb11	2.55969399	1.25E-19	2.89E-16
ENSDARG00000063916	NADH dehydrogenase subunit 4L	mt-nd4l	1.421884812	1.54E-18	2.67E-15
ENSDARG00000045367	tubulin, alpha 1b	tuba1b	1.467085015	1.41E-16	1.87E-13
ENSDARG00000043531	Jun proto-oncogene, AP-1 transcription factor subunit	jun	1.609258909	2.16E-15	2.07E-12
ENSDARG00000102899	cAMP responsive element modulator b	cremb	4.294154877	2.81E-15	2.60E-12
ENSDARG00000097456	cytochrome C oxidase assembly factor 3b	coa3b	3.93089882	8.15E-15	7.30E-12
ENSDARG00000030106	stathmin-like 4	stmn4	1.270972818	1.85E-09	8.24E-07

Gene stable ID	Gene description	Gene name	Log2FC	PValue	FDR
ENSDARG00000027740	adenylate cyclase activating polypeptide 1b	adcyap1b	1.577985712	4.12E-08	1.36E-05
ENSDARG00000099744	growth associated protein 43	gap43	1.374709774	9.99E-08	3.12E-05
ENSDARG00000039268	ER membrane protein complex subunit 4	emc4	2.853612962	1.47E-06	0.000384837
ENSDARG00000044114	cytochrome b561 family, member D2	cyb561d2	2.794442915	5.43E-06	0.001236105